A SYSTEMATIC STUDY ON ENERGY PROPERTIES OF IONIC THERMOELECTRIC MATERIALS DURING PHASE TRANSITION

LIU JIN

PhD

The Hong Kong Polytechnic University

2023

The Hong Kong Polytechnic University

School of Fashion and Textiles

A Systematic Study on Energy Properties of Ionic Thermoelectric Materials during Phase Transition

LIU Jin

A thesis submitted in partial fulfilment of the requirements for the degree of

Doctor of Philosophy

December 2022

CERTIFICATE OF ORIGINALITY

I hereby declare that this thesis is my own work and that, to the best of my knowledge and belief, it reproduces no material previously published or written, nor material that has been accepted for the award of any other degree or diploma, except where due acknowledgement has been made in the text.

_____(Signed)

LIU JIN (Name of student)

ABSTRACT

With the expanding growth of wearable electronics and Internet of Things, the efficient and environmental-friendly power sources are urgently needed. Thermoelectric generators (TEGs), which can harvest energy from waste heat and directly convert it into electricity, can be one of the possible solutions. Different from conventional TEGs made by electronic thermoelectric (TE) materials, ionic thermoelectric (i-TE) materials have been explored as candidates for TEGs with superior TE performances comparing with electronic TE counterparts at room temperature. However, simple i-TE systems made by salt aqueous solutions still possess unsatisfied performances for applications and the enhancement of output thermopower needs either complicated mechanisms or uncommon ion species which are difficult to synthesis. This thesis, based on the analysis about the ionic transportations in i-TE systems, systematically studies the energy properties (including thermopower (or ionic Seebeck coefficient), electrical conductivity, thermal conductivity and ionic figure of merit (ZT_i)) of i-TE materials during phase transition and establishes an analytical model that can describe the ionic transportations in phase-transitional i-TE systems. Starting with the analysis and investigation about the effects of phase transition in four different types of i-TE materials (non-phase-transition, thermal sol-to-gel, thermal gel-to-sol and UV-induced sol-to-gel phase-transition), this thesis, for the first time, reports a discovery of a 6.5-fold (from 2.5 mV/K to 15.4 mV/K) and 23-fold (from less than 0.03 to around 0.68) increment of the thermopower and ionic figure of merit during the thermal-induced sol-to-gel phase transition in a poloxamer/LiCl aqueous i-TE material. A large drop of thermopower during the gel-to-sol phase transition in an agarose/LiCl system

is also observed, which indicates the possibility of this method to modify the TE performances of the i-TE materials.

In order to reveal the operational mechanism, this thesis provides a semi-quantitative model based on Onsager relations and Eastman entropy theory, which can cover the pre-, post- and during-transition stages. Based on the analysis model, six dimensionless influencing factors that may affect the change of thermopower during phase transition are probed and derived. The analysis result confirms that gigantic increment (larger than 1000 times) of the thermopower can possibly be achieved in the i-TE systems during phase transition. In addition, the theoretical analysis also speculates the universal applications of phase transition in i-TE materials, which means that the modifications of TE performances in i-TE systems can be achieved by phase transition regardless the type of causes for the sol-gel phase transition and the prediction is further confirmed by the rise of thermopower in epoxy/LiCl system during the phase-transition caused by UV irradiation.

The phase-transitional i-TE systems share similar drawbacks with other thermodiffusive i-TE systems, which are the decay of output current with time when connected to the external load. This thesis, further investigates these limitations, provides possible solutions by using thermogalvanic effects (adding redox couples) or metal electrodes, and observes a continuous current output in the phase-transitional i-TE systems by using these methods. This thesis, for the first time, systemically studies the energy properties of i-TE materials during phase transition, points out a possible, novel and universal-applicable method to modify the TE performances of the i-TE systems, which may lead to a new perspective for future tunable i-TE devices for low-heat energy harvesting applications.

Key words: Ionic thermoelectric materials, phase transition, thermoelectric performances, energy harvesting, theoretical analysis, simulations.

List of Publications and Conference

Presentations

Journal publications based on this thesis work:

(* corresponding author)

1. **Jin Liu**, Wei Zeng, and Xiaoming Tao*, Gigantic Effect due to Phase Transition on Thermoelectric Properties of Ionic Sol–Gel Materials, *Adv. Funct. Mater.* **2022**, 2208286

2. **Jin Liu**, Qiutong Liu, Shuping Lin, Man Yui Leung, Yuan Ma, Xiaoming Tao*, Wearable Thermoelectric Generators: Materials, Structures, Fabrications and Applications, *Phys. Status Solidi RRL*, 2200502, **2023**.

Journal publications during my PhD study but not included in this thesis:

(* corresponding author)

1. Shuping Lin, Lisha Zhang, Wei Zeng, Dongliang Shi, Su Liu, Xujiao Ding, Bao Yang, **Jin Liu**, Kwok-ho Lam, Baolin Huang & Xiaoming Tao*, Flexible thermoelectric generator with high Seebeck coefficients made from polymer composites and heat-sink fabrics, *Communications Materials*. **3**, 44, **2022**.

2. Junhong Pu, Kit-ming Ma, Yonghui Luo, Shenyang Tang, Jing Yang, **Jin Liu**, Tongyao Liu, Ruomu Hui, Manyui Leung, Xiaoming Tao*, Textile electronics: manufacturing and post-processing for wearable applications, accepted by *Int. J. Extrem. Manuf.*, 2023.

Conference presentations

1. **Jin Liu**, Wei Zeng, Xiaoming Tao, "Gigantic Effect due to Phase Transition on Thermoelectric Properties of Ionic Sol–Gel Materials", Oral Presentation, The Fiber Society 2022 Fall Meeting and Technical Conference, Raleigh, North Carolina, USA, Oct. 2022.
2. **Jin Liu**, Wei Zeng, Xiaoming Tao, "Gigantic Effect due to Phase Transition on Thermoelectric Properties of Ionic Sol–Gel Materials", Virtual Poster Presentation, MRS Spring Conference and Exhibition, San Francisco, California, USA, Apr. 2023.

ACKNOWLEDGEMENTS

When I recalled the memory in my previous study, a great of deal fascinating moments came to my mind. As for me, the PhD study is quite comprehensive, the happy times let me enjoy the pleasure of learning while the tough times make me grow up. I would like to express great gratitude to many people who have provided help and supports to me both in my study and life.

The greatest appreciation goes to my supervisor Prof. Tao Xiao-ming. She is and remains one of my best role models for a scientist, mentor and teacher. Prof. Tao has guided me for doing the whole project and enlightened me in both material and physics area. Prof. Tao has wide experiences not only in textile, electronic, materials and physics research field, but also in fostering students. The discussion on diversity and interdisciplinary subjects in every week's group meeting has inspired me overwhelmingly. Prof. Tao has been supportive and has given me the freedom to explore in the research field without objection. I am also very grateful to Prof. Tao for her scientific advice and knowledge together with many insightful discussions and effective suggestions. Thanks a lot to Prof. Tao for bringing me up to speed on this novel research program.

In addition, I would like to specially appreciate the great help from my former groupmate, Prof. Zeng Wei, who was a PostDoc researcher in our group. With his help and guidance, I started my research on thermoelectrics and learned a lot from his research experience, especially in experiment designs and material preparations. The idea of this project is also shared by Prof. Zeng wei and I also seek help from him when I'm working on this project.

Besides, I would like to appreciate the help from the present and past group members: Dr. Yang Bao, Dr. Zhang Lisha, Dr. Lin Shuping, Dr. Yang Su, Ms. Ying Li, Dr. Liu Su, Ms. Ma Linlin, Ms. Ma Kit-Ming, Dr. Xiong Ying, Mr. Pan Linqi, Dr. Li Jun, Dr. Zhang Ziheng, Mr. Tang Shengyang, Mr. Luo Heng, Dr. Pu Junhong and the collaborator from department of Mechanical Engineering Dr. Ma Yuan and his student Ms. Liu Qiutong.

I also would like to express my sincere appreciation to the panels for their commitment of efforts and reviews in this process. I would like to thank The Hong Kong Polytechnic University for a postgraduate scholarship. The technical supports from the laboratory, general officers and technicians are also highly appreciated.

At last, I would like to specially thank the support from my girlfriend Yuanbao, who accompanied me during my whole Ph.D. study. Her supports, patience and her love encouraged me when I faced with troubles and problems. I think it should be the suitable time for me to express my love to her in my thesis.

CONTENTS

ABSTRACT I

List of Publications and Conference Presentations IV

ACKNOWLEDGEMENTS VI

CONTENTS VIII

LIST OF FIGURES AND TABLES XI

NOMENCLATURE XIV

General Symbols XIV
Abbreviations XV

CHAPTER 1 Introduction 1

1.1 Research background 1
1.2 Problem Statement 5
1.3 Objectives 6
1.4 Methodology 7
1.5 Research Significance 11
1.6 Outlines of the thesis 12

CHAPTER 2 Literature review 15

2.1 Introduction of Thermoelectric Effect 15
2.2 Thermoelectric materials 17
2.2.1 Thermoelectric fundamentals 18
2.2.2 Electronic TE materials 24
2.2.3 Ionic TE materials 35
2.2.4 Comparison and summary of TE materials 39
2.3 Enhancement of TE performances 41
2.3.1 Electrical properties 41
2.3.2 Thermal properties 45
2.4 Structure design and fabrication of flexible TEGs 48
2.4.1 Design of the electric circuit 48
2.4.2 Fabrication of wearable TEGs 51
2.5 Application of thermoelectric device 57
2.5.1 Principle of wearable applications 57
2.5.2 Demonstration of wearable applications 59

2.5.3 Challenges and future in application of wearable TEGs 69
2.6. Summary and perspectives 71
CHAPTER 3 Thermoelectric properties of phase-transitional i-TE systems during phase change 74
3.1 Introduction 74
3.2 Methodology 77
3.2.1 Preparation and fabrication 77
3.2.2 Characterization 82
3.3 Result and discussion 86
3.3.1 I-TE materials and phase-transition 86
3.3.2 Thermopower 90
3.3.3 Thermal, electrical conductivity and ZT values 95
3.4 Summary 100
CHAPTER 4 Mechanisms and theoretical models 102
4.1 TE performances of the i-TE cells 102
4.2 Mechanisms of ionic thermodiffusion 103
4.2.1 Illustration of thermopower 103
4.2.2 Eastman entropy of transfer 109
4.3 Analysis of ionic transportations 114
4.3.1 Before phase-transition 115
4.3.2 After phase-transition 116
4.3.3 During phase-transition 118
4.3.4 Analysis model 120
4.3.5 Experimental proofs 129
4.4 Generalization of the model 132
4.5 Summary 134
CHAPTER 5 Enhancement of output current and generation of continuous output ... 135
5.1 Figure of merit and efficiency of energy conversion 135
5.1.1 Figure of merit and efficiency of electronic TEGs 135
5.1.2 Figure of merit and efficiency of ionic TEGs 138
5.2 Increase output current by thermogalvanic effect 141
5.3 Effects of active electrodes 147
5.4 Summary 150
CHAPTER 6 Conclusions and Suggestions for Future Research 151
6.1 Conclusions 151
6.2 Limitations and outlooks 153
6.3 Recommendations on future work 155

Appendix 157

Appendix I Simulations from COMSOL Multiphysics 157

Appendix II Onsager relations 160

Appendix III Matlab codes 162

References 167

LIST OF FIGURES AND TABLES

Figure 1.1 The timeline for the development of ZT values in bulk TE materials.

Figure 2.1 A schematic diagram of a common structure of a flexible TEG.

Figure 2.2 Schematic diagrams of thermoelectric effects.

Figure 2.3 Thermoelectric properties of PEDOT:PSS at various dedoping times.

Figure 2.4 TE effect in electronic TE and i-TE materials.

Figure 2.5 Operation principle of i-TE thermodiffusion cells.

Figure 2.6 DFT calculations of two-band model.

Figure 2.7 ZT values of anisotropic SnSe crystals along different axial directions.

Figure 2.8 Introduction of dislocation arrays has a large effect on thermal conductivity but a small effect on electronic conductivity.

Figure 2.9 Electric circuit connections of TE cells.

Figure 2.10 Examples of flexible TEGs with different structures.

Figure 2.11 Schematic figure and photo of a flexible TEG structure.

Figure 2.12 Schematic figures of different techniques for surface modification.

Figure 2.13 Schematics of requirements for wearable applications.

Figure 2.14 Examples of body-heat powered watch.

Figure 2.15 Examples of applications of wearable TEGs with rigid structures.

Figure 2.16 Examples for applications of wearable TEGs with flexible structures.

Figure 2.17 Medical applications of wearable TEGs.

Figure 2.18 Summary of several demonstrations about the performances of recent wearable TEGs.

Figure 3.1 Schematic illustrations of the i-TE systems.

Figure 3.2 Schematic figures of the preparation process for the i-TE cells.

Figure 3.3 Photos of the equipments used in the characterization of the TE materials.

Figure 3.4 Photos of the preparations for the i-TE materials and i-TE cells.

Figure 3.5 Liquid-to-gel phase transition of LiCl/P407 solution.

Figure 3.6 Sol-gel phase transition of P407 with different concentrations.

Figure 3.7 Thermopower-temperature relationship of the salt/10% (w/v) poloxamer systems.

Figure 3.8 Thermopower and viscosity of the transitional i-TE materials.

Figure 3.9 Characterization of a gel-to-sol phase transition i-TE system.

Figure 3.10 Bode's plot of 1 mol/L LiCl / 18% (w/v) Poloxamer i-TE material at different temperature.

Figure 3.11 Electrical and thermal conductivity of the i-TE system.

Figure 3.12 Cyclic voltammetry curves of the 18% (w/v) P407-based 1 mol/L LiCl ionic solution under room temperature.

Figure 3.13 Temperature-ZT_i relations of 18% (w/v) P407-based 1 mol/L LiCl ionic solution.

Figure 4.1 Hydrodynamic calculation of the single-ion heat of transport.

Figure 4.2 Schematic of the diffusion process of cations and anions under a temperature gradient within transitional i-TE system in liquid-state (before phase-transition).

Figure 4.3 Schematic of the diffusion process of cations and anions under a temperature gradient within transitional i-TE system in gel-state (after phase-transition).

Figure 4.4 Schematic of the diffusion process of cations and anions under a temperature gradient within transitional i-TE system in quasi-state (during phase-transition).

Figure 4.5 Analysis about the change of thermopower during phase-transition.

Figure 4.6 3D-plot relations between γ and other six parameters in the Equation 4.47.

Figure 4.7 Proof of the concentration differences of Cl- ions at different ends of the i-TE cell.

Figure 4.8 Output thermopower of UV-light induced sol-gel transitional i-TE materials.

Figure 5.1 Schematic figures of the TE effect in electronic TEGs.

Figure 5.2 Calculated maximum conversion efficiency of TEGs.

Figure 5.3 Schematic figures of the TE effect in ionic TEGs.

Figure 5.4 Evidence of capacitances working mode of the phase transitional i-TE materials.

Figure 5.5 Comparison of the TE performances between the phase-transitional i-TE materials with/without redox couples.

Figure 5.6 Output voltage of the i-TE materials with different electrodes.

Table 2.1. Summary of some popular electronic TE materials: types and ZT values at different temperatures.

Table 2.2 Several demonstrations about the performances of recent wearable TEGs.

Table 3.1 Details of i-TE systems.

Table 3.2 Different components of the ionic-TE materials shown in Figure 3.4c.

Table 4.1 Diffusion coefficient of some different ions in water at 25°C.

Table 4.2 Single-ion heat of transport at infinite aqueous solution.

Table 4.3 Lists of conditions in Figure 4.5

NOMENCLATURE

General Symbols

ΔT	Temperature Difference
n	Carrier Concentration
μ	Carrier Mobility
T	Temperature
κ	Thermal conductivity
q	Electrical charge
σ	Electrical conductivity
S	Seebeck coefficient
τ	Time constant

Abbreviations

TE	Thermoelectric
TEG	Thermoelectric generators
UV	Ultra-violet
PMMA	Poly(methyl methacrylate)
ZT	Figure of merit
PDMS	Polydimethylsiloxane
FTEGs	Flexible thermoelectric generators
DI water	Deionized water
PF	Power Factor
P407/Polo.	Poloxamer 407
Aga.	Agarose
i-TE	Ionic thermoelectric

CHAPTER 1 Introduction

1.1 Research background

The uses of natural fossil fuel to generate electricity have not only caused the energy crisis but the air pollution together with the global warming as well. However, as the increasing of the global population and development of industrialization, the demand of energy, especially the electricity, has reached an unexpected level.[1] The increasing demand of energy and the drawbacks of the natural fossil fuel have aggravated the energy crisis and environmental problems which human beings are dealing with in the present time. To cope with the global warming, air pollution and high energy costs, researchers in the past decades have tried to find other forms of environmental-friendly energy, including the energy from solar, wind and biomass. Apart from the discovery of new forms of energy, the growing interest in renewable energy, which can harvest energy from natural waste resources, such as radiation, thermal, light etc., to provide sustainable, environmental-friendly and cheap electrical power has also provided another potential solution to the energy crisis and the related problems in environments.

As one of the representatives of waste energy, thermal energy is one of the abundant resources which could be found in almost everywhere of the surroundings, such as the electronic devices (PC, mobile phone, electronic heater, etc.), vehicles and even human or animal body. With such kind of sufficient amount, the uses of thermal energy attract so many interests and one of the representatives is thermoelectric applications, which are mostly based on thermoelectric generators (TEGs).[2] TEGs are devices which are based on

the Seebeck effect, made by thermocouples and could convert the thermal energy into electricity. Furthermore, TEGs made by flexible materials to fulfill the requirements of working in large mechanical deformation conditions have attracted increasing interests attribute to their advantages of light-weighted, high-flexibility and environmental-friendly. With the development of this area in the past few decades, the flexible thermoelectric generators (FTEGs) have been chosen as potential candidate for the power supplier of the wearable electronic systems since they can directly acquire the heat from human body and convert it into electricity.[3,4]

The key point of making FTEGs is the choice of the materials, which are normally be called as thermoelectric (TE) materials. TE materials are the materials that can directly conduct the heat-to-electricity conversion and can also convert the electricity into temperature gradient reversely. Researchers have put many efforts in finding the TE materials with satisfied performances and one of the most significant factors is efficiency. In order to evaluate the performance and the efficiency of TE materials, researchers have defined a dimensionless parameter based on the TE properties of the materials, which is called dimensionless figure of merit (ZT). The ZT value is defined by equation as:

$$ZT = \frac{S^2 \sigma T}{\kappa}$$

where S is Seebeck coefficient, σ is electrical conductivity, κ is thermal conductivity and T is temperature, respectively. It can be clearly observed from the equation that for a certain temperature, a high efficiency or a high ZT value requires S and σ to be high and κ to be low. Normally, high S and high σ guarantee the TE material can generate a high electrical

output while low κ helps maintain the differences between the temperature of hot side (T_H)and temperature of cold side (T_C).

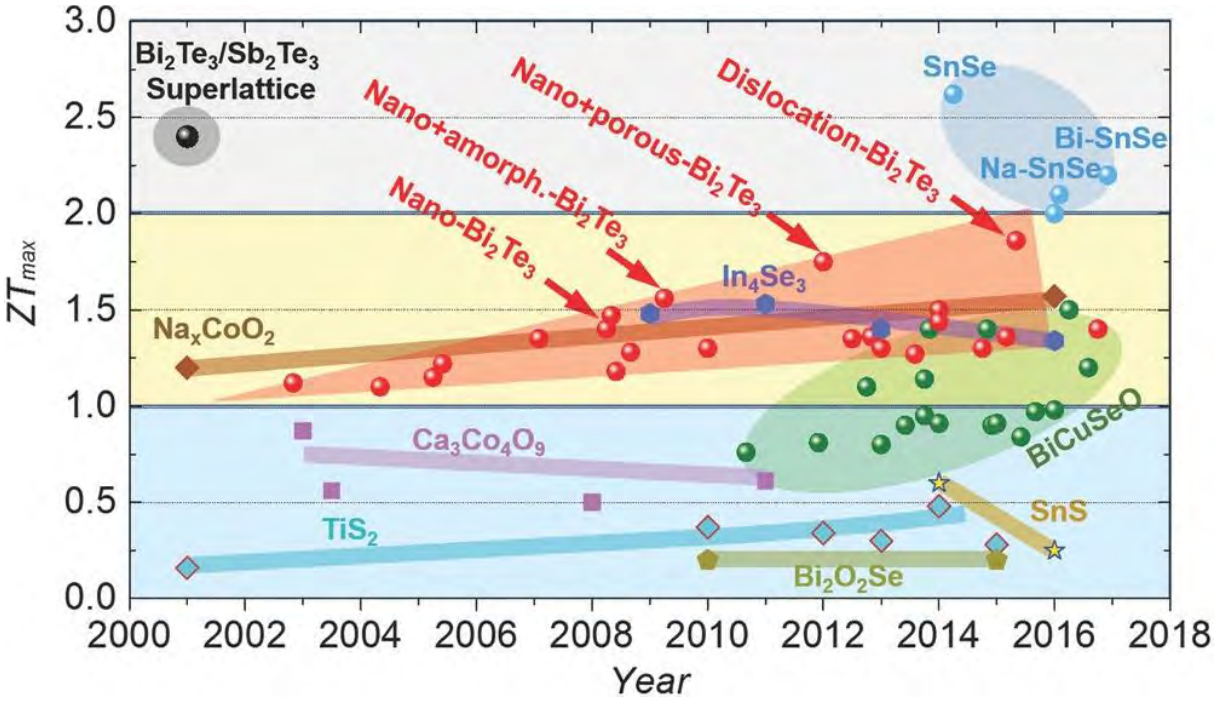

Figure 1.1 The timeline for the development of ZT values in bulk TE materials.[5]

Figure 1.1 shows the timeline for the development of ZT values in bulk TE materials. Conventional TE materials used in industrial production or basic research areas are mainly focused on solid state materials, including Bi_2Te_3, PbTe, SiGe, SnSe and some organic materials such as poly(3,4-ethylenedioxythiophene) polystyrene sulfonate (PEDOT:PSS). However, the traditional solid-state materials are facing serious challenges, including multiple bending, large mechanical deformation and some high-level demands. Recently, researchers have tried many methods to enhance the flexibility of the TE materials. In a recent work, printing pastes were made from the fabrication of Bi_2Te_3 and Sb_2Te_3, which

can be simply manufactured on curved surfaces such as human body or wearable textiles.[6] Apart from printing pastes, researchers also tried to fabricate thin films with high flexibility or divide the large solid-state TE materials into several small parts and addict them onto flexible substrate thus fulfill the flexible requirements. However, due to the inter-relations of the S, σ and κ, the TE performance, especially the ZT values of the previous mentioned FTEGs are not satisfied.

To break the strong inter-relations of those parameters and improve the TE performances of the TE materials, researchers have also made some attempts. Some of them tried to use composite materials instead of homogenous materials by affecting the energy level and density of states (DOS) of the certain materials thus break the inter-relations between the S and σ.[7] Another routine is using ions as charge carriers instead of electrons, which can break the inter-relations that have been mentioned above and thus improve the output thermopower. The ionic thermoelectric (i-TE) materials normally can work based on two different mechanisms, which are named as thermodiffusion effect and thermogalvanic effect, respectively. The previous one is on the basis of the thermal diffusion of different ion species while the later one is attributed to the redox reactions happen at different temperature.[8,9] Recently, researchers have discovered a giant thermoepower of ionic gelatin matrix modulated with ionic providers (KCl) and redox couple [$Fe(CN)_6^{4-}$/ $Fe(CN)_6^{3-}$] which could achieve a rather high thermopower of 17.0 mV/K while maintaining an applicable σ (1.4 S/m).[10] In addition, a rather high thermopower of 43.8 mV/K and ionic conductivity of 19.4 mS/cm have been reported in the ionogels of poly(vinylidene fluoride-*co*-hexafluoropropylene) (PVDF-HFP) and 1-ethyl-3-methylimidazolium dicyanamide (EMIM:DCA) doping by sodium dicyanamide

(Na:DCA).[11] These works have demonstrated the TE performances of i-TE systems and the outstanding performances may help them become good candidates for wearable applications. Most of the previous research have focused more on the choices of ion species and tried to choose the proper ions that might be suitable for different conditions. Therefore, in order to achieve a rather high output thermopower, researchers need to try many times for different combination of ion species or synthesize i-TE materials with complex polymer components. It will be valuable if we can find out a universal method that can be used in most of the i-TE systems to modify the output thermoelectric performances, including increase and decrease of output thermopower. Therefore, instead of putting efforts on choosing different ion species, locating the target on the electrolyte, where the ions are transported, might provide a completely different aspect for research in i-TE materials. This novel idea might provide an opportunity to enhance the performances of those i-TE materials with unsatisfied TE performances and make them suitable for energy harvesting applications.

1.2 Problem Statement

FTEGs have many potential applications basing on the ability to harvest thermal energy from the surroundings and convert into electricity. However, most of the industrial or commercial applications are not satisfied due to the low converting efficiency. As mentioned in the previous part, ZT depends on three dependent parameters at a certain temperature. Conventional TEGs made by narrow band-gap semiconductors which use either electrons or holes as charge carriers always suffer from the inter-relations the S, σ

and κ thus cannot achieve a high converting efficiency. Therefore, in order to generator a useful output voltage under room temperature condition, researchers need to integrate several tiny TEG components together, which limited the applications of conventional TE materials for wearable electronic devices.

Researchers have tried several methods, including doping and nanostructure designs to break the inter-relations between these parameters. However, most of these generators are still made from solid-state materials, which could increase the difficulty of the applications under high mechanical deformation conditions. Another routine is to use ionic liquid or ionic hydrogels which use ions as carriers instead of conventional TE materials which use electrons as carriers. Therefore, the inter-relations between the S and σ can be weakened. A high ZT value requires the TE materials to have a rather high S together with a high σ. Comparing with the semiconductors, ionic-liquids or ionic-gels are normally lack of σ. Therefore, the way to improve the S together with maintaining a rather high σ could be quite significant in the study of i-TE materials. Previous research on i-TE materials mostly focused on the choices of ion species but ignored the matrix or environments that the ions are transported. The theoretical study about the transportations of ions in i-TE systems is lacked. Besides, how to enhance the mechanical strength of the target materials to fulfill the requirements of working in high mechanical deformation conditions could also be a quite important factor to be considered.

1.3 Objectives

As mentioned in the previous parts, i-TE materials can partially break the inter-relations between the S, σ and κ, which thus enhance the ZT values and TE performances. Therefore,

this thesis will mainly focus on i-TE materials with satisfied TE performances, find out the working mechanism of i-TE systems and attempt to assess the TE properties of the i-TE systems.

This thesis will mainly focus on the study of i-TE systems and discover certain effects of the environments (the solvent in i-TE liquids) on transportation of ions. Based on this point, the thesis will try to introduce several novel mechanisms into the i-TE systems, including different types of phase-transition, to find out the relations between ionic transportation and TE performances.

The objectives of this thesis are listed below:

(1) To prepare the liquid-state i-TE by using ionic liquids and examine the TE performances.
(2) To examine the TE performances of different i-TE systems and find out the relations between phase-transition and TE performances, especially the thermopower.
(3) To study the working mechanism in the system and try to establish an analysis model to describe the phenomena.
(4) To investigate the working mode of the i-TE systems and try to enhance the output power.

1.4 Methodology

This thesis mainly focuses on the study of i-TE materials, especially the TE performances. However, most of the i-TE systems in this thesis are in liquid-state. Therefore, the i-TE materials need to be fabricated into a test cell before the characterizations. Before starting this project, a comprehensive review about the previous works of this area, including the study of different types of TE materials, design and fabrication of flexible TEGs and applications of flexible TEGs for wearable applications needs to be performed. After finished the review, the related techniques and methods are selected to solve the main problems and tasks step by step. This section will introduce the methodology of this project in details including the main techniques for the fabrication, characterization as well as the study of the mechanisms.

(1) Firstly, the comprehensive literature review will be conducted on flexible TEGs, or wearable TEGs. The literature review will cover the choices of TE materials, fabrication and design of TEGs and the wearable applications. The characterization methods and mechanisms of these materials need to be explored and summarized before conducting the research of this project in the literature review. After that, evaluation about the performance and limitations of the previous work in this area needs to be illustrated in detail thus the novelty and reliability of this project can be examined. Based on these fundamental works, the methodology of this study can evaluate the whole validity and reliability of this work.

(2) In this work, basing on the investigation about the previous research, i-TE materials will be the research targets. Different from the i-TE systems that haven been reported from previous works, the i-TE systems in this project involve phase-

transition mechanism, which means the i-TE system will experience phase change between liquid-state and hydrogel-state during the whole experiments.

(3) After chose TE materials, the TE performances of the targets need to be explored, which means the S, σ and κ of the material need to be examined. Therefore, several various types of characterization methods need to be conducted and illustrated as below:

Seebeck coefficient:

The Seebeck coefficient is measured by the magnitude of the induced thermoelectric voltage divided by the temperature difference across the material. Therefore, the key point of the measurement is to measure the voltage difference between the ends with different temperatures of the target TE materials. In this thesis, the output voltage of the target TEG is measured and recorded by an electrochemical workstation (CHI660E, CHInstrument, USA). The temperature differences are produced and maintained by a Whatlet TEC temperature controller and the real-time temperature is measured and recorded by Anbat AT4516 thermocouple thermometer.

Electrical conductivity:

The electrical conductivity of solid-state materials is quite simple. Normally, researchers could use four-point probe (FPP) measurer to accurately achieve the electrical conductivity by measuring the resistivity of the target materials. However, it is quite difficult to apply the FPP methods onto liquid-state or gel-state materials. Therefore, an indirect measurement needs to be explored. Researchers have found

that i-TE materials are likely to work in capacitor modes, which means the i-TEGs work like supercapacitors. Therefore, the measurement and calculation of electrical conductivity in this project will be similar with the methods on capacitors. In this project, the ionic σ will be analyzed from the electrical impedance of the material, which can be measured by electrical impedance spectroscopy (EIS). The EIS test is conducted also on electrochemical workstation (CHI660E, CHInstrument, USA).

Thermal conductivity

Thermal conductivity refers to the thermal conductivity of the i-TE electrolytes but not the conductivity of whole cells. The thermal conductivity should be evaluated by Thermal Conductivity Measurement Instrument (Hotdisk, TPS2500s) for samples in fluid form. The performed experiments should be controlled in suitable T to make sure the i-TE materials can be maintained at liquid-state during the whole test process.

Other electrical measurements and ZT:

Other electrical properties, such as the output power and power factor, can be calculated from the result measured by the electrochemical workstation (CHI660E, CH Instrument, USA). The ZT value is calculated as $ZT = \frac{\sigma S^2}{\kappa} T$.

Fabrication of TEGs and performance assessment

In this work, liquid-state i-TE materials will be fabricated into test cells by poured into the container with electrodes on the bottom and top sides. A single test cell can

be directly characterized for the TE properties, especially the electrical output, including open-circuit voltage and close-circuit current, which are measured by electrochemical workstation (CHI660E, CHInstrument, USA) and the temperature is monitored by thermocouple thermometer (Anbat AT4516, USA). Then the TEGs can simply be built by connecting several test cells together and find out the electrical output.

1.5 Research Significance

This thesis is meaningful and the novelty of this work lies in the following aspects:

(1) Ionic liquid-state TE materials have been discussed and synthesized in previous studies. However, the i-TE systems which include the phase-transition has never been studied before. This work will study the i-TE systems with phase-transition for the first time and observe the large change of TE performances that the i-TE materials can have during phase-transition.

(2) Theoretical analysis of ionic transportation under temperature gradient has been studied by Onsager's relations. This work will modify the theory and successfully describe the transportations of ions under temperature gradient in phase-transitional i-TE system for the first time. From the analysis of the model, this work also predicts the gigantic increase of thermopower that can be achieved by phase-transition in i-TE systems.

(3) The i-TE systems based on thermodiffusion effect normally work in capacitance mode. Therefore, the output current will experience a sudden decay when

connected to the external resistance. The enhancement by adding thermogalvanic effect into the i-TE system in the view of current will be studied in this work for the first time. In addition, the effect of unsymmetric electrodes is also investigated in this work.

1.6 Outlines of the thesis

This thesis will discuss the background information of thermoelectric effects and demonstrate the whole study about i-TE materials. This thesis will be stated in six chapters and the main contents are briefed as follows:

Chapter 1 is the introduction chapter. In this chapter, the basic information about TE effects and TE materials are discussed. Apart from the introduction, the limitations and problems about the previous works in this area will be stated and the objective, the value and novelty of this project are also discussed.

Chapter 2 is the literature review chapter. This chapter provides a comprehensive review of the previous works on thermoelectric materials and some applications based on wearable TEGs fabricated by TE materials. This chapter starts with the review about the fundamental thermoelectric effects and introduces different types of TE materials, including the electronic TE materials and ionic TE materials and gives a comment about the comparison of different materials. The fabrication, structural design and applications of wearable TEGs are also reviewed in this chapter, which can provide a guideline for future research on the design of wearable TEGs based on the i-TE materials studied in this work. This chapter

provides the fundamental knowledge about this area and gives a strong background foundation of the whole thesis.

Chapter 3 is the one of the three main parts of this whole project. In this chapter, the characterizations of phase-transitional i-TE materials are demonstrated in detail. First, a short introduction of this chapter is stated and the methods of the characterization and fabrication of the four different types of i-TE systems in this chapter have been listed, which are non-transitional, thermal induced liquid-to-gel, thermal induced gel-to-liquid and UV-induced liquid-to-gel i-TE materials, respectively. After that, the characterizations of the target TE materials are demonstrated in detail, including the output thermopower (or ionic Seebeck coefficient), σ, κ and the calculated ionic figure of merit ZT_i.

Chapter 4 is the theoretical analysis of the relationships between the output thermopower of the i-TE systems and the transportations of ions. Based on the Onsager's relations, this chapter illustrates an analysis model that can describe the transportations of ions at pre-, post- and during phase transition processes. In addition, this chapter also introduces an equation with six dimensionless parameters that can influence the output thermopower during the phase-transition. The analysis result from this equation also predicts a gigantic enhancement of thermopower that can be achieved by phase-transition and explained the experiment result in previous chapter. This model is also examined universal for i-TE systems with different phase-transition mechanisms (either UV-induced or thermal induced).

Chapter 5 starts with the limitations of the i-TE systems in previous chapter. The i-TE system based on only thermodiffusion effect normally works in capacitance mode.

Therefore, the output current will experience a sudden decrease when connected to the external load and thus the continuity of output power is a problem. This chapter try to find out the solution by introducing the redox couple into the system and using asymmetry electrodes to maintain a constant output current. This chapter will focus on the current aspect, where previous works always ignored, and provide a possible solution to enhance the output current of the thermodiffusive i-TE systems.

Chapter 6 is the last chapter of this thesis. It gives a summary and conclusion of the present works, provides the limitations of the work at this stage and some recommendations for studies for next step. After the end of all chapter of the thesis, the appendix parts will list some supporting information for the whole thesis which may not be suitable to directly put into the main text.

CHAPTER 2 Literature review

2.1 Introduction of Thermoelectric Effect

With the rapid development of Internet-of-things (IoTs), the need of power supply without cables or batteries has attracted intensive research interests.[12,13] Harvesting energies from daily environment is one of the most promising solutions. In general, the power supply for wearable applications can be realized by either active or passive approaches.[14] Active approaches are normally based on wireless power transmittance and can maintain a long-term operation but limit the movements of the devices to a long distance from external power sources.[15] Passive approaches, on the other hand, can use the human body as power sources and harvest energy produced from daily activities like walking, running or simply heat dissipation.[16–18] Thermoelectric (TE) effect, which can directly harvest waste heat from human body and directly convert it into electricity, has received broad attention from both academia and industry.[19–21]

Thermoelectric generators (TEGs) are the most conventional and basic applications of TE materials, which can directly convert the heat into electricity or reversely. Most of the conventional TEGs are rigid and have been developed for applications such as power production, cooling and sensing for temperature.[22] In recent years, flexible TEGs, which are deformable, light-weighted, cost effective and environmental friendly, have been explored for wearable applications where high flexibility and deformation stability are greatly demanded.[1,23] A schematic structure of a common flexible TEG is shown in **Figure 2.1**. Current studies on wearable TEGs can be mainly categorized into two groups, namely

developing high-performance flexible TE materials and fabricating flexible TEGs by structural design.[3] High performances TE materials have already been explored for a long time but most of the research focused on rigid materials. Organic TE materials and ionic thermoelectric (i-TE) materials have attracted growing research interests thanks to the potential applications in flexible TE devices.[24,25] In the meantime, TEGs made from thin-film or fiber are reported for wearable applications attribute to the perfect ductile, curving and in-plane shear proeprties.[26]

Despite the aforementioned advantages, the applications of wearable TEGs also meet many challenges. The conversion efficiency for most TE materials, either in rigid form or flexible form, are relatively low at temperature range for wearable applications.[27] Moreover, fabrication and design issues contact resistance, thermal resistance and deformation of wearable TEG are not fully understood.[28,29] Furthermore, the tradeoff between performance and durability of the wearable TEGs also needs to be resolved.

This chapter critically summarized the state-of-the-art TEGs with respect to the growing demand of powering wireless wearable IoTs as well as the generation of renewable energy. This review covers the study of wearable TEGs in the choice of materials, design of structure, fabrications, and applications. Theoretical studies of the wearable TEGs will also be comprehensively reviewed, followed by a critical discussion on the opportunities and challenges of the TEGs for wearable applications.

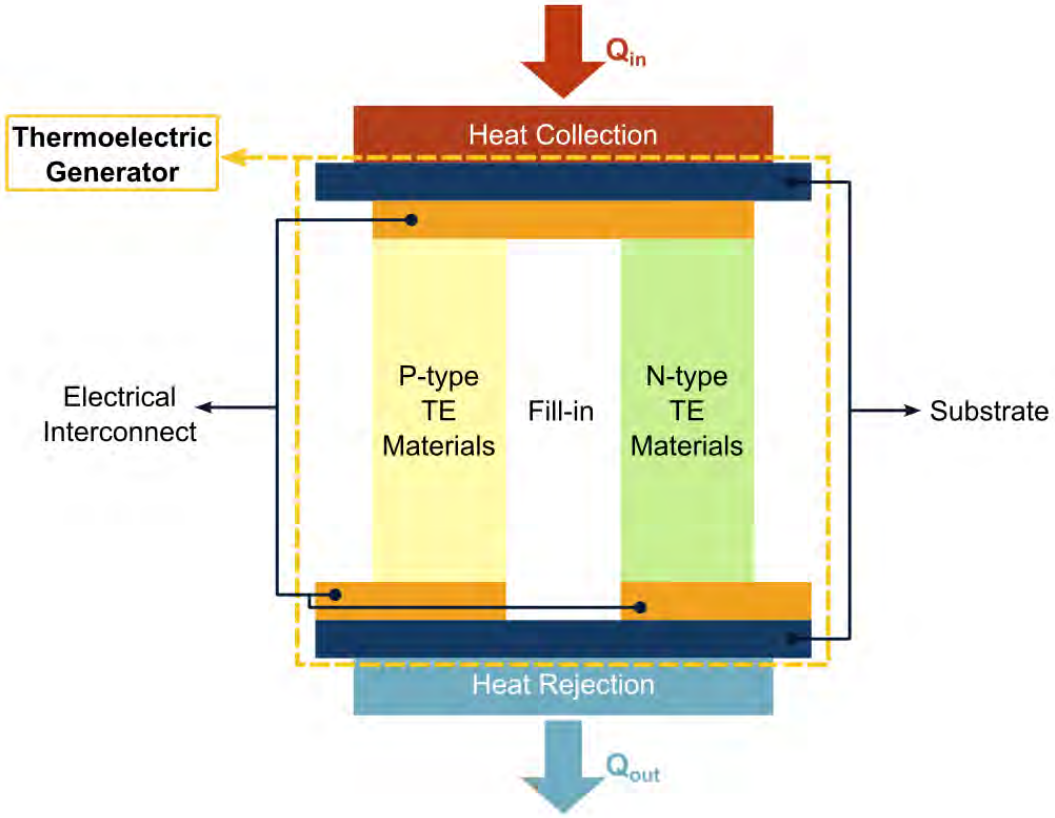

Figure 2.1 A schematic diagram of a common structure of a flexible TEG.

2.2 Thermoelectric materials

This section will mainly focus on the mechanisms of thermoelectric effect and common materials used in wearable TEGs including electronic TE materials, ionic TE materials, and polymer-based TE materials. Discussions about the requirements for other components of the wearable TEGs and summarize the choices of materials in wearable TEGs will also be introduced.

2.2.1 Thermoelectric fundamentals

Thermoelectric effects normally include three basic effects that describe the conversion between heat and electricity, namely, the Seebeck effect, the Peltier effect and the Thomson effect.[7,30] Seebeck effect describes the voltage difference generated between two different electrical conductors or semicondutors when a temperature gradient is present. In a typical Seebeck process, the electrons in the target materials transport under the temperature gradient and the resulted asymmetrical electron distribution generate an electromotive force. This is also the fundamental effect for TEGs.[31] The Seebeck effect can be described as:

$$S = \frac{\Delta V}{\Delta T} \tag{2.1}$$

where S is the Seebeck coefficient, ΔV and ΔT are the voltage and temperature differences between two different ends of the materials, respectively.[7] The whole process of the Seebeck effect is explained in **Figure 2.2a**. The Peltier effect can be regarded as the reversal process of the Seebeck effect, where a small heating or cooling effect can be generated when an electric current goes through a thermocouple (**Figure 2.2b**).[7] The Thomson effect refers to the effect that a changeable cooling or heating can take place in a homogenous conductor when electric current and temperature gradient coexist.[7] This phenomenon is shown in **Figure 2.2c**.

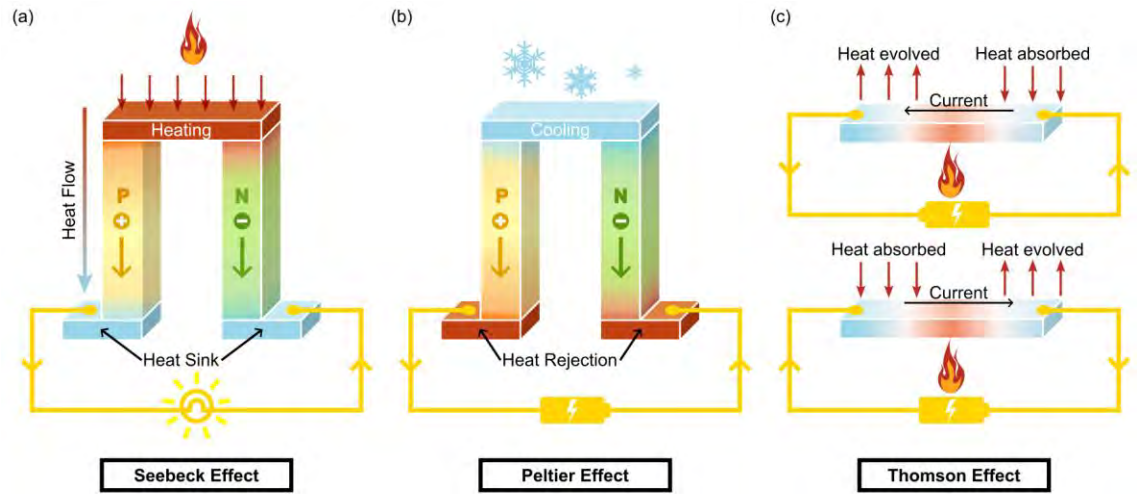

Figure 2.2 Schematic diagrams of thermoelectric effects: **a.** the Seebeck effect, **b.** the Peltier effect, and **c.** the Thomson effect.

In energy harvesting systems, the Seebeck effect dominates the energy conversion process. The dimensionless figure-of-merit ZT, which can describe the energy conversion efficiency, is defined as:

$$ZT = \frac{S^2 \sigma T}{\kappa} \tag{2.2}$$

where S is the Seebeck coefficient, σ is the electrical conductivity, T is the temperature and κ is the thermal conductivity.[32] From this definition, a general rule for choosing suitable TE materials with satisfying TE performances can be observed: the material should have high S, σ, but low κ. The strong interrelations between these parameters, however, limits achievable ZT values and make the choice of suitable high-ZT TE materials challenging.[33]

Start with the Seebeck coefficient, a Mott-Schottky analysis can be applied to express its temperature dependence, which is:

$$S = \frac{\pi^2 {\kappa_B}^2 T}{3q} \left[\frac{1}{\sigma(\varepsilon)} \frac{d\sigma}{d\varepsilon} \right]_{\varepsilon=\varepsilon_F} \tag{2.3}$$

where κ_B , T and q are Boltzmann constant, temperature and electrical charge, respectively.[34–36] In addition, $\sigma(\varepsilon)$ can be further expressed as:

$$\sigma(\varepsilon) = n(\varepsilon) e \mu(\varepsilon) \tag{2.4}$$

where n and μ are the carrier concentration and carrier mobility, respectively. The carrier concentration can be further expressed by:

$$n(\varepsilon) = D(\varepsilon) f(\varepsilon) \tag{2.5}$$

where D is the density of states and f is the Fermi-Dirac distribution. Combining (2.3) and (2.5), the Seebeck coefficient can be expressed by the following equation:

$$S = \frac{\pi^2 {\kappa_B}^2 T}{3q} \left[\frac{1}{n} \frac{dn(\varepsilon)}{d\varepsilon} + \frac{1}{\mu} \frac{d\mu(\varepsilon)}{d\varepsilon} \right]_{\varepsilon=\varepsilon_F} \tag{2.6}$$

From (2.6), it can be observed that the S and σ of a material cannot increase at the same time, which means a material with high S always has a σ and vice versa. Apart from Mott's formula, the Seebeck coefficient can also be expressed in other forms:

$$S = \frac{8\pi^2 {\kappa_B}^2 T m^*}{3q\, h^2} \left(\frac{\pi}{3n} \right)^{2/3} \tag{2.7}$$

where m^* and h are effective mass and Plank's constant, respectively.[37,38] This expression of S also shows the inter-relations between the S and σ. From the equations, it can be easily observed that a material has a high S should normally have a σ at the same time.

Furthermore, apart from the interrelations between S and σ, the strong interrelations between κ and σ cannot be ignored. The total thermal conductivity (κ_T) of a certain material normally consists of the contributions from electrons and lattice because the charge carriers in the materials, especially semiconductors, can bring both heat and electrical charge. The thermal conductivity from the contribution off electrons (κ_E) can be expressed as

$$\kappa_E = L\sigma T \tag{2.8}$$

where L is the Lorentz number. This equation is also well known as the Wiedemann-Franz law.[39] κ_T can then be further expressed as:

$$\kappa_T = \kappa_L + L\sigma T \tag{2.9}$$

where κ_L is the κ from contributions of lattice, respectively. It can be observed that a natural material normally has either high or low κ and σ at the same time. Therefore, one way to get a high ZT value with a high σ but low κ, is to reduce κ_L.[40] In all, the strong relationships between S, σ and κ is one of the key obstercles for improving ZT in bulk materials since the advances in 1950s.[5]

Similar to the electronic TE materials, the ionic thermoelectric (i-TE) systems can also generate an electrical potential across the temperature gradient. The S in i-TE systems

should be replaced by ionic Seebeck coefficient, or thermopower, which is calculated as $S_i = -\Delta V/\Delta T$.[41] Therefore, the ionic figure of merit (ZT_i) is identified as:

$$ZT_i = \frac{S_i \sigma_i T}{\kappa_i} \tag{2.10}$$

where S_i is ionic Seebeck coefficient (or thermopower), σ_i and κ_i are the electrical and thermal conductivity of the ionic system, respectively. The i-TE materials use ions as carriers for charge, which can break the interrelations between S, σ and κ and thus result in high TE performances.[42] Most of i-TE systems work in two very different mechanism, namely thermodiffusion effect and thermogalvanic effect. Thermodiffusion effect describe the migration of cations and anions under temperature differences, which can also be called as Soret effect,[43] whereas the thermogalvanic effect denotes the redox reactions of redox couples at two electrodes maintained at different temperatures.[44]

As an important group of i-TE materials, thermodiffusion cells are governed by Soret effect. The Soret effect describes the component flux as a result of thermal gradient:

$$\nabla c = -cS_T \nabla T \tag{2.11}$$

where the coefficient S_T is called Soret coefficient and sign should be determined by the properties of ions.[45] Most of the solutes are 'thermophobic', which means the ions will move from hot region towards cold region ($S_T > 0$).[41] In general, the Soret effect is a thermodynamic process explained by theories for irreversible process. Onsager's relations are well accepted to explain this effect.[46,47] According to Onsager's theory, the thermodiffusive i-TE system can be viewed as a system with heat flow and mass flow and

both of them can drive the other flow. The current flow J_i of the the certain ions (i) can be stated as:

$$J_i = -L_{ii}\frac{1}{T}\nabla\mu - L_{iq}\nabla\frac{1}{T} \tag{2.12}$$

where the first term represents the Fick diffusion (or can be called as mass diffusion) with coefficient L_{ii} and the later term represents the thermodiffusion according to the cross coefficient L_{iq}.[48,49] The coefficient L_{ii}, L_{iq} can be obtained from experiments and theories and the term represents the potential in this system should be modified by electrochemical potential.[50] After simplification, the thermopower of the i-TE materials can be stated as:

$$S_{td} = \frac{n_+ D_+ \hat{S}_+ - n_- D_- \hat{S}_-}{e(n_+ D_+ + n_- D_-)} \tag{2.13}$$

where D, e and n are mass diffusion coefficient, charge of electrons and ionic concentrations, respectively. $\hat{S}$ represents the transferred entropy from Eastman's illustration and the different signs represents ions with opposite charges. This equation is widely adopted in many recent works on the thermodiffusion effect in i-TE systems. [10,48,51] The diffusion that has been driven by temperature differences have a thermal mobility defined as $D\hat{S}/k_B T$.[10] The $\hat{S}$ is directly related to the transportation heat (Q^*), which is determined by the ionic size and ε of the solutes from the Born model.[43,52,53] Therefore, the choice of suitable ion species is closely related to the TE performances of thermodiffusive i-TE cells.

Another group of i-TE systems are on the basis of the thermogalvanic effects. The electronic power in these systems can be generated continuously since the redox reactants can be rebalanced by ion diffusion after redox reactions.[54] The thermopower in the

thermogalvanic systems should be expressed by another term called temperature coefficient (which can also be taken as S_i) as:

$$\alpha_R = \frac{S_R - S_O}{nF} \quad (2.14)$$

where S_O and S_R are the molar entropy of the redox species in the redox reaction $O + ne \leftrightharpoons R$. It can be observed from this equation that the α_R of the thermogalvanic system is closely related to S_O and S_R. Therefore, the choice of redox couples is quite important in thermogalvanic systems.

2.2.2 Electronic TE materials

The choice of thermoelectric materials for wearable TEGs is the first and the most important step. A good candidate should not only have good TE performances but also fulfill the requirements of flexibility. One of the most common choices of thermoelectric materials is semiconductor-based electronic thermoelectric material. Generally, either holes or electrons are the major carriers in p- and n-type semiconductors, respectively.[55] Tuning the amount of carriers in electronic thermoelectric materials is an significant step to generate high ZT values. The relations between the parameters S, σ, κ and the properties of carriers should also be examined.

Originally, researchers observed and made use of the electronic thermoelectric effect in thermocouples formed by different metals at their junctions.[32] Recently, more suitable candidates with satisfactory TE properties have been demonstrated. Many recent reviews have comprehensively summarized the developments of electronic TE materials in past

decades, for instance, metallic alloys, metal oxides, metal chalcogenides and some semiconductors, including Bi-Te alloys, Skutterudites compounds, Tetrahedrites compounds, Half-Heusler (HH) compounds and other oxides,[56–58]Some typical electronic thermal electric materials together with their reported ZT values are listed in **Table 2.1** and demonstrated in the figure that is combined. The details will be discussed below.

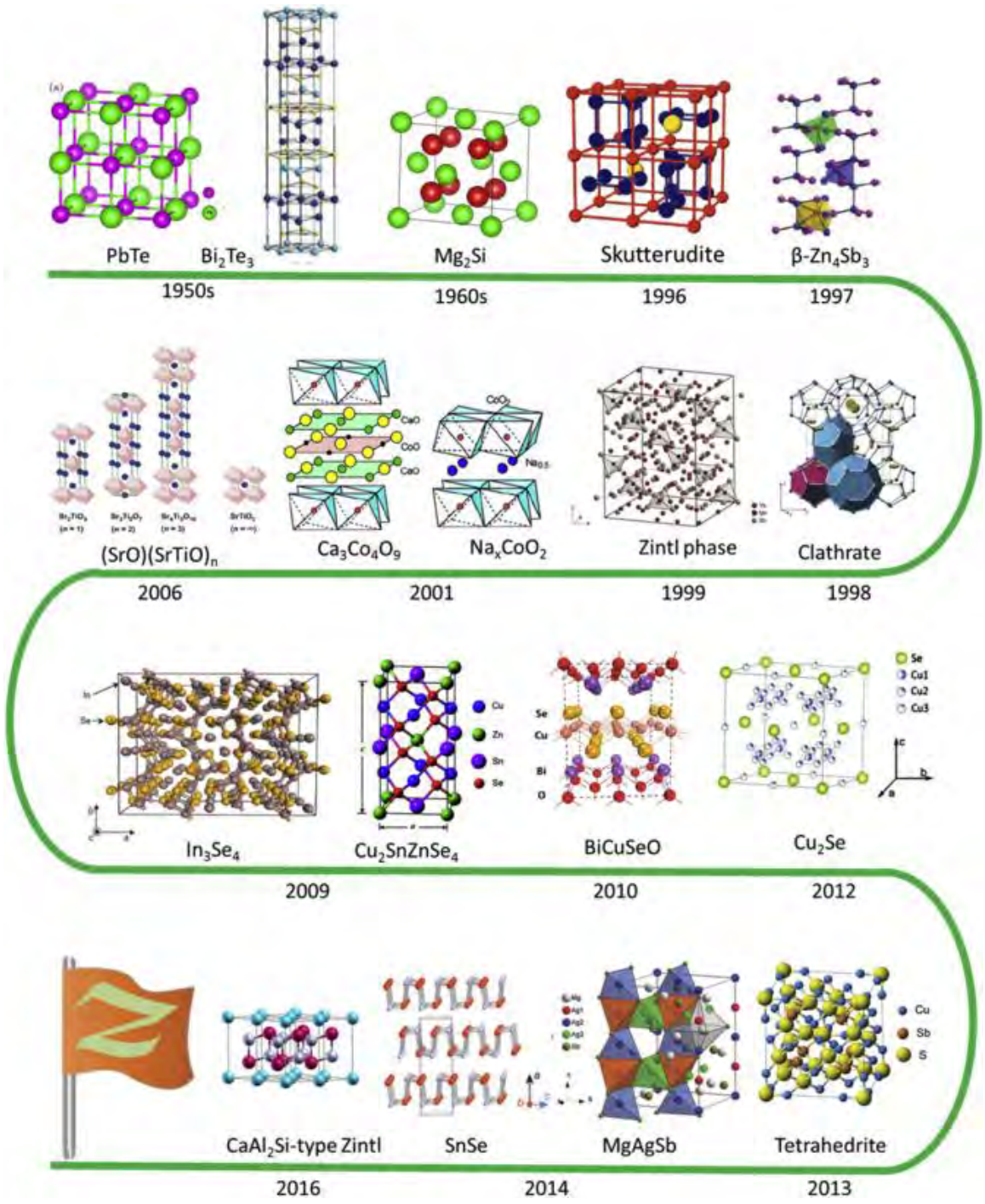

Timeline of selected TE materials.[59]

Table 2.1 Information of some popular electronic TE materials.

Category	Materials	ZT values	T(K)	Ref.
Oxides	Nb-doped $SrTiO_3$	~1.42	~1050	[60]
	$Li_{1-x}NbO_2$	0.125	970	[61]
	$Ba_{1/3}CoO_2$	~0.55	873	[62]
	$Bi_{0.94}Pb_{0.06}CuSe_{1.01}O_{0.99}$	1.6±0.2	873	[63]
	$Zn_4Sb_{2\cdot94}In_{0.06}$/1 wt% ZnO	1.16	700	[64]
Half-Heusler	$FeNb_{0.88}Hf_{0.12}Sb/FeNb_{0.86}Hf_{0.14}Sb$	~1.5	1200	[65]
	$Zr_{0.5}Hf_{0.5}NiSn_{0.985}Sb_{0.015}$ (p-type)	0.92	1000	[66]
	$Zr_{0.5}Hf_{0.5}CoSb_{0.8}Sn_{0.2}$	1.07	850	[65]
Skutterudites	$(Sm,Mm)_{0.15}Co_4Sb_{12}$	2.1	850	[67]
	$Yb_{0.3}Ca_{0.1}Al_xGa_{0.1}In_{0.1}Co_{3.75}Fe_{0.25}Sb_{12}$	1.7	823	[68]
	$Yb_{0.3}Co_4Sb_{12}$/0.1Si	1.37	823	[69]
	$Co_4Sb_{11}Te_{0.7}Sn_{0.3}$	1.13	711	[70]
Tetrahedrites	Cu_3SbS_3-Fe doped	0.62	848	[71]
	$Cu_{12}Sb_4S_{13}$-0.7vol% BiI_3	1.15	723	[72]
	$Cu_{11}ZnSb_4S_{13}$	1	720	[73]

	Cu_3SbS_3	0.57	623	[71]
	$Cu_{11}MnSb_4S_{13}$	1.13	575	[74]
Chalcogenide	$Cu_{1.94}S_{0.5}Se_{0.5}$	2.3	1000	[75]
	$Cu_2S_{0.08}Se_{0.92}$	2.0	1000	[76]
	$Cu_{1.97}S$	1.7	1000	[77]
	$Cu_{1.97}S$ (with melt-solidification)	1.9	973	[78]
	$Cu_2S_{0.2}Se_{0.8}$	1.65	950	[79]
	SnSe	2.6±0.3	923	[80]
	MoS_2 (oxygen-doped)	0.16	750	[81]
	*WSe_2 (monolayer)	1.4	~300	[82]
		2.14	500	
	*SnSe (single layered)	2.06	300	[83]
Tellurides (Bi-Te, Pb-Te)	PbTe (PbI_2 doped)	0.9	600	[84]
	Bi_2Te_3 bulk	0.96	380	[85]
	*Bi_2Te_3 nanostructure	~1.16	323	[86]
	*p-type Bi_2Te_3/Sb_2Te_3	~2.40	300	[87]

	*n-type $Bi_2Te_3/Bi_2Te_{2.83}Se_{0.17}$	~1.46	300	[87]
	*Bi_2Te_3 thin film on glass	0.7	300	[88]

* Selected works with good TE performances at low temperature range, which might be suitable for wearable applications.

Metal oxides are also a large group of TE materials. The research on oxides can be traced back to Japanese researchers and now a great demands of materials have been studied.[89–92] Even though the crystal structure of the oxides are different with each other, most of the oxides can be chosen as great TE materials due to the high stability at high temperature and low cost.[93] These advantages, together with their high ZT values at high temperature, make them suitable choices for harvesting industrial waste heat with rather high temperature.[63,64]

Similarly, half-Heusler compounds have also attracted many research interests over last few decades due to the high stability in high temperature, high bending strength and satisfactory ZT.[94] These compounds with formula ABX have cubic crystal structures (MgAgAs type), forming three interpenetrating FCC sublattices and one vacant sublattices.[94] By using nanocomposite approaches, the ZT of this group of compounds can exceed 1.[65]

Tetrahedrites and skutterudites are typical minerals applied in thermoelectric. Skutterudites has cubic unit cell with 32 atoms and its crystal structure implies the high σ and low κ, which are quite important factors for thermoelectric materials.[95] Similar to skutterudites,

tetrahedrites also have large unit cells. By cold pressing and high-pressure torsion on commercial skutterudites powders, a record-high maximum ZT of around 2.1 can be achieved in bulk $(Sm,Mm)_{0.15}Co_4Sb_{12}$ at 850K.[67]

Metal chalcogenides, such as $Cu_2Te/Cu_2Se/Cu_2S$, $Ag_2Se/Ag_2S/Ag_2Te$, are mixed ionic-electronic conductors.[96–100] In these materials, the mobile ions can induce static and dynamic disorders, which can cause a strong disruption of phonon and perform a 'phonon-liquid' behavior.[101] At the same time, the rigid sublattice provides conductive paths for either electrons or holes, which performs an electron-crystal behavior. Therefore, through the balancing from mobile ions, conduction electrons, and lattice phonons, the TE performances of these group of materials can be enhanced.[99] Even though these Cu_2Se-like chalcogenides still has rather high ZT values (more than 1.5) at around 1000K and seems to have more suitable applications in high temperature range,[76–79] a recent outstanding work discovered a colossal Seebeck effect in metallic Cu_2Se at room temperature range with a huge ZT exceeding 400.[102] The abnormal thermoelectric properties were explained to arise from the phase-transition of Cu_2Se from oriented and non-cubic-shape α-Cu_2Se to the random and cubic β-Cu_2Se.[103] Nevertheless, the stability of these superior TE performances in wearable TEGs made by these materials still needs to be examined. Apart from these Cu_2Se-like materials, other metal chalcogenides such as WSe_2 and SnSe also possess good TE performances at room temperature range, which make them potential candidates for wearable TEGs.[82,83]

Tellurides are another good example of traditional thermoelectric materials. Among them, Pb-Te based thermoelectric materials have been applied in many aerospace areas, such as the NASA space missions in 1960s.[104] In recent decades, the research on Pb-Te-based

thermoelectrics never stops and the ZT value boosted from 1.0 to 2.5 for p-type and 1.8 to 2.2 for n-type.[105] Most of the Pb-Te-based thermoelectrics, however, achieve their highest ZT values at high temperature range (normally >600K), limiting the applications for energy harvesting from low-temperature senarios. Tetrahedrites, skutterudites, half-Heusler compounds, and Pb-Te based Tellurides works best at high temperature,[60,61] making them good candidates in harvesting industrial waste heat but less ideal in wearable devices at room temperature range. [67–74]

Bi_2Te_3-based Tellurides thermoelectrics, on the other hand, have demonstrated their outstanding thermoelectric performances at temperature around 300K (room T). The reported ZT of Bi_2Te_3 bulk or thin films reached 0.96 and 0.7 at around 300K.[85,88] Furthermore, with nanostructuring, ZT value of Bi_2Te_3 has achieved 1.16 at 323K. ZT of nanostructured p- or n-type Bi_2Te_3 based alloys further reached 2.4 and 1.4 at 300K for [87] The increased ZT values of these tellurides mainly rely on the reduction of κ_L, which are realized by dense point-defect scattering, dislocation arrays or grain boundaries.[106] The modification of lattice thermal conductivity, however, will inevitably affect the electrical conductivity, which thus limits the increase of ZT values. Therefore, theoretical exploration about the dynamics from molecules of electron and phonon transportations in Bi_2Te_3 alloys can guide materials development in obtaining high ZT values.[107]

Even though the highest stable ZT of electronic TE materials can exceed 2.5, their working temperature range do necessarily match the working condition of wearable applications.[108] To fulfill the requirements of harvesting waste heat from human body, the working temperature of the TEGs should be targeted towards 310K. Considering such constraint, potential candidate electronic TE materials are Bi-Te compounds and metal chalcogenides.

Considering that these candidates are bulky and brittle, the fabrication techniques need to be carefully designed to make them suitable for wearable TEGs with high flexibility.

Apart from traditional inorganic materials, organic materials, especially polymer-based materials have attracted research interests on their TE performances. Comparing with bulk inorganic materials, polymers normally have high mechanical strength and flexibility, which make them a good candidate for applications under high mechanism deformation conditions. Different from the inorganic materials, the parameters which may affect the ZT values can be largely influenced by the orientation of the materials. As an example, κ, especially the κ_L, can be anisotropic for polymers. The huge differences between κ_L at different orientations of polymers, which may allow the material to scatter the phonons while not to affect the motions of electrons at the same time, thus decompose the relations between electrical conductivity and thermal conductivity. There are many conducting polymers have been tested as potential materials for TE applications, such as polyacetylene (PA), polypyrrole (PPY), polyaniline (PANI) and Poly(3,4 - ethylenedioxythiophene) (PEDOT).

PA can be regarded as one of the first conducting polymers chosen as candidates for TE applications. Highest result was achieved from stretch-aligned PA films doped with $FeCl_3$, showing a significantly large σ_{max} of 30,000 S/cm at temperature of 220 K.[109] The polymer has been further investigated by introducing different types of dopants into it and the most satisfied result was found for 28% iodine-doped PA, in which the σ can achieve 10,000 S/cm at around 300K.[110] At the same time, the Seebck coefficient of the polymer has been investigated and observed for a high value when doping levels were quite low(~0.8 %),

with S around 120 μV/K. Studies on the κ of PA films were also performed, showing a rather small thermal conductivity (κ =0.21 W/mK).[111]

Apart from PA, the TE performance of PPY has also been investigated. Different from PA films, the reported electrical conductivity was quite low (8 to 26 S/cm) in electrochemically grown PPY films doped by silver p-Tos at different grades of doping.[112] For lightly doped films, the Seebeck coefficient could achieve 5 μV/K at 200 K and reach a largest number of about 7.2 μV/K at 300 K. Apart from this work, similar treating methods for other polymers are lately proved to be extremely effective for enhancements of the TE properties and the ZT of materials.

PANI has also attracted many research attentions due to its high σ. In 1997, the PANI films prepared with camphorsulfonic acid were investigated and the TE performances at different doping level were also illustrated. A maximum electrical conductivity of 583 S/cm at 215K can be achieved for 60% doping level, which is still quite low compared with PA films.[113] Apart from the σ, the κ of the target material was also measured and showed a relatively low value of 0.20 W/mK, together with an estimate ZT value of 0.001.[114]

Beside these, the research on the TE performances of PEDOT and its derivatives is also currently underway, which has already been commercialized in several current applications, including the applications in vivid films, prepared as electrodes in capacitors and as hole-injection layers in OLED devices.[115] PEDOT, mixed with Tos, PSS or fine-tuning by dedoping, has also been confirmed to possess the most satisfied TE performance recently as organic compounds.[116]

A great deal of studies have proved that the σ and κ of PEDOT:PSS or PEDOT:Tos films can be tuned. With different treatments, the TE properties of PEDOT:PSS films can be easily modified (**Figure 2.3**).[117]

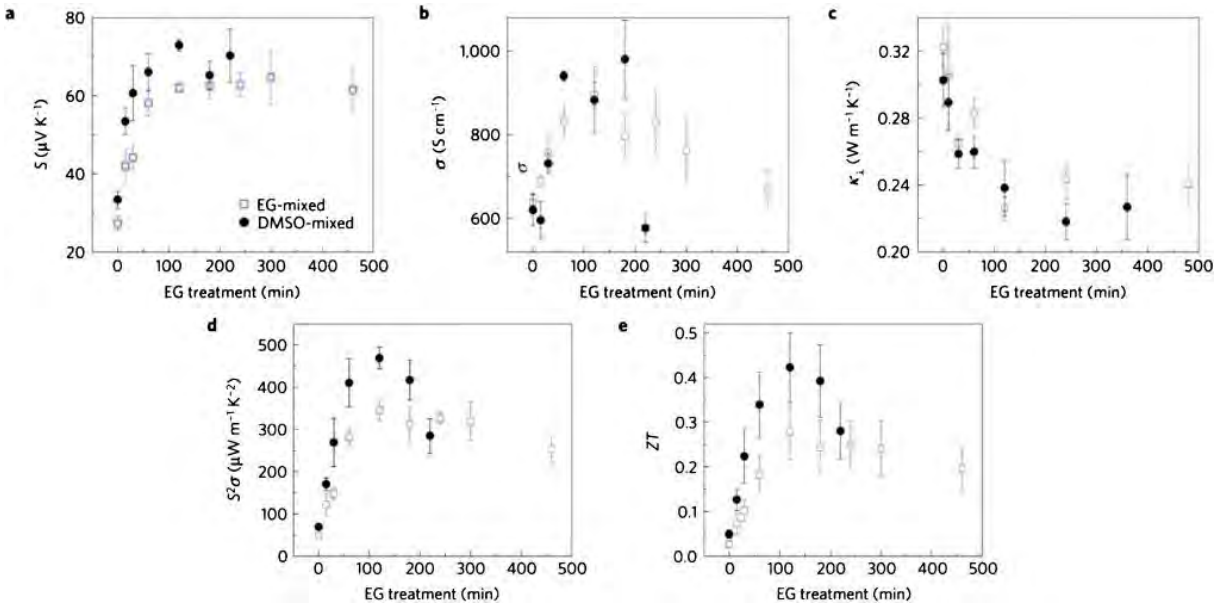

Figure 2.3 Thermoelectric properties of PEDOT: PSS at various dedoping times. The figures **a** to **e** represents the different parameters of the thin film with different lengths of dedoping treatments.[117]

In that work, an impressive ZT of 0.42 at around 300K can be observed, together with rather high σ (around 1000 S/cm) and relatively low κ (0.20 W/mK). Even the S is not quite high, the TE performance of this material is quite satisfied. In summary, it can be observed that compared with inorganic materials, organic compounds, especially polymers, normally have smaller ZT values. However, due to the good flexibility and high mechanical strength of the polymers, the TE performances of polymers are still deserved to be explored.

2.2.3 Ionic TE materials

Both thermodiffusion and thermogalvanic effects can be utilized to build TE devices for energy harvesting but their working mode are quite different. The thermodiffusion cells operate in a capacitive mode while the thermogalvanic cells can generate the electricity continuously.[54,118] However, regardless of the working mechanism, the output current will gradually decay after the i-TE system is connected to the external load.[8,118] **Figure 2.4** shows a comparison between thermoelectric effect in electronic TE materials and i-TE materials (typically thermodiffusion cells). Therefore, for materials that have exactly the same ZT, the maximum ability for conversion should be different. The efficiency of electronic TEGs will be higher than that of i-TE materials.[119] As such, the thermopower and normalized output power are more suitable than ZT_i to describe the TE performances of i-TE materials.[20]

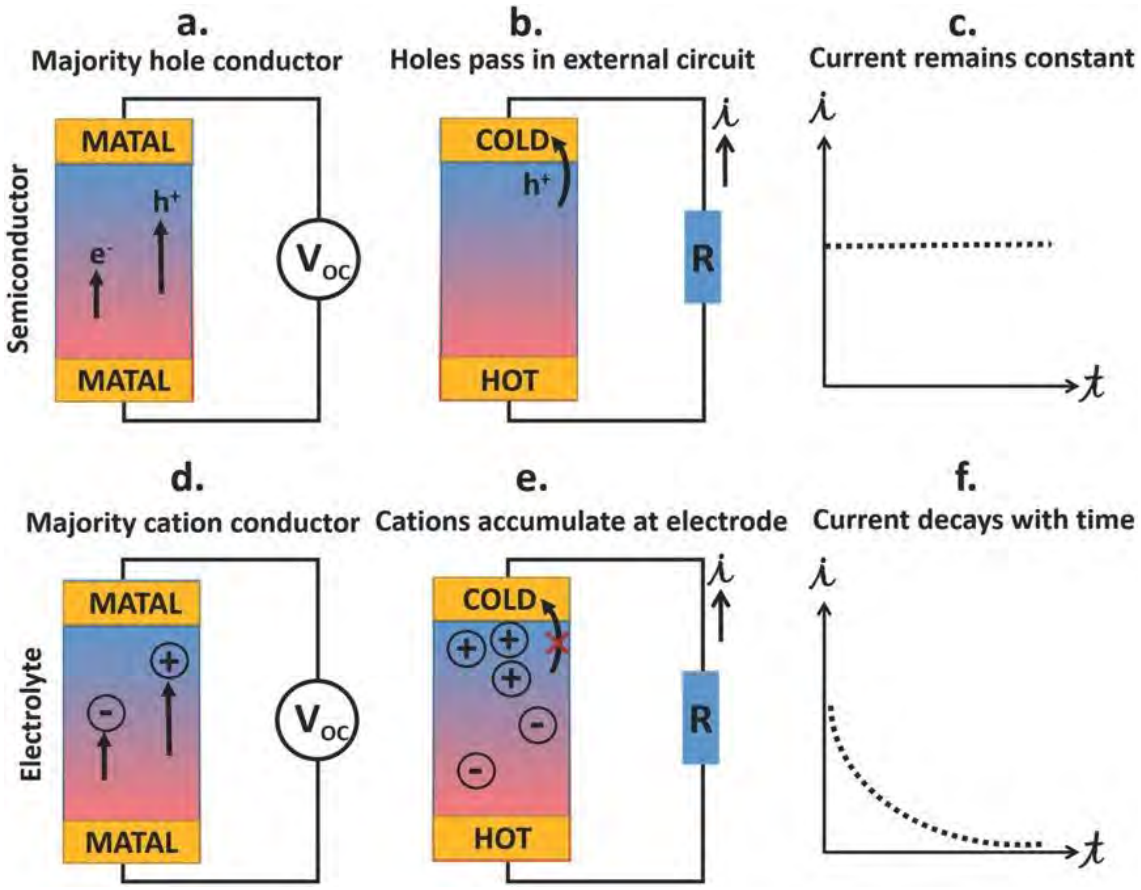

Figure 2.4 TE effect in electronic TE and i-TE materials. (**a**) and (**b**) demonstrate the transport of holes in electronic TE materials displaying majority hole conduction. (**c**) Continuously output current and power in electronic TE materials as TEGs. (**d**) and (**e**) demonstrate the transport of ions in i-TE materials and indicate the ions cannot pass through the interface between electrode and electrolyte. (**f**) Output current decays with time. Modified from ref. [119]

As mentioned above, ions cannot go through the boundary between the electrolytes and electrodes, meaning that the ionic TEGs based on thermodiffusion effect can only work in capacitance mode. Normally, this type of ionic TEGs needs a charge-discharge process to

harvest the energy and power an external load. The basic operations are schematically stated in **Figure 2.5**:

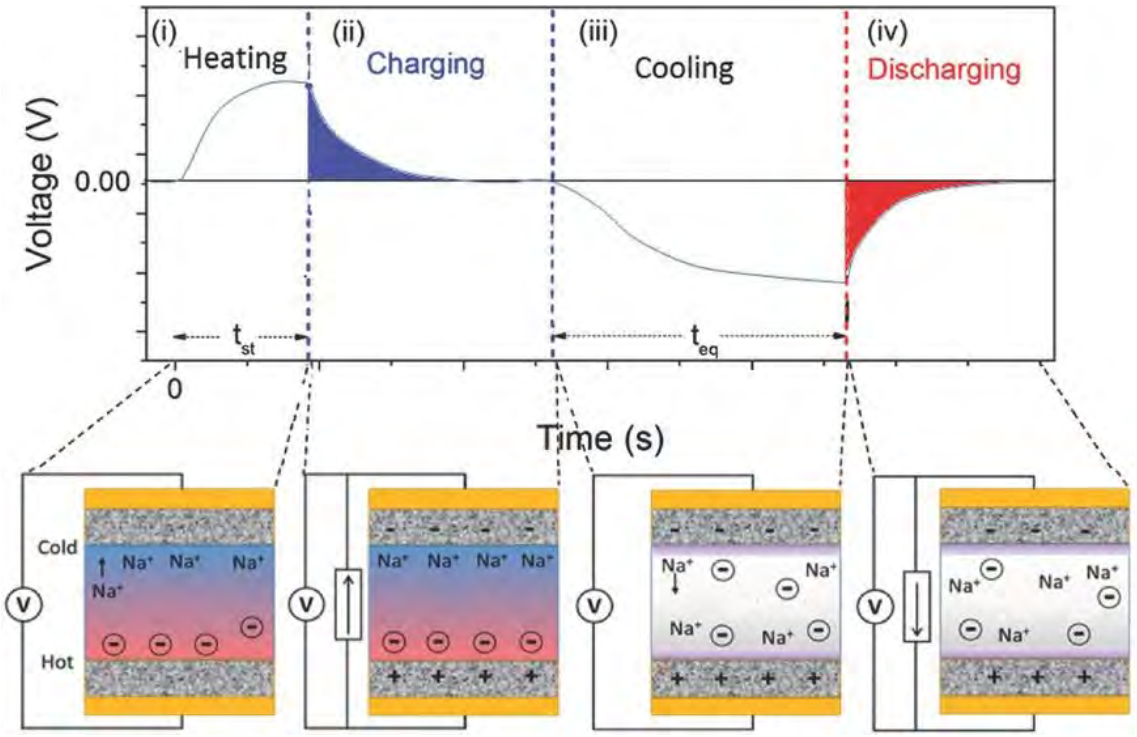

Figure 2.5 Operation principle of i-TE thermodiffusion cells. Open circuit voltage and mechanism sketch of a full charge and discharge cycle of the i-TE material working in capacitance mode. The details are shown in text. Modified from ref. [119]

From Eq. 2.13, the expected thermopower of i-TE materials with certain ionic composition can be calculated using the entropy of transfer defined by Eastman and diffusion coefficient and the expected thermopower of NaCl and HCl should be 51 μV/K and 221 μV/K, respectively.[120] These values are quite close to the Seebeck coefficient or conventional electronic TE materials. By changing the compositions of ions and electrolytes, the thermopower can be boosted significantly. A large thermopower of the electrolyte which

composed of Tetrabutylammonium nitrate (TBAN) in dodecanol can reach 7 mV/K as reported in 2011.[121] In addition, a remarkable output S_i of 10 mV/K can be achieved in a polymetric electrolyte which consist of polyethylene oxide (PEO) and NaOH.[9] Zhao et al also presented a completed working cycle of the ionic thermodiffusive cell in capacitance mode and demonstrated the potential applications by harvesting and storing the heat from sun light.[9]

Apart from the liquid-state i-TE materials, the TE performances of non-liquid-state (or gel-state) ionic polymer gels were also reported and the S_i of the gels with ions can be modified at the range of -4 ~ 14 mV/K by changing the compositions.[122] Further research on ionic liquid polymer gels achieved high S_i of 26.1 mV/K.[123] Recently, by using the doping techniques, a highest S_i of 43.8 mV/K was reported.[11] In summary, the S_i of the thermodiffusive i-TE materials can be rather high (several orders larger) when comparing with that of conventional electronic TE materials.

Another group of i-TE materials are designed on the basis of the thermogalvanic effect, which utilize the temperature dependence of different electrochemical redox potentials to produce continuous electrical power.[54] Recently, redox couples such as Co^{2+}/Co^{3+} couple[124], Fe^{2+}/Fe^{3+} couple[125], I_3^-/I^- couple[126] and $[Fe(CN)_6^{4-}/ Fe(CN)_6^{3-}]$ couple[8,127,128] were reported with an absolute thermopower of a few millivolts per Kelvin. Although the output thermopower of the thermodiffusive i-TE materials is lower than those based on thermodiffusion effect, the continuous current output from these thermogalvanic cells enables potential applications. By introducing a crystallization and dissolution process which are sensitive to temperature into the $[Fe(CN)_6^{4-}/ Fe(CN)_6^{3-}]$ thermogalvanic system, a rather satisfactory converting efficiency of 11.1% for liquid-state thermocell near room

temperature was achieved.[8] In the same work, Yu et al built a device based on the thermocell modules and used it to successfully powered the electric fan, LED array and even charged the mobile phone,[8] which indicated the possibility for using i-TE materials based on thermogalvanic effect to build wearable TEGs.

Apart from the i-TE materials using only on effect (either thermogalvanic or thermodiffusion), efforts have also been devoted to combine these two effects together to build an i-TE material using synergy effect. With this combination, gigantic S_i of 17.0 mV/K in a flexible gel-state electrolyte built by gelatin matrix together with ion providers and [$Fe(CN)_6^{4-}$/ $Fe(CN)_6^{3-}$] redox couples was achieved and a continuously output current was also maintained.[10] This proved the possibility of the synergetic effect between the mentioned two different effects in i-TE systems and provided another route to choose i-TE materials.

In summary, most of the i-TE systems are either in liquid or gel form, which fits the basic requirements of flexibility for wearable TEGs.[10,129] However, the high and stable output of the ionic system is still an important issue. Normally, the thermodiffusive cells based on can generate high voltage output but lacks continuous current output due to its capacitive working mode. On the contrary, the redox systems can generate continuous current but the output voltage is low. The i-TE materials that are designed on the basis of the synergistic effect is proved to be possible but the application still needs to be explored.

2.2.4 Comparison and summary of TE materials

As introduced in the above texts, each group of TE materials has their advantages and disadvantages, which are summarized and compared as follow:

1) Electronic TE materials: Most of the electronic TE materials (inorganic) are rigid, which limit their direct applications in wearable TEGs. In addition, when choosing electronic TE materials for wearable applications, the working temperature should also be considered. Therefore, electronic TE materials have satisfied TE performances at room temperature and can be easily fabricated into thin films or flexible structures are good candidates. Under this scope, we believe metal chalcogenides, (such as WSe_2, SnSe), Bi_2Te_3-based composites and graphene-based composites can be good candidates for applications in wearable TEGs after appropriate treatment. Different from rigid semiconductors, most of the polymers have good flexibility and low thermal conductivity, which already fulfill the basic requirement of flexibility for wearable devices. However, most of the polymers suffer from low ZT values, which limit their ZT performances in wearable energy harvesting applications. Therefore, some techniques need to be applied, such as doping or nanostructure fabrication, when using polymers for design of wearable TEGs.

2) Ionic TE materials: Most of the i-TE materials are in either liquid-state or hydrogel-state, which fulfill the basic requirement of flexibility for wearable devices. However, the encapsulation of liquid-state i-TE materials and mechanical strength of gel-state i-TE materials are the key issues to be concerned. Meanwhile, the continuity of the power generation, especially a stable output current without any decay, should be taken into consideration. These two problems are the main problems to be considered when choosing i-TE materials for wearable applications.

In all, the choice of materials for design of wearable TEGs should be the first and very important step. Each type of TE materials has their advantages and disadvantages, which means no best TE materials but most suitable TE materials can be chose in different conditions. Sometimes two or more types of TE materials can be used together to fulfill the different requirements of the applications. Therefore, the research on discovery of TE materials with good TE performances at different conditions can be significantly important.

2.3 Enhancement of TE performances

As indicated from the previous part, restricted by the strong interactions between S, σ and κ, the increasing of TE performances, especially ZT, is quite difficult to be achieved. Researchers have put efforts to find out how to enhance the TE performance and they have generally established two main ways to enhance TE performance.[140,141] One is to optimize the power factor (PF) from electrical properties, including band convergence engineering,[130,131] resonant energy level,[142] carrier filtering effect etc.[132,133] The other method is to minimize the lattice thermal conductivity through nanostructuring engineering, defect engineering etc.[134,143,144]

2.3.1 Electrical properties

From the previous discussion, it can be observed that a strong relation existed between the σ and S. The Mott's expression of S shows that it has a negative relationship with carrier concentration while the σ has the positive one. Therefore, the key factor to improve the TE performances from electrical properties is strongly linked to the carrier concentration.

Researchers firstly tried doped semiconductors and found that as the concentration of doping increased, the σ increased while the S decreased. Therefore, a maximum of the PF can be found at different doping concentration and chemical potential, which is closely related to and even affected by the band structure of electrons.

To investigate the improvements of TE performances for TE materials, the electronic band structures of the materials need to be explored. By using the Boltzman's theory,[145] which describes the statistical behaviors of the thermodynamic system in non-equilibrium state, researchers can find out how the physical parameters can be affected, such as viscosity, κ and σ. The Bloch–Boltzmann expressions for electrical conductivity (in one dimension or x-axis) and Seebeck coefficient are given by[146]

$$\sigma_x = e^2 \int_0^\infty g(E) v_x^2(E) \tau(E,T) \left(-\frac{\partial f(E)}{\partial E}\right) dE$$

$$S = \frac{k_B}{e} \left[\frac{\int_0^\infty g(E) v_x^2(E) \frac{E-E_F}{k_B T} \tau(E,T) \left(-\frac{\partial f(E)}{\partial E}\right) dE}{\int_0^\infty g(E) v_x^2(E) \tau(E,T) \left(-\frac{\partial f(E)}{\partial E}\right) dE} \right] \quad (2.15)$$

The factor shows the truth that at a certain temperature with finite value, only the electrons have energy near the Fermi level could make contribution to the process of conduction. From the previous equations, it can be observed that the electrical conductivity depends on two energy dependent factors, which are the band structure (can determine the g(E) and v(E)) and the scattering time τ(E,T) (related to band structure), respectively.

Previous parts have introduced the Mott's formula, which indicates the inter-relations between Seebeck coefficient and electrical conductivity:

$$S = \frac{\pi^2 {\kappa_B}^2 T}{3q}\left[\frac{1}{n}\frac{dn(\varepsilon)}{d\varepsilon} + \frac{1}{\mu}\frac{d\mu(\varepsilon)}{d\varepsilon}\right]_{\varepsilon=\varepsilon F} \quad (2.16)$$

Therefore, the key point to discover the highest TE performance or the highest power factor is the band structure. Researchers have studied the optimal band gap, E_g, of TE semiconductors with indirect band gaps and found that the band gap that has the most satisfied performances should be from $6k_BT$ to $10k_BT$ (**Figure 2.6**).[147] It is concluded that large band gap (larger than $8k_BT$) could suppress the contributions of the carriers for minorities to the TE transport, thus improve the TE performances.

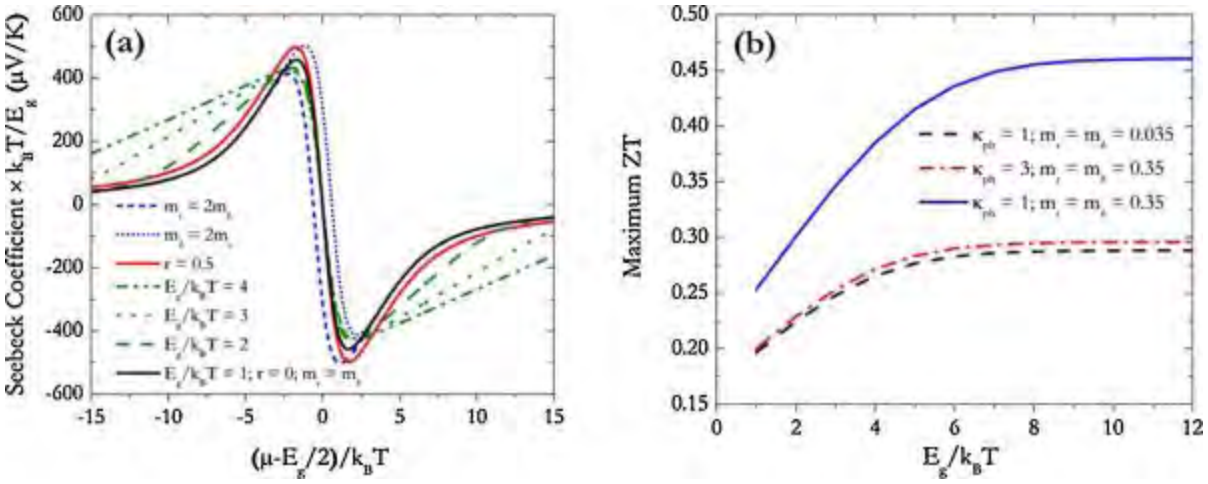

Figure 2.6 DFT calculations of two-band model. (a) Calculated S. (b) Calculated maximum value of ZT. High ZT values can be obtained with large band gap (larger than $6k_BT$).[147]

Apart from the feature of band structure, researchers have also put insights on another parameter or factor named density-of-states (DOS) effective mass, m*. Normally,

materials with large DOS effective mass have large Seebeck coefficient but have low carrier mobility, which will decrease the electrical conductivity. To suppress the inter-relations between the σ and S, researchers have tried many ways based on these theories. They showed that multi-valley semiconductors with low masses are good choices to increase the DOS m* by not hamper the carrier mobility.[141] As the scattering through valleys is decreased or even disappeared, the concept confirmed that the multi-valley semiconductors with small inertial masses could have higher ZT values comparing with their bulk conterparts.

Another idea is based on the change from isotropic band masses to anisotropic, which generate high average Fermi velocity because of the light mass directions. This idea also is based on band structures of multivalley. Although high mobility in the direction of current flow is required to enlarge the weighted mobility, high m* along the same crystal direction is not required. Therefore, a satisfied chance can be found to enhance highly anisotropic structures. This idea provides a new routine for the choice of TE materials, which is the choice of anisotropic materials. Recently, researchers have observed an unprecedented ZT values of 2.6 at 923K. This value is achieved when measuring SnSe single crystals along the b-axis (**Figure 2.7**).[108] At the same time, the ZT of the crystal measured along a axis and c axis are relatively low compared with the value measured from b axis. Even through this interesting result mainly depends on the ultra-low κ, the contribution of the electrical properties is still very important.

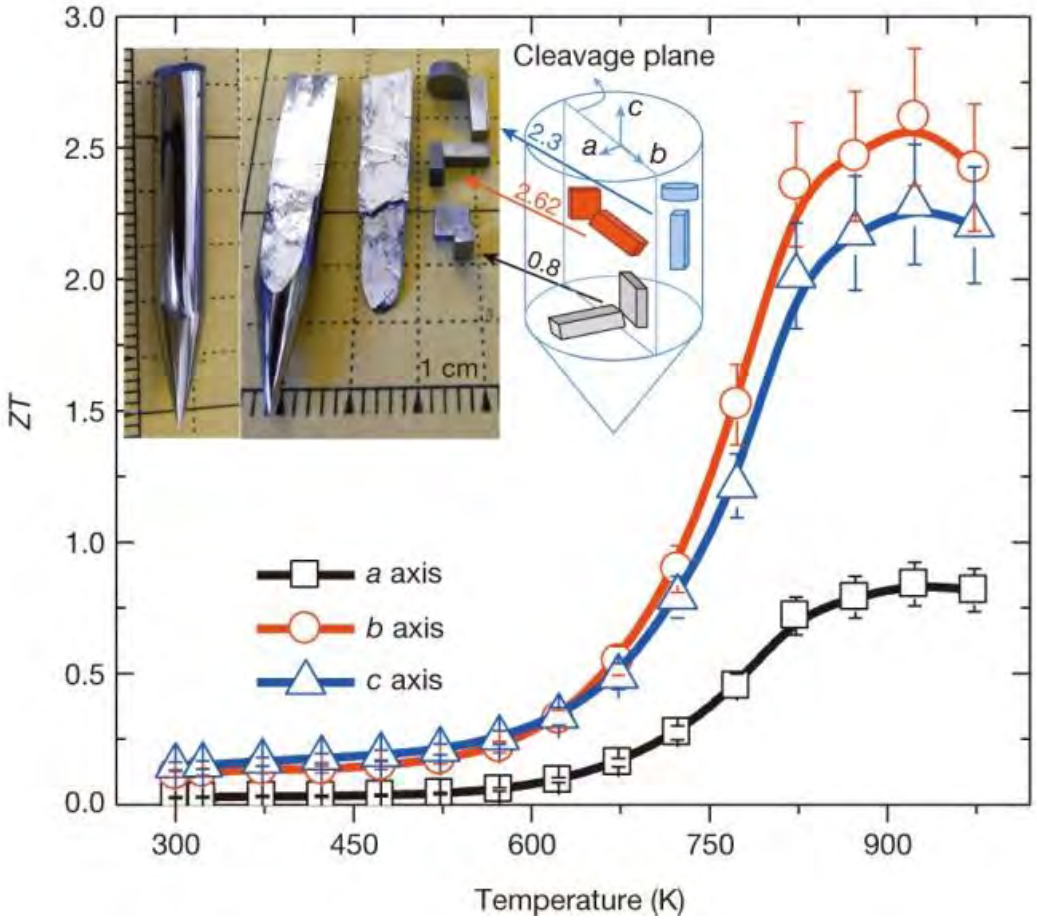

Figure 2.7 ZT values of anisotropic SnSe crystals along different axial directions.[108]

2.3.2 Thermal properties

Apart from electrical properties, thermal properties, especially the thermal conductivity, are also important factors which could affect the TE performances. To study the thermal conductivity of the crystal, the effect of phonons needs to be explored in detail. Heat-carrying phonons can go through a wide-ranging spectrum of frequencies (ω) and $\kappa_{lattice}$ can be expressed in another form, as the total contributions from different frequencies:

$$\kappa_{lattice} = \int \kappa_s(\omega) d\omega \tag{2.17}$$

The spectral κ_{lat} can be expressed as

$$\kappa_s(\omega) = C_p(\omega) \times v^2(\omega) \times \tau(\omega) \tag{2.18}$$

where Cp, v and τ are spectral heat capacity, velocity and scattering time of phonons, respectively. Phonons from materials with crystal structures are scattered by each other's, which normally exhibits a $\tau_U^{-1} \sim \omega^2$ dependence and combining this expression with the Debye approximation for phonons that carry heat, it can be found that $\kappa_s(\omega)$ should be a constant. Therefore, a broad scale of phonon frequencies will promote to the κ.[148]

Normally, there are several methods to reduce the κ of the TE materials. The most commonly used methods is based on nanoscale microstructures to induce edge scattering of phonons, which occurs at the interface of compounds or grain boundaries of the TE materials.[149,150] Other methods, such as point defects and grain boundaries are also effective methods to reduce the κ by affecting the phonon-scattering at high and low frequencies, respectively. However, to maintain a satisfied ZT, the carrier mobility of the target material cannot be reduced to much when introducing the scattering into the system. Thus, the reduction of the κ_{lat} from phonon-scattering should not reduce the carrier mobility by electron scattering to maintain a high ZT value.

Recently researchers have found an interesting fabrication method and successfully reduced the κ of the $Bi_{0.5}Sb_{1.5}Te_3$ crystal but maintained the electrical conductivity. Through this methods, the ZT value can be improved to 1.86 at temperature of 320K, which

can be regarded as the highest ZT matched with other TE materials at the same time (**Figure 2.8**).[151]

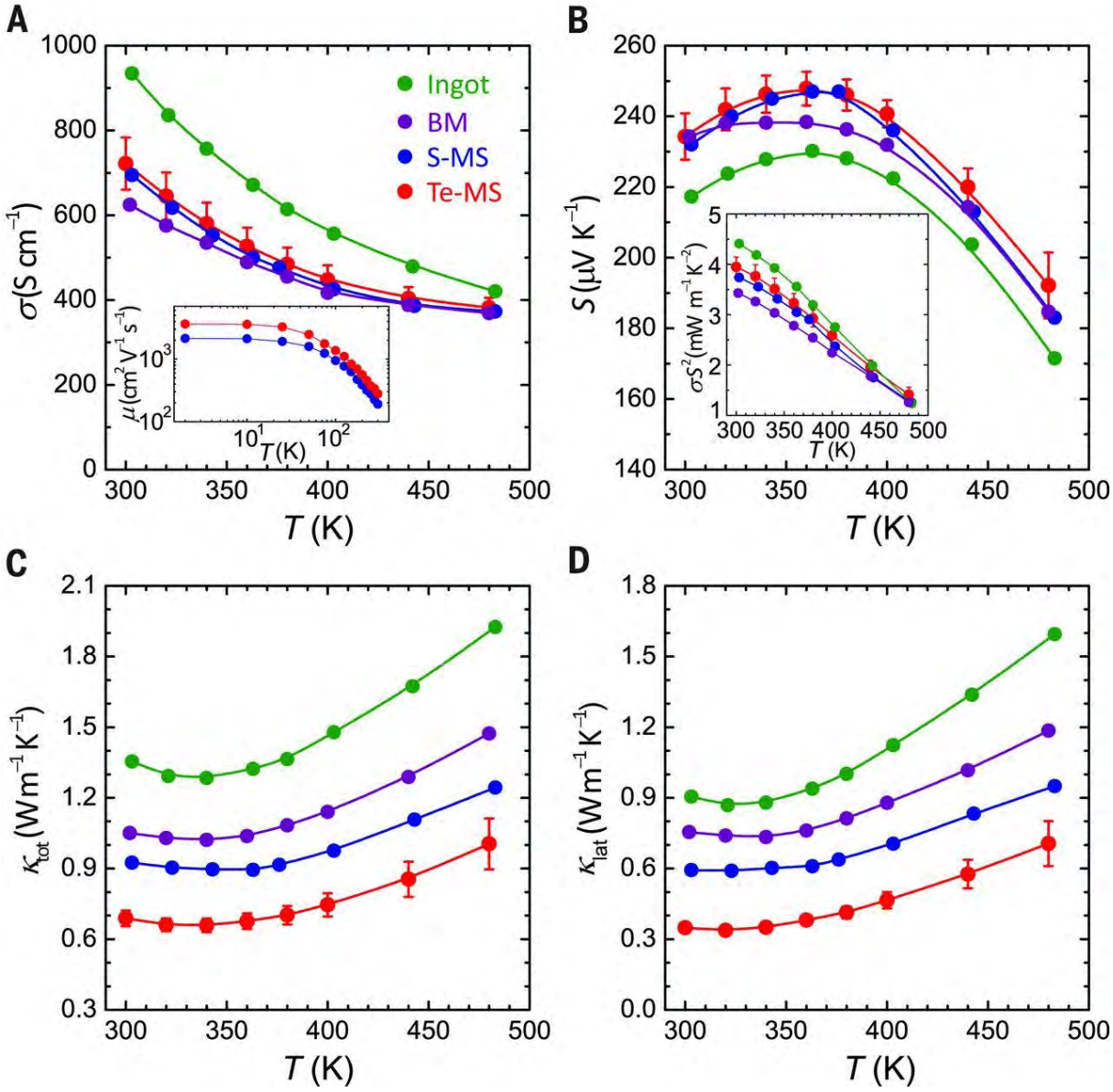

Figure 2.8 TE performances of a $Bi_{0.5}Sb_{1.5}Te_3$ crystal with different fabrications. Figure a to d represents the different parameters with respect to the temperature.[151]

2.4 Structure design and fabrication of flexible TEGs

In this part, the structures in flexible TEGs will be reviewed. During the design of the structure, the electric circuit, flexibility, contact resistance and mechanical reliability should be considered. This part will illustrate the structure design of wearable TEGs from the viewpoints of these aspects and point out the issues need to be considered during the structural design of wearable TEGs and introduce some fabrication techniques

2.4.1 Design of the electric circuit

As mentioned in the previous parts, majority of TE materials have the S at the magnitude of mV/K or even μV/K, which means the generation of a useful voltage at the range of 1~ 5 V at daily environments with only temperature difference of around 10-20 K requires the integration of a great number of small TE elements or voltage booster for DC to DC conversions.[152] No matter which method is applied, the first step of building a TEG is to connect single TE elements together. There are two ways to connect the TE elements together, namely N-shaped and π-shaped (**Figure 2.9**). The method of connection is determined by the type of TE elements used: if only one type (either p- or n-type) of TE material is applied, N-shaped connection should be applied; if both type (p- and n-type) are applied, π-shaped connection should be used. These connection methods ensure the TE cells are in series connections and generate the maximum output voltage. Both methods can be applied together and the output voltage of each element by the temperature gradient should be aligned.

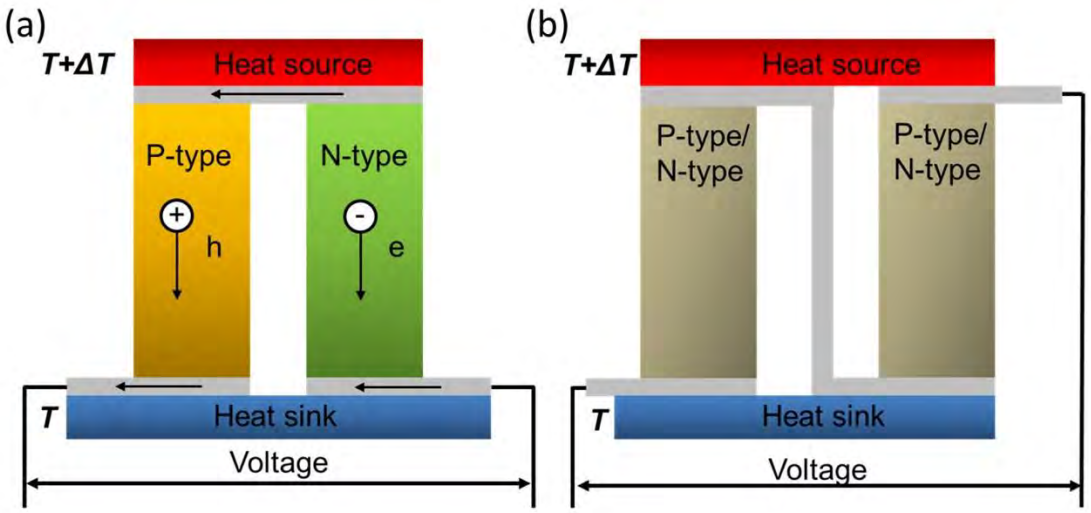

Figure 2.9 Electric circuit connections of TE cells. Schematics of **(a)** π-shape **(b)** N-shape connections.

On most occasions, designing flexible devices will allow only one flexible TE materials to be fabricated and N-shape connections are therefore applied. The N-shape connection is often found in film structures but rarely in sandwich designs because the electrodes in the film structures can be easily fabricated in the same plane. When it comes to material selection, flexible organic TE materials are typically preferred, while inorganic - organic composite materials are also favorable for the device assembly. Gao and co-workers reported an Ag/Ag_2Se composite based TE film fabricated on a porous nylon membrane.[153] In this process, the raw materials of Se nanowires reacted with $AgNO_3$ and was deposited on a leachy nylon film, followed by a hot pressed annealing process. The film was then divided into 8 legs with dimension of 6 mm×20 mm (**Figure 2.10a**). These legs were

adhered to the polyimide film connected with silver adhesive in sequence, finally forming the “N” structure flexible TE device. Lin et al also have fabricated a lateral “N” shape thermoelectric bracelet using the reduce graphene oxide (rGO)/ Polydimethylsiloxane (PDMS) 3D printed soft grids (**Figure 2.10b**).[154]

On the contrary, if both types of TE materials can be synthesized, the TEGs can use π-shape connections. This form of connection can be found in membrane and sandwich systems. Cho's group recently used screen printing to fabricate $Bi_{0.3}Sb_{1.7}Te_3$ (p) and $Bi_2Se_{0.3}Te_{2.7}$ (n) legs, prepared a TEG with lateral π-structure on a SiO_2/a-Si/quartz (**Figure 2.10c**). The device has been initially crammed with stiff quartz substrate, which was expertly removed in the special procedure by using laser to lift.[155] This standalone sandwich-like wearable TEG is flexible and lightweight. Similarly, Son et al recently applied an approach like printing to create flexible and shape-conformable TEGs.[156,157] The researchers introduced a novel kind of f-TE materials with satisfied performances in their study and performed multiple π-structural TEGs designs. Both types of materials (p and n) with editable shapes and geometric adaptability were newly investigated and could be coated on any uneven surface without any further treatments.

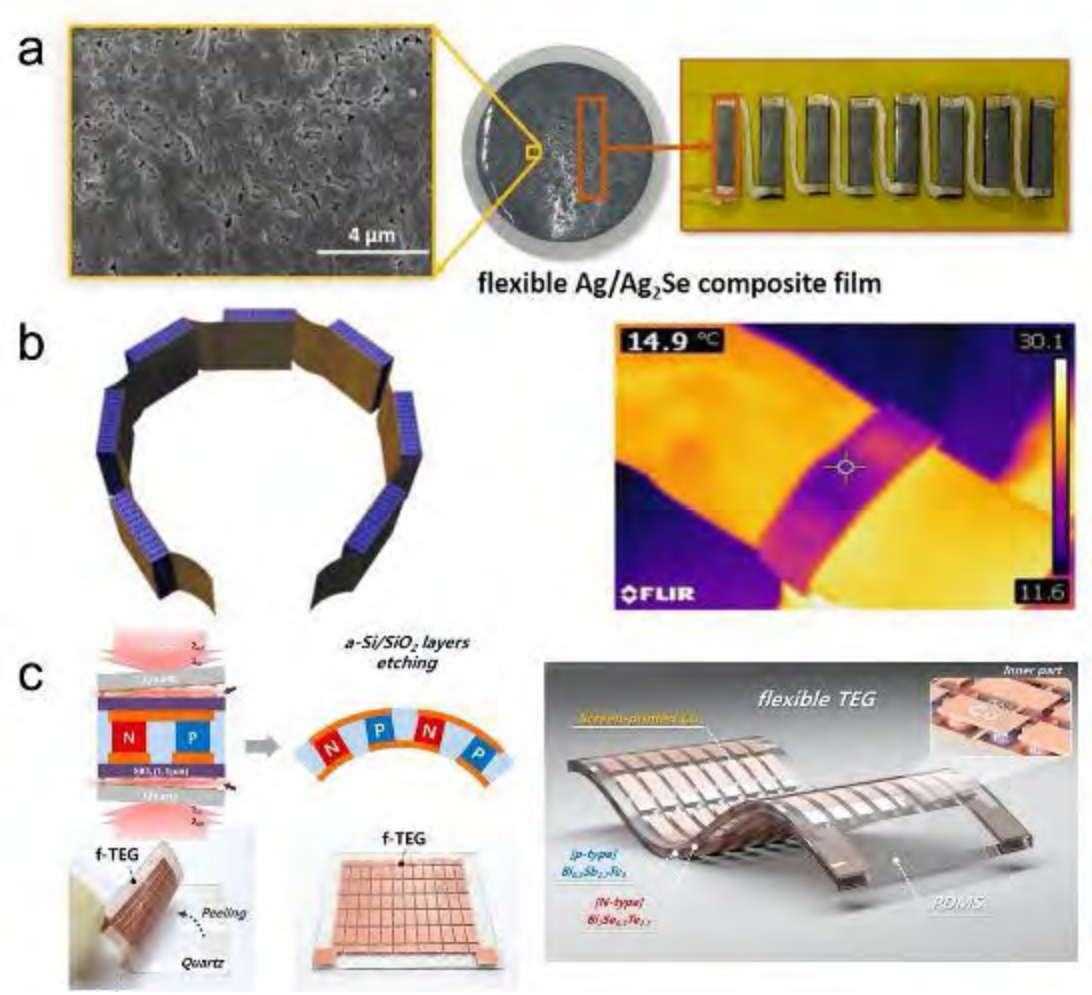

Figure 2.10 (**a**) Actual model of "N"- shape TEG.[153] (**b**) Images of the thermoelectric bracelet.[154] (**c**) Process flow and product of a "π" structure TEG.[155]

2.4.2 Fabrication of wearable TEGs

The basic function for wearable TEGs is to harvest heat from human body. However, since the human body is curved, the conventional TEGs with stiff structures may not be the best choice for wearable applications. Therefore, the study on fabrication techniques of flexible

TEGs is necessary for wearable applications. The manufacture methods can be categorized into two different groups: embedding and surface modification.

The embedding methods are used to fabricate flexible TEG with embedded structures. When TEGs are used in wearable systems, the flexibility should be guranteed to provide direct and close thermal contact between the human body and the TEG. In order to realize a TEG with flexible structure, possible solutions including using flexible TE materials (i.e. i-TE materials in liquid or gel form, polymer-based TE materials) and using innovative structures to bond the rigid electronic TE materials can be utilized.[169,170] The key points in fabrication of embedded flexible TEG structures should be the design of electric circuit and the choice of materials for fill-in and substrate.

Conventional electronic TE materials, especially the bulk rigid semiconductors, are commonly used in building TEGs. Conventional TEG consists of the electrodes, TE modules and rigid substrates, where the TE modules and electrodes are connected in either π-shape or N-shape. The embedded structure is quite similar with the structure of conventional TEGs. The difference is that the substrate of the embedded structure is a flexible substrate but not a rigid ceramic substrate. **Figure 2.11** shows a schematic diagram and an actual photo of the embedded structure of the flexible TEG.[170] The copper electrodes are exposed and can directly contact the human skin, which can absorb the heat from human body. In order to ensure the mechanical strength of the whole generator, the empty spaces in the modules should be filled with proper polymer materials with low thermal conductivity. The integration process started with the arrangement and bonding of the rigid TE materials onto the patterned copper thin film where the pattern provided the electric

connections. After preparation, the empty space was filled with polymer material with thermal conductivity of 0.03 W/(mK^2).[170]

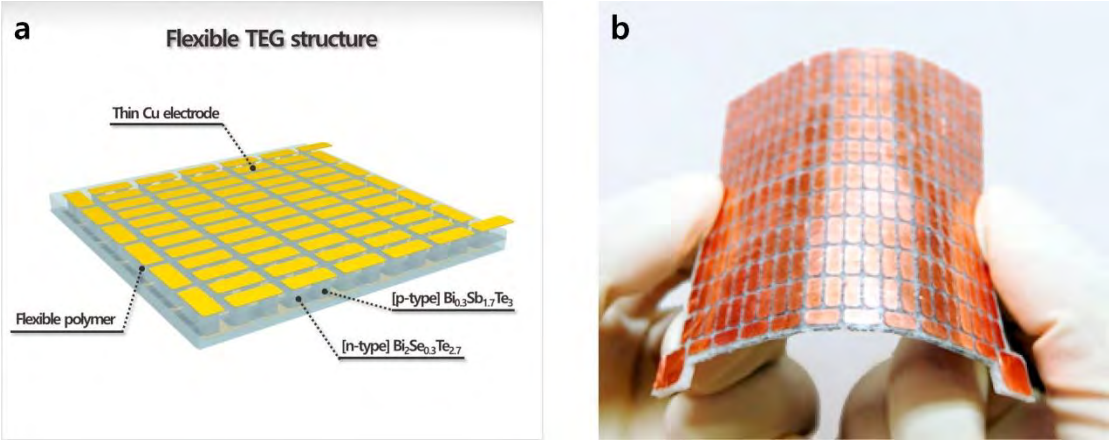

Figure 2.11 Schematic figure and photo of a flexible TEG structure. (**a**) Schematic figure of a flexible TEG structure. (**b**) Photo of an example of actual fabricated flexible TEG device. [170]

Since the embedded structure is quite similar with the structure of conventional rigid TEGs, the fabrication procedure is quite similar. However, the rigid TE modules in flexible TEGs based on embedded structure hinder the wearable applications due to the lack of flexibility. In order to solve this problem, the TE modules can be flexible from fabrication by 3D printing methods, which have already been reported in fabrications of TEGs based on TE materials (organic or inorganic).[171–175] The 3D printing technique involves the preparation of ink like TE materials and the fabrication of TE modules through printing process, which enable the fabricated TE modules with high flexibility and high controllability. These advantages strengthen the choice of 3D printing over other annealing technique in the fabrication of flexible TEGs with embedded structures. However, the key challenge of the

fabrication on embedded structures is the improvement of flexibility together with maintaining the TE performances, which limited the fabrications of TEGs by these methods.

Apart from the embedding structures, another category of flexible TEG structures is based on the flexible substrate with TE materials deposited on it. The fabrication techniques for these structures can be classified as surface alteration, which includes the accumulation of TE materials on flexible targets, such as fibers, yarns and fabrics. After the deposition, the flexible substrates with TE materials can be applied to manufacture the flexible TEG devices.

Techniques by surface alteration include drop casting/ink printing, dip coating, spin coating, sputtering, thermal vapor deposition, screen printing and others.[32] The basic objective for all these techniques is to deposit the TE materials onto the flexible substrates. Drop casting and ink printing are representatives of the widest used techniques due to the simple execution procedures with no requirements for high temperature or vacuum. In these methods, the TE materials were firstly prepared in the form of inkjet and then simply deposited or printed onto flexible substrates.[176] Many works have used these methods and a schematic diagram about the preparation of a flexible TEG using drop casting method is shown in **Figure 2.12a**.[177] Similar to drop casting, spin coating is also a well applied technique.[178] Spin coating starts with dropping solution containing TE materials onto a flat substrate and rotate the substrate to make sure the solution distributed uniformly. The schematic about the process of spin coating is shown in **Figure 2.12b**.[179] However, these methods mainly focus on flat substrate and may not be suitable for substrate such as fibers or fabrics. In order to coat on fibers, dip coating is good choice because the process is directly immersing the substrates into the particular solutions (**Figure 2.12c**).[180] Apart from

these operation methods with simple procedures, sputtering, especially radio-frequency (RF) magnetron sputtering, is also applied in fabrication of flexible TEGs. The process includes spattering elements of the TE compounds precisely onto the substrate as shown in **Figure 2.12d**.[181] However, the low pressure requirements for this technique limited its usage for production.[32] Apart from sputtering, evaporation deposition methods, including thermal evaporation and flash evaporation, are also applied to fabricate the flexible TEGs. The process starts with the evaporation of the TE materials by high temperature or other methods and then deposits the TE materials onto the substrate.[182] The process is shown in **Figure 2.12e**.[183] However, these techniques also have their limitations, such as high temperature or vacuum condition, which limit their usage on flammable substrates. Comparing with these methods, screen printing can be a better choice for fabrication of TEGs on fabric substrates. The screen-printing technique also use the ink form TE materials and print the toner onto the substrates across the made screen.[184] The sequences of screen printing are shown in **Figure 2.12f**.[185] Recently, many flexible TEGs manufactured by screen printing approaches have been published. After the preparation of liquid-state pastes of Bi_2Te_3 (n) and Sb_2Te_3 (p) TE materials, the flexible TEGs can be fabricated by screen printing approaches onto the fabric made by brittle materials or Si/quartz substrate.[155,186]

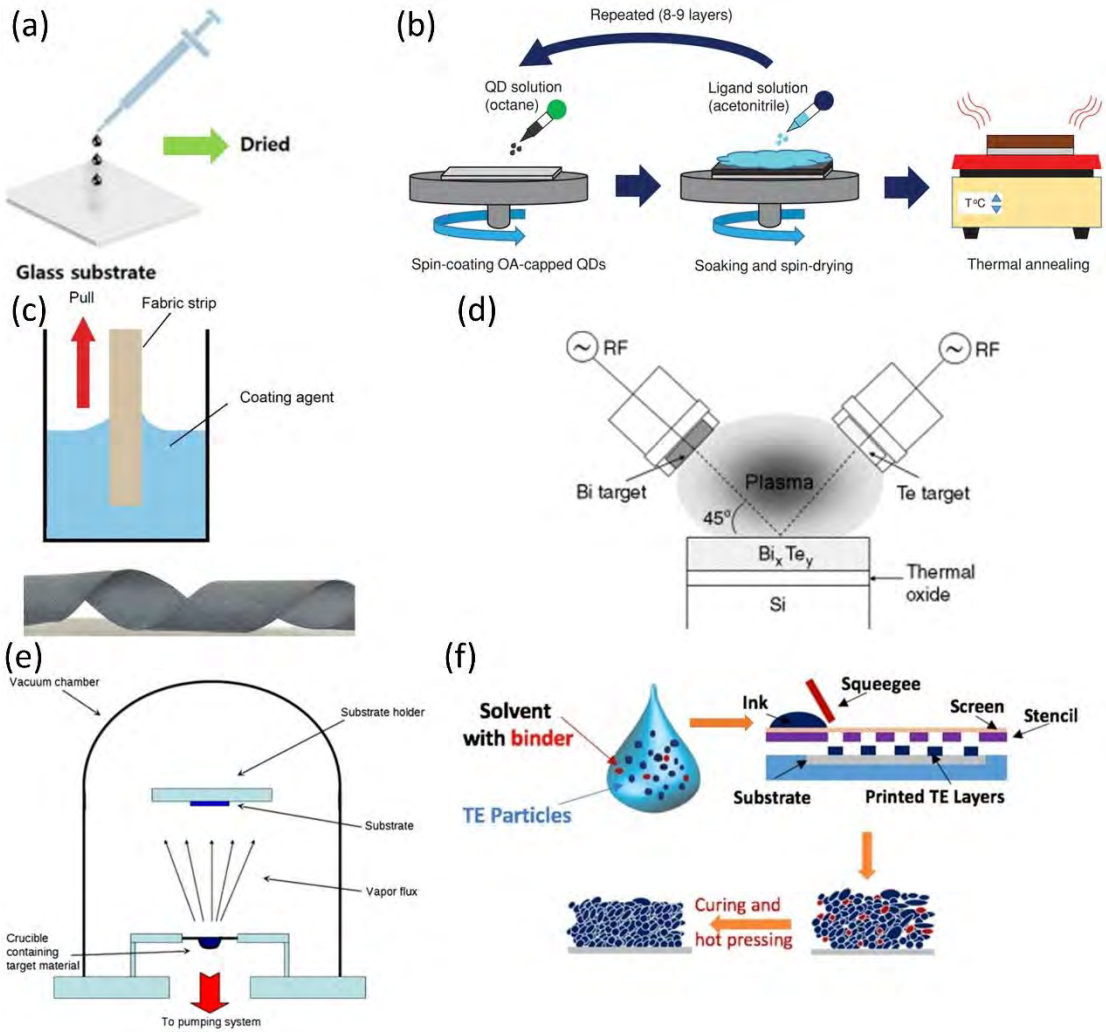

Figure 2.12 Schematic figures of different techniques for surface modification. (**a**) Schematic figure of drop casting.[177] (**b**) Schematic figure of spin coating.[187] (**c**) Schematic figure of dip coating.[188] (**d**) Schematic figure of RF magnetron sputtering.[189] (**e**) Schematic figure of thermal evaporation.[190] (**f**) Schematic figure of screen printing.[185]

Surface modification includes a large group of techniques for fabrication of flexible TEGs with different substrates. Most of them can be applied to flexible substrates such as fibers, yarns and fabrics without extreme conditions (i.e. high temperature, vacuum). However,

flexible TEGs in wearable applications should not only fulfill the requirement of flexibility but also possess an enough size to maintain the temperature gradient and thermal resistance. Therefore, flexible TEGs based on thin films may not be the most suitable choice for wearable applications.

2.5 Application of thermoelectric device

This part mainly focuses on the applications of thermoelectric materials as generators for wearable devices and the efforts made towards specific applications, such as increasing flexibility, power or voltage output, energy conversion efficiency, and long-term effective performance.

2.5.1 Principle of wearable applications

Most intelligent wearable devices involve only a small power input (around 100 μW~ 1 mW) to operate. Driving these devices by the electronic generators often demands bulky wiring and excessive planning of circuit layouts. Besides, the power supply should correspond to the devices' lifespan. Many wearables such as GPS and health monitors are designed for long-term working status. Batteries, currently the most used power supply system in wearables, however, limit these autonomies as the power will run out and charging is troublesome due to geographical constraints. The recharging process signifies a strong limitation on the working time of wearable electronic devices. This strong

limitation implies the demand for further research on powerful wearable energy harvesting devices that can enhance both the quantity and the operation time of electrical power. With the advantage of safe, environmentally friendly, reliable, small and lightweight, TEGs are ideal choices for wearable applications.

According to estimates,[191] the conversion efficiency for mechanical energy from human body is around 15-30%, which indicates that the majority of energy that consumed by human are wasted in the form of heat. Therefore, the harvesting of energy from waste heat can be strongly demanded. According to the Carnot's equation, [192] the maximum efficiency (η_{max}) of a heat engine (the system that can conduct the energy conversion from heat energy to electricity) can be calculated as:

$$\eta_{max} = \frac{T_{body} - T_{ambient}}{T_{body}} \tag{2.19}$$

where T_{body} and $T_{ambient}$ are the temperatures of human body and environment, respectively. [191] The efficiency of TEG (η_{TEG}) is lower than that of heat engines mentioned above:[193]

$$\eta_{TEG} = \eta_{max} \cdot \frac{\sqrt{1+ZT}-1}{\sqrt{1+ZT}+\frac{T_{ambient}}{T_{body}}} \tag{2.20}$$

Different positions of human skin can exhibit in different temperatures according to different environmental temperatures as shown in **Figure 2.13a**. The principle of wearable TEGs is converting waste heat to electrical power by using the temperature difference between the environments (room) and human-beings (**Figure 2.13b**).[194] Taking the T_{body}

as 37°C and $T_{ambient}$ of 0°C, Eq. 2.20 indicates that the real efficiency of the device with ZT = 1 could reach around 2.15%.

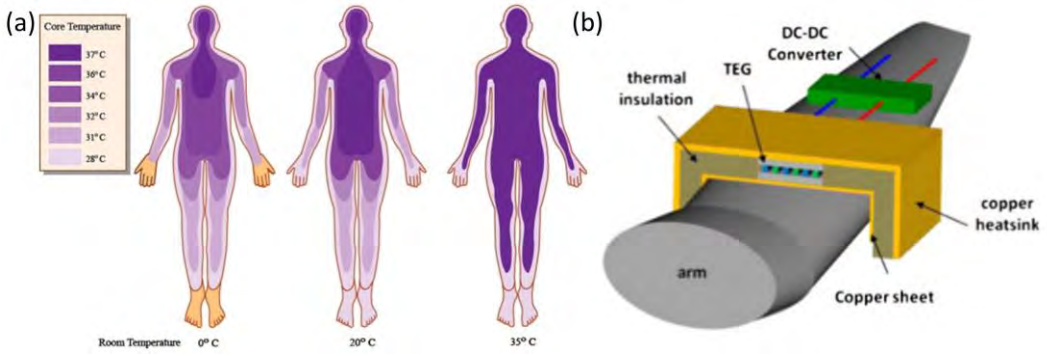

Figure 2.13. (a) Human skin temperature with different room temperature.[195] (**b**) Schematic figure of the applications of wearable TEGs on arms.[194]

2.5.2 Demonstration of wearable applications

The first TE watch powered by TE effects was SBET001, which was designed by Seiko and Citizen in 1998 (**Figure 2.14a).**[196] The Seiko watch generated electrical output of 22 with an open-circuit voltage of 300 mV and efficiency of about 0.1%. Another commercial example is the Dyson TE bracelet developed at 2009 (**Figure 2.14b**), which can absorb body heat and charge a battery of mobile phone or other mobile devices.[197]

Figure 2.14 Photo of (**a**) body heat powered watch Seiko thermic[196] (**b**) Dyson energy bracelet.[197]

More attempts to use TEGs for powering wearable devices were explored by academia and reported in literatures. At the early stage, rigid TEGs were chosen for wearable applications. A wireless pulse oximeter, which can also be used as sensor for compounds, has been created, manufactured and examined by Torfs et al. in 2006 as shown **Figure 2.15a**.[198,199] The device records content of oxygen in main blood powered by a TEG with the size compatible with watch. It has power output at the range of 100–600 μW during the whole day and night time. Leonov et al. integrated 17 small thermoelectric modules on a T-shirt to drive an ECG system which consums 10 μW (**Figure 2.15b**). The thickness of each

module is less than 6.5 mm to make the person who wear it feel comfortable and only a thumb-size of the human body area was utilized to get the essential power. The system can also endure the washing processes and dry processes by washing machine.[200] AimeLay-Ekuakille et al. demonstrated of a WTEG that can be used as the power source for devices that can support hearing (**Figure 2.15c**).[201] Design of TEGs that are on the basis of power from body heat can be applied for biomedical devices. It should be noted that the power generated from WTEG needed to go through a conditioning circuit and a backup battery is also needed for reliable performance. Leonov et al. incorporated thermopiles into a test shirt where every single thermocells (40 × 30 × 1 mm) was sandwiched between 30 mm-diameter round plates of different temperatures. The system (16 modules into shirt) can maintain the continuously power output at around 5 mW for more than 10 hours a day from the environmental temperature of around 295K. The wearer have no complains about the comfort since the thickness of the whole wearable systems is less than 4mm.[202] V. Leonov et al also demonstrated a glove worn that can keep the temperature of the wearer's hands at high temperature even in cold environments (**Figure 2.15d**).[203]

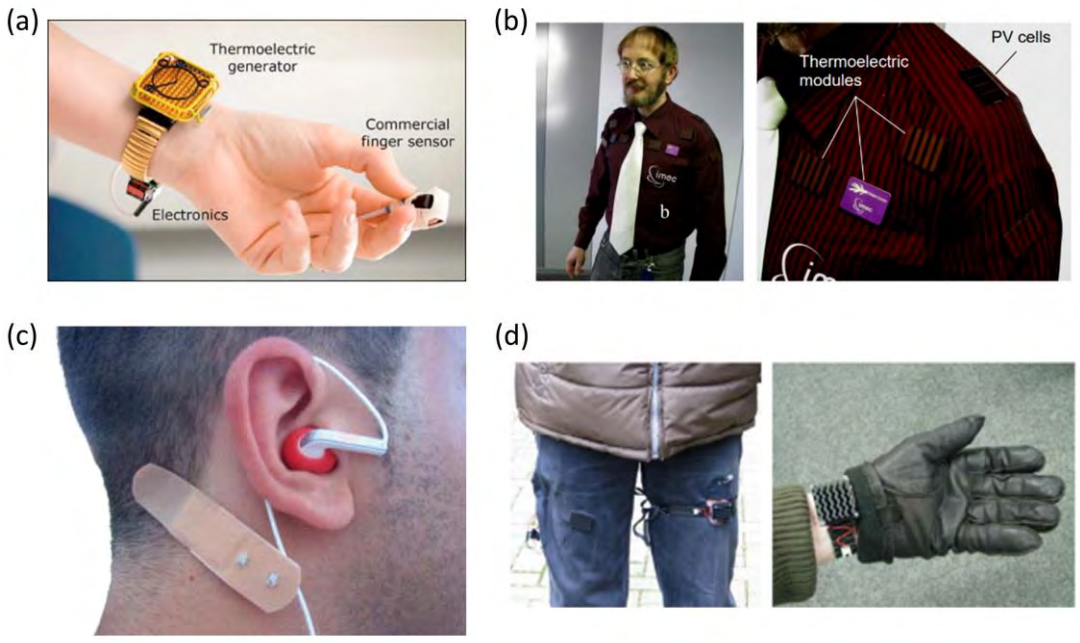

Figure 2.15 Demonstrations of some applications. (**a**) Body-powered pulse oximeter[199] (**b**) Electrocardiography shirt and some of its modules.[200] (**c**) Hearing aids powered by TEGs[201] (**d**) A TEG-based glove worn for warming of the wearer's hands.[203]

Due to the expanding research on f-TE materials and the design of f-TEGs, more applications using flexible TEGs for have been demonstrated. Kim et al successfully demonstrated a TE generator with rather satisfied flexibility (bending radius less than 20 mm, no degradations on performances after repeated bending for 120 cycles). Then they integrated FTEG devices with glass fibers and attached to the wrist (**Figure 2.16a**), which generated an V_{open} of 2.9 mV at room temperature.[88] Kim et al used a FTEG to demonstrate a self-powered wearable electrocardiograph(ECG) (**Figure 2.16b)**, which required a 3.3V power supply.[204] Xu et al. built a f-TEG made by bulk materials and included multifunctional Cu electrodes for heat absorption and dissipation(**Figure 2.16c).** It can

provide the enough intensity of light for reading a paper in the room without any other light sources at 17.5°C by integrating 100 pairs of the TE modules together.[167] Kim et al incorporated the TEG into the shirt from fabrics.[205] With the measured temperature of skin and environment of 32°C and 5°C respectively, the 12-couple prototype device generated 146 nW power. The output power per cm^2 was 292.4 nW/cm^2. Such TEG could generate 4.7 mW from the entire skin area of an adult (around 1.6 m^2). Micropelt et al established the modules (W: 3.3, L: 4.2, H: 1.1 mm) can generate a continuous power output at different temperature gradients (1 mW for 10 K and 10 mW for 30 K).[206] Yuan et al. designed a self-powered multifunctional electronic skin system by using TE models enclosed on the surface of hand and the liquid crystal display (LCD) on the other side can be powered (**Figure 2.16d**).[207] Hong et al. designed a new concept of TE device and the simulations showed the flexibility of the devices can be enhanced by around 30%.[159] It can generate a V_{open} of 74.5 mV, P_{output} of 4.5 mW/cm^2 when worn by people sitting indoor with normal temperature. Wang et al. also developed a TEG can be worn by people for operating a shrunken accelerometer to identify human body motion.[208]

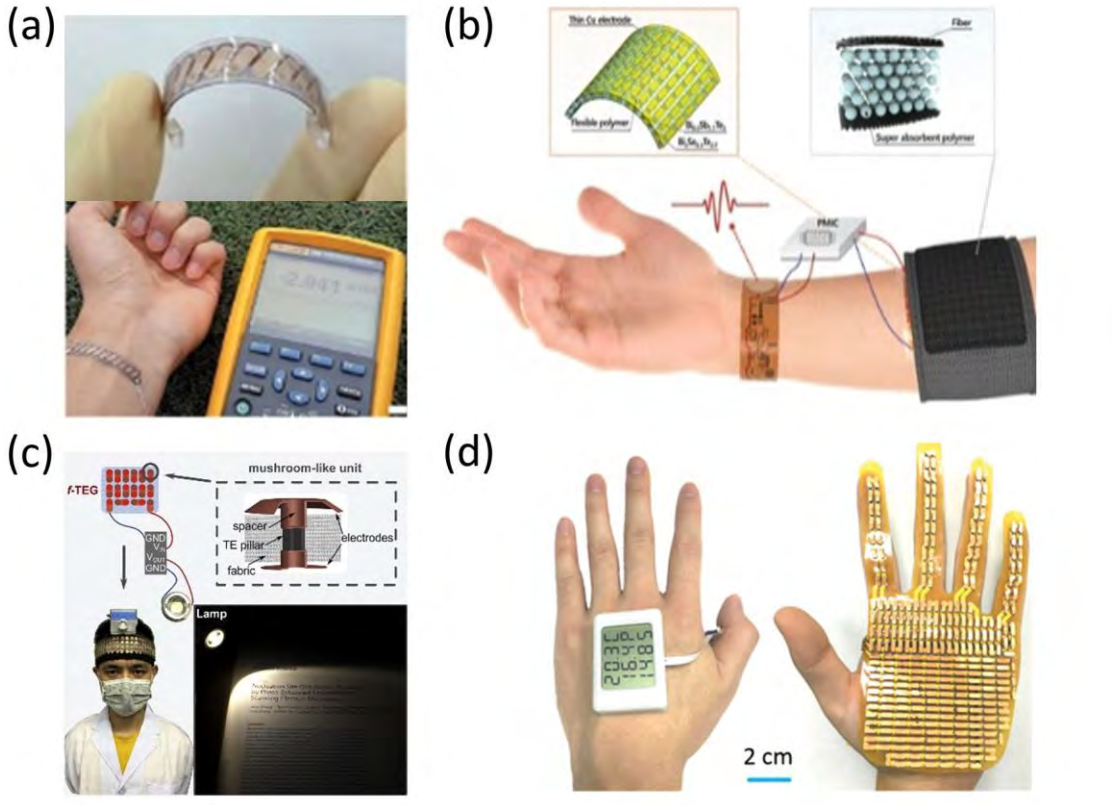

Figure 2.16 Examples for applications of wearable TEGs. (**a**) FTEG devices with glass fibers.[88] (**b**) A self-powered wearable electrocardiograph(ECG) by TEG.[204] (**c**) The bulk-material-based FTEG to illuminate a paper for reading. [167] (**d**) Illustration of an electronic skin system.[207]

In the medical domain, TEGs are mainly used to power implanted organs and assistive devices in the human body to enable them to function properly over time, such as artificial hearts or cardiac pacemakers. Many companies have manufactured nuclear-powered pacemakers radioisotope thermoelectric generator(RTG), as shown in **Figure 2.17**.[209]

Figure 2.17 Pacemaker(left) and RTG battery(right).[209]

Table 2.2 Several demonstrations about the performances of recent wearable TEGs.

(Flexibility here is characterized by Minimum bending radium)

Materials	**No. of Pairs**	**Size**	**Voltage/ power**	**Flexibility**	**Working time**	**scenario**	**Ref.**
Bi-Te	>50	2×2×1.3 mm^3	> 1 μW	*	Around 3 days	Powered a wristwatch	[196]
*	17	1-2 cm^2	0.8-1 mW	*	1.5-2 years	As a power supply by spreading TEGs over the shirt	[200]

						compared with AA batteries	
*	450	Thickness 500μm	*	*	*	Hearing aid	[201]
*	*	3×4×0.65 cm^3	10-25 $\mu W/cm^2$	*	*	Hands warm	[203]
$Bi_2Te_3$and Sb_2Te_3	11		3.88mW/cm^2 (ΔT=50 K)	20mm	*	Built a band-type flexible TE generator to patch on wrist	[88]
*	*	40 cm^2	38μW/cm^2	*	22h	Drive an ECG system by combined a flexible heat sink	[204]
*	50	100 cm^2	10 $\mu W/cm^2$	*	*	illuminate a paper for reading by	[167]

			ΔT = 25K			wearing on the head	
$Bi_{0.5}Sb_{1.5}Te_3$ (p-type) and $Bi_2Se_{0.3}Te_{2.7}$ (n-type)	12	1.6 m^2	292.4 nW/cm^2	13mm	*	Shirt	[205]
*	*	64 cm^2	3 $\mu W/cm^2$	10 mm	22h	To power a liquid crystal display (LCD) module	[207]
n-type BiTeSe and p-type BiSbTe	50	6×6×1 mm^3	48μW/cm^2	25 mm	*	Integrated with an ECG System into a Shirt	[209]
*	142	4.5 mW/cm^2	74.5mV 4.5 mW/cm^2	30 mm	>8 h	Built a thermoelectric band	[159]

$Mg_{3.2}Bi_{1.498}Sb_{0.5}Te_{0.002}$ (n) and $Bi_{0.4}Sb_{1.6}Te$ (p)	18	28.8×15.2×2.5 mm^3	13.8mW/cm^2	13.4mm	150 s	Light a LED lamp	[210]
P-type ($Bi_{0.5}Sb_{1.5}Te_3$) N-type ($Bi_2Se_{0.5}Te_{2.5}$)	52	43.5 × 26.5 × 2.6 mm^3	16.7 μW/cm^2	20mm	*	powered a miniaturized accelerometer to detect human body motion	[208]

* Data not provided

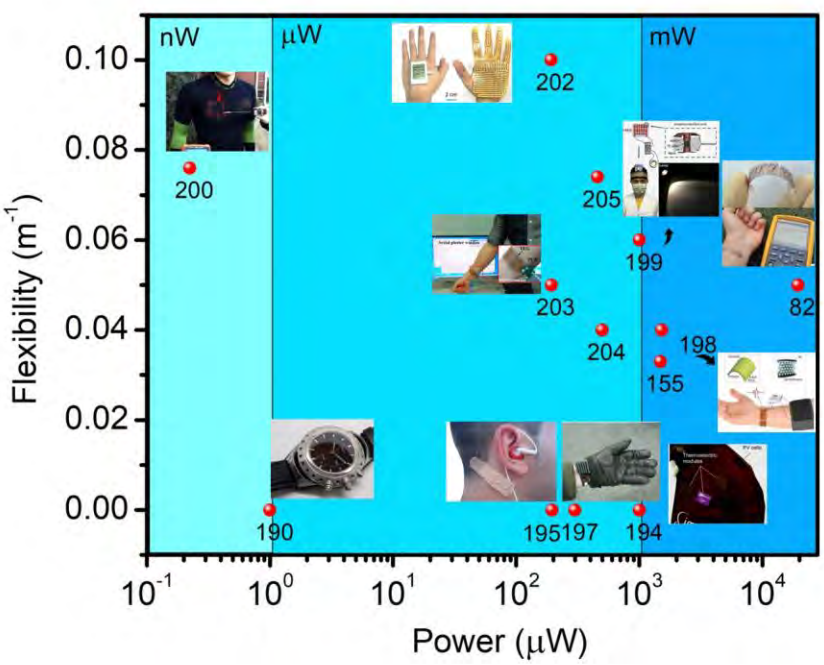

Figure 2.18 Summary of several demonstrations about the performances of recent wearable TEGs (Flexibility here is characterized by the reciprocal of minimum bending radium)**.**

2.5.3 Challenges and future in application of wearable TEGs

With various applications in wearable devices, wearable TEGs have demonstrated themselves as effective power supplies. For successful integration with wearable devices, however, the structure and material of TEGs needs to be carefully designed and optimized. We summarized several examples of wearable applications and compared the performances (**Table 2.3** and **Figure 2.18**). The result shows the bendable radius of characterized flexibility has been reduced from 30 to 10 mm[210] and the power supply

integrated in wearable devices has reached the milliwatt level, which better satisfied the power demand of wearable devices.

In spite of the developing progress, studies in the application of wearable TEGs still faces many challenges ahead.[211]

1) To meet the requirement of power supply, a great number of thermoelectric pairs needs to be integrated, taking up large skin area on human body. This significantly sacrifice the comfortability of wearable devices.

2) Secondly, in the existing demonstrations of wearable TEGs, a lot of efforts are devoted to the conversion between heat and electric power but the effective operating time are less discussed. In the data available, the effective conversion time of some devices varies from 8h to 22h, but in many wearable applications, such as GPS or health monitoring, the need for long-term effectiveness operation is essential.

3) The comprehensive evaluation methods for the entire life cycle of wearable TEGs have not yet been established, especially in the harsh service environment such as dynamic temperature field. The performance stability and reliability design of TEGs materials and devices still lack systematic evaluation criteria. Therefore, it is important to establish the failure assessment model of thermoelectric components and the theory and method of device reliability and service life evaluation.

4) Finally, the present benefit-cost-ratio of TEGs is low, which limits its advances to industry. The current commercially available thermoelectric devices are mainly bismuth telluride, lead telluride, and silicon-germanium alloy systems. For them,

expensive Te and Ge made cost reduction very difficult. The price for a rigid TEG system was around USD30 for each W in 2014. It should be as low as around USD5 for each W to satisfy the requirements of economy.[212]

2.6. Summary and perspectives

In this chapter, a critical and board review of the wearable TEGs including the choices of TE materials, design of structure, fabrications and applications was presented. Inorganic TE materials have limited applications in flexible devices due to their rigid and fragile nature, even though they have outstanding TE performances. Organic TE materials are flexible compared with inorganic counterparts but suffer from unsatisfied TE performances. I-TE materials can have high flexibility together with outstanding TE performance but the continuity of the power output can be a design concern. Based on the comparison between different kinds of TE materials, Bi_2Te_3-based TE materials are the most common choice for wearable TEGs. Other functional materials besides the TE modules in flexible TEGs were also introduced and summarized. The structures of the wearable TEGs have also been summarized and compared, followed by the introduction and comparison two main types of fabrication methods. Since the wearable TEGs requires a certain size to maintain the temperature gradient and heat flow, the embedded structure seems to be a better choice comparing with the coating structure. Meanwhile, the thermal and electrical contact resistance are also key issues that need to be concerned during the structural design and fabrications. With the exploration of TE materials and fabrication methods, the applications

of wearable TEGs have expanded rapidly. In recent years, the bendable radius of characterized flexibility for wearable TEGs has been reduced from 30 to 13 mm and the power supply integrated in wearable devices has reached the milliwatt level, which better satisfied the power demand of wearable devices.

Although the research works at this stage have already demonstrated several successful applications of wearable TEGs, the study of wearable TEGs is still deserved to be further explored. What are the limitations and drawbacks of the current wearable TEGs? Can wearable TEGs take the roles of batteries in wearable electronics? The answers are complicated. Firstly, the performances and stability of the TE materials for wearable TEGs at this stage can still be improved. Conventional electronic TE materials are rigid and facile, polymer-based TE materials have poor TE performances and i-TE materials cannot generate high power output continuously. Each type of the TE materials has their advantages and drawbacks, which limited the applications of wearable TEGs based on these materials. Therefore, as the most important component of the wearable TEGs, the research on flexible TE materials with high TE performances should have high priority. Second, the structures of flexible TEGs are similar with each other and most of them are designed using embedded structure or coating films. However, TEGs based on thin films may not be suitable for applications since the thickness is too small, making it difficult to maintain the required temperature gradient. The embedded structure can have enough thickness but may hinder the flexibility for wearable applications. In addition, the contact electrical resistance, contact thermal resistance, structural stability and heat absorption/rejection from substrates should also be considered when design a wearable TEG. Based on different structures and TE materials, the fabrication methods for electronic

TE materials and organic TE materials are sufficient but the fabrication methods for i-TE materials scarce. Until now, 3D printing is one of the most commonly used methods for fabrications of wearable TEGs based on gel-state i-TE materials. The fabrication methods for liquid-state i-TE materials that can maintain the flexibility and provide good sealability still deserves to be explored. At last, although several successful applications of wearable TEGs have already been demonstrated, the working life and long-time stability of the wearable TEGs still meet some challenges. In addition, the high cost of effect may also hinder the applications of wearable TEGs compared with other generators. With all the limitations tackled, we believe wearable TEGs can have boarder applications and become a significant component for IoTs.

CHAPTER 3 Thermoelectric properties of phase-transitional i-TE systems during phase change

The change of phase from liquid form to gel form in ionic thermoelectrical (i-TE) materials can generate huge quick change in gluiness and transport process of ions, which means it can generate extreme differences in TE performances, critical in harvesting energy of small amount like waste heat for Internet of thing (IoT) and wearable electronic applications. This chapter will demonstrate three types of ionic thermoelectric systems including i-TE systems without phase change, thermal induced phase change from liquid to gel and thermal induced phase change from gel to liquid. After the preparation, the TE performances will be examined. The result will be summarized and compared in detail.

3.1 Introduction

Accompanied by the unpredictable increase of elastic, light and wearable electronics, the usage of nodes and sensors in IoT has quickly come close to the forecasted trillion pieces.[213,214] Nevertheless, the blockage that obstructs the broad usage of IoT and wearable technologies has arisen due to the shortage of light and effective power supplies that are friendly to environment.[10] Thermoelectric generators (TEGs) in solid forms, which are able to directly absorb the waste thermal energy from surroundings or people and change it into electricity devoid of any mobile parts can be one of the desirable solutions.[215,216]

TE materials can use ions and electrons as charge carriers and they are investigated for good choices of TEGs. TE materials using electrons as charge carriers are mostly narrow band-gap semiconductors as broadly explored or applied and charge carriers can be either holes or electrons. Compounds with metal elements and oxygen group elements, such as Tin selenide, Lead(II) Telluride and Tin telluride, or other compounds with metal elements, for example, Cu_2Se, can be frequently broadly explored TE materials using electrons as carriers.[99,102,103,108,217,218] However, the S of these materials are normally quite small (around the order of several hundreds of microvolts per K)[219], which implies to generate a functional voltage (1 ~ 5V) near environment T (around 300K) needs an combination of a great numbers of small TE cells[220] or requires a voltage booster for direct current inputs to direct current outputs, which equally enhance the complication in apparatus or manufacture procedure.[221] Furthermore, according to the tough interactions among the S, σ and κ,[35,39] the control for each individual parameter in order to enhance whole TE properties, particularly ZT, turns out to be a contest. Therefore, researchers attempted to find out many approaches, including merging and compressing of electronic band structures or DOS distortion to improving the TE performances of the electronic TE materials.[218,222,223]

On the other hand, unlike the electronic TE systems, the different ions in ionic thermoelectric (i-TE) materials are charge carriers and these materials are normally prepared on the basis of two different effects (thermodiffusion or thermogalvanic effect). The effects that i-TE system use generate a thermopower, or ionic Seebeck coefficient (S_i), which has a rather high value (up to several orders) comparing to the conservative semiconductor materials at room temperature.[8,9] For example, around one millivolt per Kelvin at room temperature[123] can be achieved by the pure water-based solution with ion

providers like LiCl or NaCl while 0.011 V/K was achieved by from a solution consists of sodium hydroxide and polyethylene oxide (PEO) solution.[9] For the objective of conquering the troubles about encapsulation[224], i-TE materials in gel form have been proved as good candidate for applications. An ionic Seebeck coefficient of 0.024 V/K, around several hundred times of scale superior than that of conventional TE materials, was attained by the same solution in the aforementioned work in enclosed nanocellulose channels.[225] In addition, an adaptable S_i from the range -4 ~ 14mV/K was achieved by altering the components of gel-state organic materials.[226] Nevertheless, the ZT of those i-TE materials in gel form are generally less than 0.1 due to the weak ionic electrical conductivity (σ_i). Lately, gels with ions created from ionic liquids and poly(vinylidene fluoride-co-hexafluoropropylene) (PVDF-HFP) possess a rather high value of S_i (around 26.1 mV/K) accompanied by an σ_i of 6.7 S/m and thus it can generate a rather high ZT (~0.75).[123] These superior TE performances of i-TE systems arises from the ionic effect called Soret effect, which rearrange the ionic positions at the hot temperature region and cold temperature region.[43] The S_i of the i-TE cells, particularly the cells with thermodiffusive effect, is affected by the concentration variations among ions with different signs at different sides. Consequently, the moving procedure of the ions is significant for superior outcomes of the flexible-state i-TE materials.

Former studies have concentrated on types of ions or chemical reactions of ions to enhance the TE properties of the certain systems. Nevertheless, the places where ions are moving, the electrolytes, should have strong effects as well. Electrolyte allows electrically management of electronic, magnetic and optical properties of materials [227] and the change of phase can affect electrochemical properties of hybrid-ion batteries in liquid form.[228] The

liquid-to-gel or reversely phase change may alter the stickiness of the system due to creation or obliteration of polymer network. Therefore, it can be predicted that the change of phase should possess a considerable influence about the moving procedure of ions which can further affect the S_i of i-TE systems.

This chapter will mainly focus on the preparation and investigation of the consequences from phase change by using different types of i-TE materials, including different performances about phase change and mechanisms (i.e. non-phase-transition, thermal-induced liquid-to-gel phase-transition, thermal-induced gel-to-liquid phase-transition and UV-induced liquid-to-gel phase-transition). This chapter, firstly exposes a widespread result of gigantic variation caused by the change of phase in i-TE systems, provides a innovative and practicable routine to expand energy conversion properties of i-TE systems by controllable phase-transition. This method can become a novel viewpoint for upcoming i-TE devices for applications about energy harvesting from waste heat with adjustable TE performances or properties.

3.2 Methodology

In this chapter, the methodology will be introduced by two parts, which are the preparation/fabrication methods and the characterization methods, respectively.

3.2.1 Preparation and fabrication

Materials

In this work, the i-TE materials are prepared with different components. LiCl (Dieckmann, ≥ 99.0%), NaCl (Dieckmann, ≥ 99.0%), KCl (Dieckmann, ≥ 99.0%), KNO_3 (Dieckmann, ≥ 99.0%), oxirane, methyl-, polymer with oxirane (Poloxamer 407, Sigma, purified, non-ionic), acrylic formulation (PolyJet Photopolymer, RGD810, Veroclear) were bought and applied without any further purification.

Preparation of i-TE materials

Details about the parameters and information about all the i-TE systems that used in this chapter are listed in **Table 3.1**.

Table 3.1 Details of i-TE systems

I-TE solutions	Mass of salts	Polymer Mass	Water Volume	Gel Volume
10%Polo+ 1 mol/L LiCl	0.05 mol (2.12g)	20g	200 mL	50 mL
18%Polo+ 1 mol;/L LiCl	0.05 mol (2.12g)	36g	200 mL	50 mL
20%Polo+ 1 mol/L LiCl	0.05 mol (2.12g)	40g	200 mL	50 mL
2% Agarose + 1mol/L LiCl	0.05 mol (2.12g)	4g	200 mL	50 mL
UV-sensitive-gel-based	0.006 mol (0.254g)	NIL	NIL	20 mL

The poloxamer 407 i-TE liquids of different concentrations are prepared by using the similar processes except for the variations on mass of each element. The first procedure was to combine the poloxamer 407 with water to set up the fundamental aqueous solution of poloxamer 407 for a certain concentration. Then the poloxamer 407 aqueous solution was stored at 4℃ for more than 12 hours to guarantee the polymer was completely dissolved. Then a certain amount of LiCl is weighted and dissolved into a certain volume of poloxamer 407 solutions. The mixture was stored at 4℃ for more than 2 hours. The i-TE liquids were suitable for further experiments after these steps. This LiCl/poloxamer 407 had a liquid-to-gel phase transition in the temperature of environment range of 15 ~ 20℃. The agarose-based i-TE liquids were also made with comparable procedures and the only change was the liquid required to be stored at high temperature (larger than 50℃) to guarantee the LiCl was completely dissolved. This system has a gel-to-liquid phase change at the temperature range of 25 ~ 30 ℃. The UV-sensitive-gel-based i-TE liquids were made by similar procedure with the exception that the whole procedures were conducted in non-UV-light environments and the salt was completely dissolved into the UV-sensitive-gel without further procedures.

Fabrication of the i-TE cells

Liquid-state materials cannot be directly measured for the TE performances. Therefore, the test cell should be fabricated to characterize the TE performances. Test cells consist of the liquid-state targe materials inside, two pieces of graphene plate (electrodes), which are adhered onto the top and bottom ends, as shown in **Figure 3.1a**. The test cells were fabricated and possessed the identical size (outer radius of 10mm, thickness of ~1mm) and the plates were also fabricated and possessed the identical size (side length 3 cm, thickness

0.05cm with the shape of square). The schematics of the test targets and experimental settings are shown in **Figure 3.1b** and the structure of the cells at different angles are shown in **Figure 3.1c**.

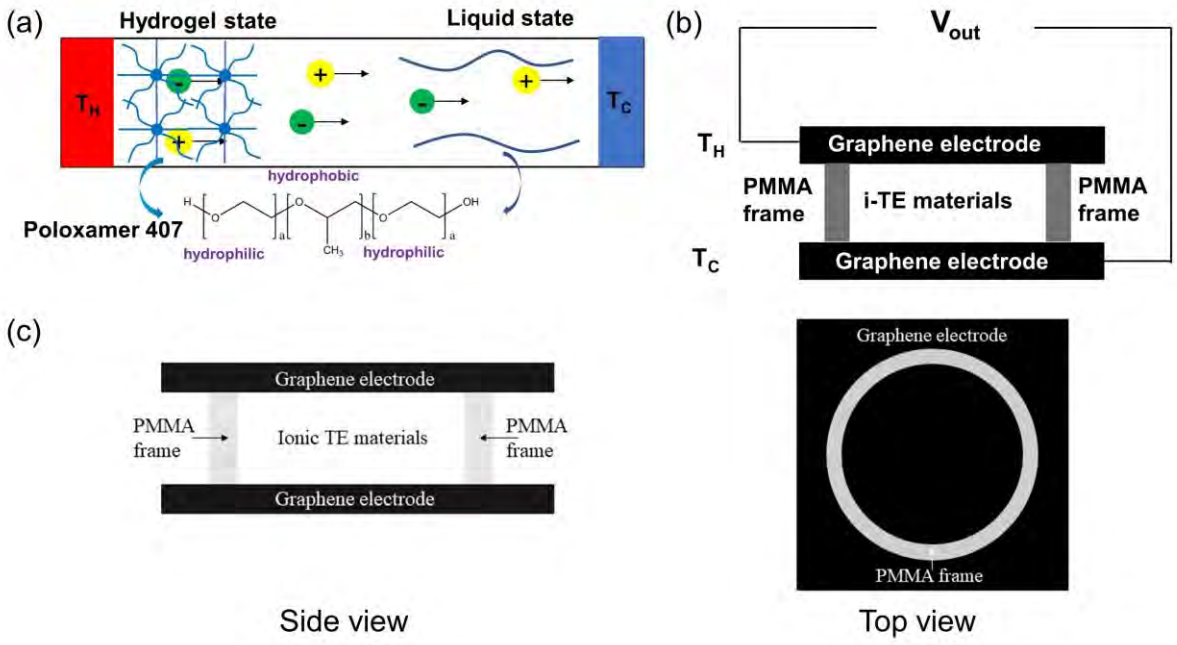

Figure 3.1 Schematic images of the i-TE systems a. Graphics of the modules of the target materials in the test TE cell. **b.** Graphs of the TE cell made for the evaluations of the TE performances. The schematic of test cell is observed from front side. **c.** The schematic figures of the container from different sides used in this project. The left one is side view (also main view) of the container. The TEG is fabricated by two pairs of thin graphene electrodes (3cm x 3cmx 0.2cm), a laser-cut PMMA frame (ring-shape, inner diameter 2cm, outer diameter 2.5cm, thickness 1cm) and the liquid-state i-TE materials (different components for different tests). The right one is the upper view of the container. To state the structure in a clearer way, the upper layer of the graphene electrode and i-TE materials are removed.

The schematic figure of the fabrication process for the i-TE cell is shown in **Figure 3.2**. In order to fabricate this test cell, the PMMA frame needs to be sticked onto one piece of graphene electrode first. In this project, a special type of glue (Fast-setting epoxy adhesive, AB type, Arlaoda) is used to stick the graphene electrode with the PMMA frame. Firstly, the A type and B type of the glue need to be mixed and the PMMA frame will then be fixed onto the electrode with the help of the glue. After waiting for 5 mins, the target liquid-state i-TE materials need to be poured into the primary container (PMMA frame with one electrode) and instantly stick the other piece of the electrode on the top end of the frame. The whole TEG is then fabricated and needs further sealing process after a short time for solidification of the glue. The fabricated TEG needs to be kept in low temperature (around 5℃) before measure. The manufactures of the i-TE cells on the basis of Agarose had the almost identical steps except that the solution was kept at 60℃ before fabrication of the test modules. The manufacture of the i-TE cells on the basis of gel that are sensitive to UV light possessed the exact identical steps excluding the manufacture could not be exposed to UV-light.

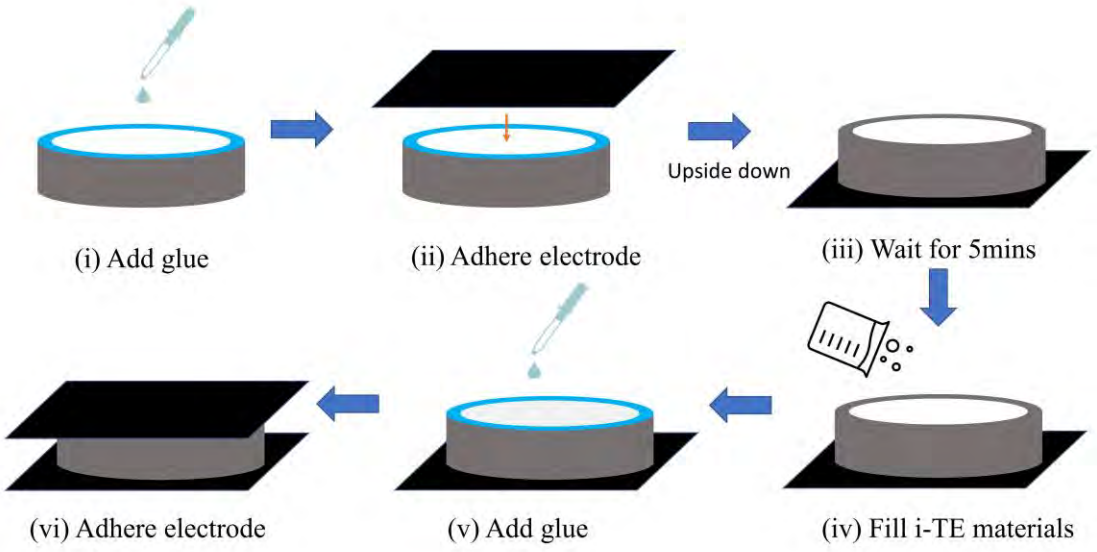

Figure 3.2 Schematic figures of the preparation process for the i-TE cells. (i) Add the mixture of A-type and B-type glue onto the top surface of the PMMA frame. (ii) Adhere one piece of electrode onto the surface of the PMMA frame with glue. (iii) Turn the frame upside down and wait for 5 minutes till the glue is dried. (iv) Fill the PMMA frame with liquid-state i-TE materials. (v) Add the mixture of A-type and B-type glue onto the top surface of the PMMA frame again. This top surface should be the bottom surface at the first step. (vi) Adhere another piece of electrode onto the PMMA frame and add more glue to seal the whole cell.

3.2.2 Characterization

In this work, most of the characterization methods are focused on the characterization of the TE performances of the TE materials. Till now, the characterization techniques for

liquid-state materials are limited. Therefore, in this chapter, some indirect measurements of the certain parameters need to be applied. This part will focus on the characterization methods for electrical properties, including S, σ and output performances (output power on the external load), cyclic voltammetry (CV) curve and thermal conductivity. The measurements for the viscosity will also be introduced.

Thermopower

The thermopower, or ionic Seebeck coefficient**,** required the measurements of electrical properties and temperature differences, which were conducted by applying a thermocouple thermometer and electrochemical workstation together. The experimental set-ups are shown in **Figure 3.2**. The test cells were put between two parallel metal plates, which supplied the temperature difference checked by the thermocouples. The electric voltage induced by different temperature differences were obtained at the range of 5 ~ 35°C, by changing the temperature of both plates together. In this work, the temperature differences between the two different sides were set as a stuck value of 3K. The ratio of the measured open-circuit voltage difference to the temperature difference was calculated as the thermopower at the cold temperature. However, the measurements in this project involved the phase-transition mechanism, so the normal method to measure the Seebeck coefficient/thermopower by using the linearly fitting ΔV to ΔT is not suitable for this project. In order to reduce the effects from random error, the measurements were replicated for 5-7 times at each temperature point and the thermopower was calculated from the average value of the maximum and the minimum result. The voltage difference was evaluated by an electrochemical workstation (CHI660E, CH Instrument, USA) in open-circuit voltage mode and the temperature difference was offered by a self-made plate with

heating, cooling temperature controlling functions. The temperature of the hot side and cold side of the TEG was checked instantaneously by a thermocouple thermometer (Anbat AT4516).

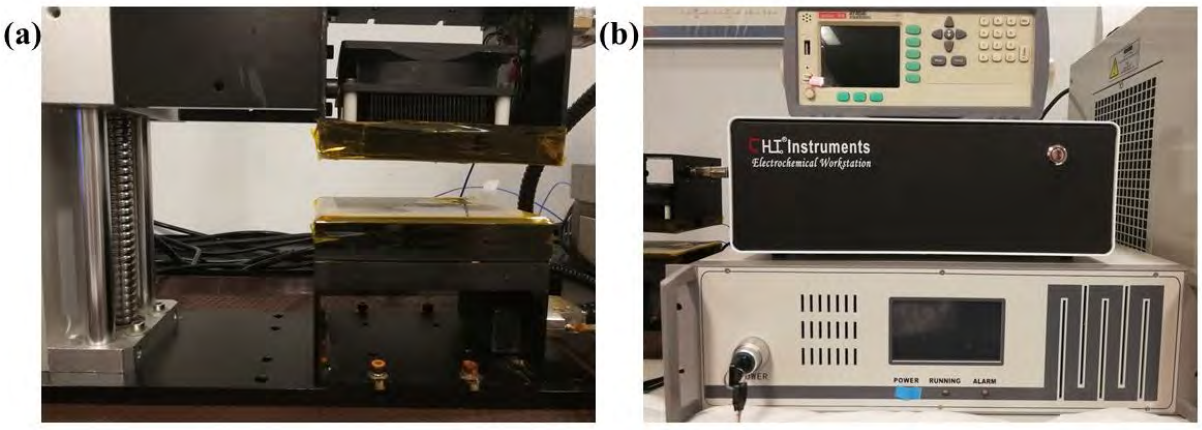

Figure 3.3 Photos of the equipment used in the characterization of the TE materials. (a) Self-made heating and cooling plates. The upper-side is heating plate while the bottom-side is the cooling plate. They can provide temperature range of -20℃ ~ 20℃ and 10℃ ~ 50℃, respectively. (b) From top to the bottom are thermocouple thermometer (Anbat AT4516), electrochemical workstation (CHI660E, CH Instrument, USA) and temperature controller of the heating and cooling plates, respectively.

Electrical conductivity

The ionic electrical conductivity was measured by a common method created for electrochemical devices.[229] The complex electrical impedance of the TE materials was achieved by the electrochemical workstation (CHI660E, CH Instrument, USA) in electrical impedance spectroscopy (EIS) mode. The set input voltage was correlated to the measured

open-circuit voltage and the chosen frequency was ranging from 10^5~10^{-2} Hz (modest differences for various materials). The electrical conductivity was assessed from the real part of the impedance at phase angle close to 0° in the Bode's plot that obtained by the EIS as:

$$\sigma = \frac{L}{Z'A}$$

where Z' is the measured real part of the impedance, L and A are the length and area of the test TEG, respectively. The calculated electrical conductivity by using this method should be the total electrical conductivity of the i-TE material but not the ionic electrical conductivity of the ions. In order to calculate the ionic figure of merit, using ionic electrical conductivity instead of total electrical conductivity should be more accurate.

Cyclic voltammetry (CV) curves

The cyclic voltammetry (CV) curves were evaluated to identify the working mode (capacitive or not) of the target TE materials. The CV curves was also evaluated by CHI660E, (CH Instrument, USA) in I-V curve mode. The scanning rate was 10 mV/s and the scanning voltage was set for the range of 0 ~ 0.4 V. All the electrical and TE characterizations of the i-TE systems were carried out on the test cells with the identical configuration and size.

Thermal conductivity

Thermal conductivity was measured by using Thermal Conductivity Measurement Instrument (Hotdisk, TPS2500s) for liquid-state samples. The experiments were conducted at room temperature.

Output power

The temperature differences between the hot and cold sides of the test cells were fixed as 3K and the external resistance load was connected to the test cells when the output voltage is stable. The maximum output power of target was chosen by the highest value of the voltage across the resistance multiplied by the spontaneous current through it.

Viscosity of the sol-gel systems

The viscosity of the samples was evaluated by Brookfield DV2T viscometer (AMETEK Brookfield, US) with the shear rate of 200 r/s and spindle No.5. 20 mL of the liquid-state samples were transferred into the 50mL breaker and the break was located into a larger 200mL breaker with ice and water inside to change the environmental temperature when measuring viscosity. The temperature during the measurements was managed by heating the larger breaker and checked by the thermometer inserted.

3.3 Result and discussion

3.3.1 I-TE materials and phase-transition

As mentioned in the experiment sessions, the i-TE systems were made and manufactured into test cells before the characterizations of the TE performances. In this chapter, the i-TE materials consist of poloxamer 407 aqueous solutions with various components and different salts as ion providers. The photos of different components of the i-TE cells, including the electrodes, PMMA frame and the photo of different i-TE materials are shown in **Figure 3.4**.

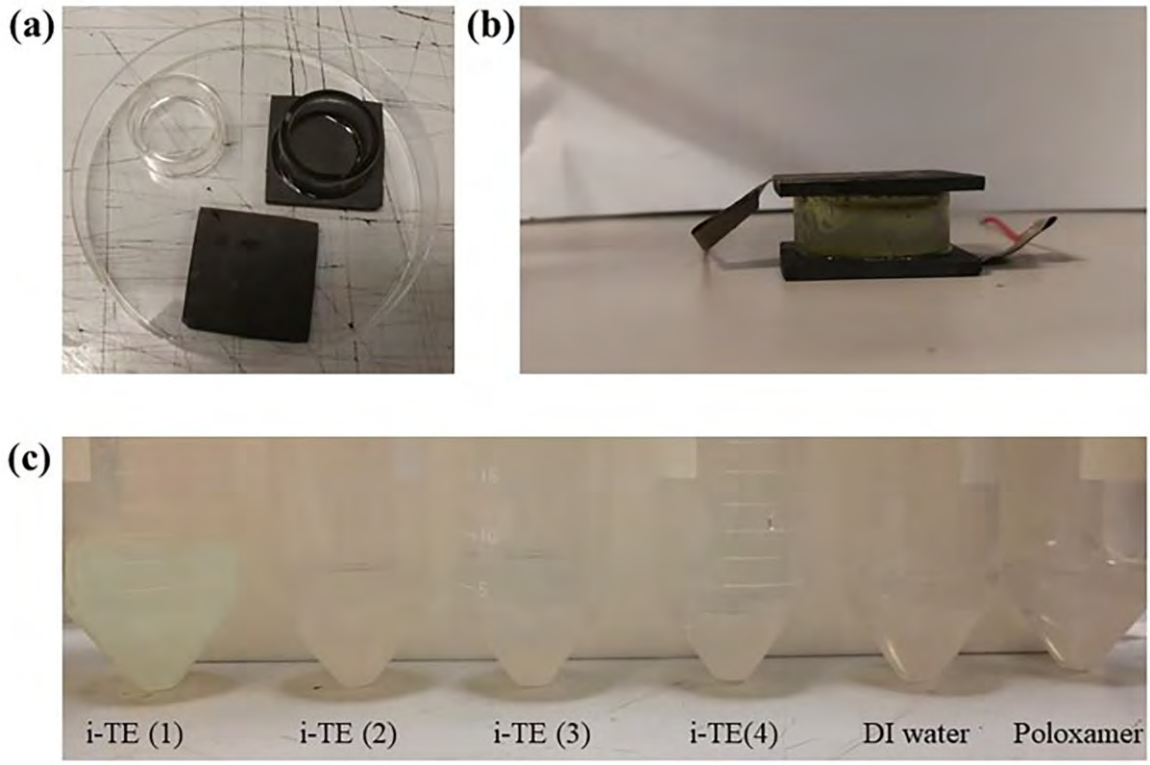

Figure 3.4 Photos of the preparations for the i-TE materials and i-TE cells. (**a**) Photo of the basic materials to prepare for the container of the i-TE materials. The container consists of two pieces of thin graphene electrodes and one ring-shape PMMA frame. The photo shows the PMMA frame and graphene electrode, together with the fundamental container made by one electrode sticked onto the bottom side of the PMMA frame. (**b**) Photo of an example of the TEG with liquid-state i-TE material inside. In this example, the i-TE material consists of 1 M/L LiCl and 18% (w/v) poloxamer 407. (**c**) Photos of different examples of the i-TE materials. The i-TE 1 to 4 represents different components, which is shown in **Table 3.1** below. DI water and poloxamer (18%) liquid are shown as reference group.

Table 3.1 Different components of the ionic-TE materials shown in **Figure 3.4c**.

i-TE (1)	1 mol/L LiCl and 2% Agarose
i-TE (2)	1 mol/L LiCl and 10% Poloxamer 407
i-TE (3)	1 mol/L LiCl and 18% Poloxamer 407
i-TE (4)	1 mol/L LiCl and UV-sensitive-gel

Figure 3.4c show appearances of the i-TE materials with different components. It can be clearly observed that most of the poloxamer based i-TE system are transparent and exhibit no color due to the colorless ions. The poloxamer 407 aqueous solution presents a change from liquid-state to gel-state at room temperature within a concentration range of 15% ~ 20% (w/v).[230] The phenomenon can be observed by adding the poloxamer solutions into a test pipe and checked the liquid surface layer by rotating the test tube at various temperature (**Figure 3.5**).

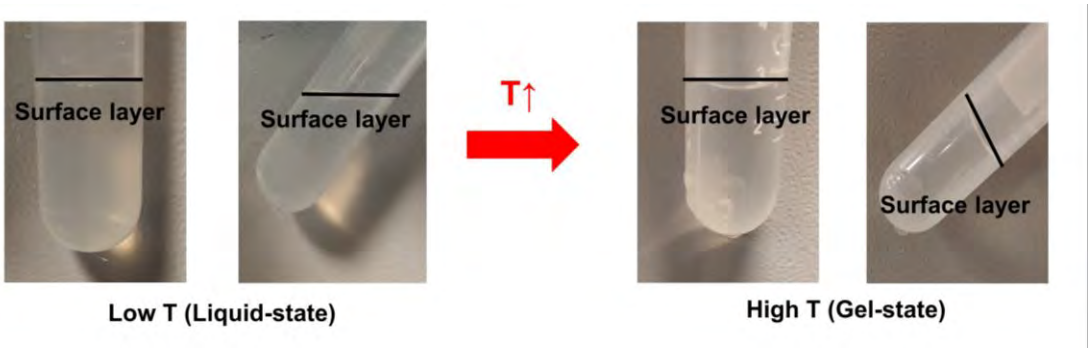

Figure 3.5 Liquid-to-gel phase transition of LiCl/poloxamer 407 solution. The surface layers of the electrolytes are shown and highlighted by thick black line from the figure. At low temperature, the surface level of the declined tube is horizontal. The level of the gel at the high temperature, however, is not horizontal.

The electrolyte shows in liquid form and the surface level keeps horizontal when rotating the test tube when temperature is quite low. At high temperature, however, the electrolyte exhibits in gel form and the upper level of the electrolyte maintains geometrically same with its initial state when rotating the test tube. The change of phase is further confirmed by the figure of viscosity vs. temperature (**Figure 3.6a**). A sudden shift of viscosity occurred at the phase change from liquid form to gel form, which can define the necessary phase-transitional concentration for electrolytes. The result shows the temperature when electrolytes transfer from liquid form to gel form reduces as the concentration of the P407 rises, which implies water-based solution with higher portion of P407 can exhibit in gel-state at lower temperature. This thermogelation property can arise from the interconnections between various portions of the polymer (**Figure 3.6b**).[231] As the temperature rises, the PO blocks that are hydrophobic in the polymer tend to dehydrate and

the molecules begin to shape in spherical structures. Followed by this step, the gel-state will show due to the oriental pack of the sufficient focused samples. Therefore, the higher concentration can enhance the gelation process which consequence the less needed temperature for the thermogelation process.

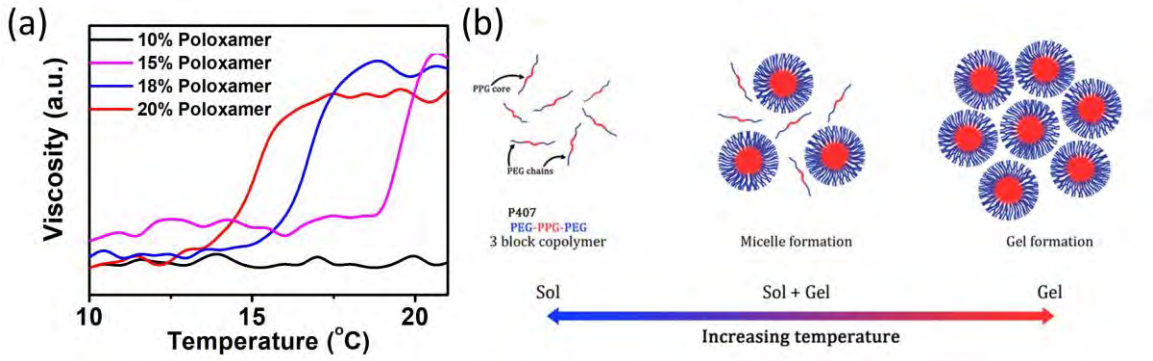

Figure 3.6 Sol-gel phase transition of Poloxamer 407 with different concentrations. (**a**) Viscosity of poloxamer 407 aqueous solutions with different concentrations. (**b**) Micellization and gel formation of Poloxamer 407 in the aqueous medium. When the concentration of Poloxamer 407 is raised when the temperature is raised above CMT, micelles are generated by the binding between hydrophobic groups in the center of the triple copolymer Poloxamer 407. When the concentration of Poloxamer 407 is further raised or the temperature is further raised, a gel composed of micelles is formed.[232]

3.3.2 Thermopower

In order to explore the TE performances of the i-TE materials, the output should be measured. One of the most important characteristics is the output S_i of the i-TE system. The i-TE systems without phase change or before phase change are investigated at first. As

shown in **Figure 3.7**, the thermopower of the solution (1 M/L LiCl + 10% (w/v) P407) is around 2-3 mV/K at room temperature and seems to have no relations with the temperature. At such low concentration, phase change can merely be observed in this system, which means it exhibited in liquid-state at room temperature. The thermopower, however, is still fairly unsatisfied when comparing with previous outputs and is at the same level with the thermopower of the thermogalvanic cells.[128,233,234] I-TE systems with other components (e.g. NaCl, KCl, $NaNO_3$ with 10% (w/v) P407) are investigated and show similar results to that of the LiCl poloxamer system (**Figure 3.7**).

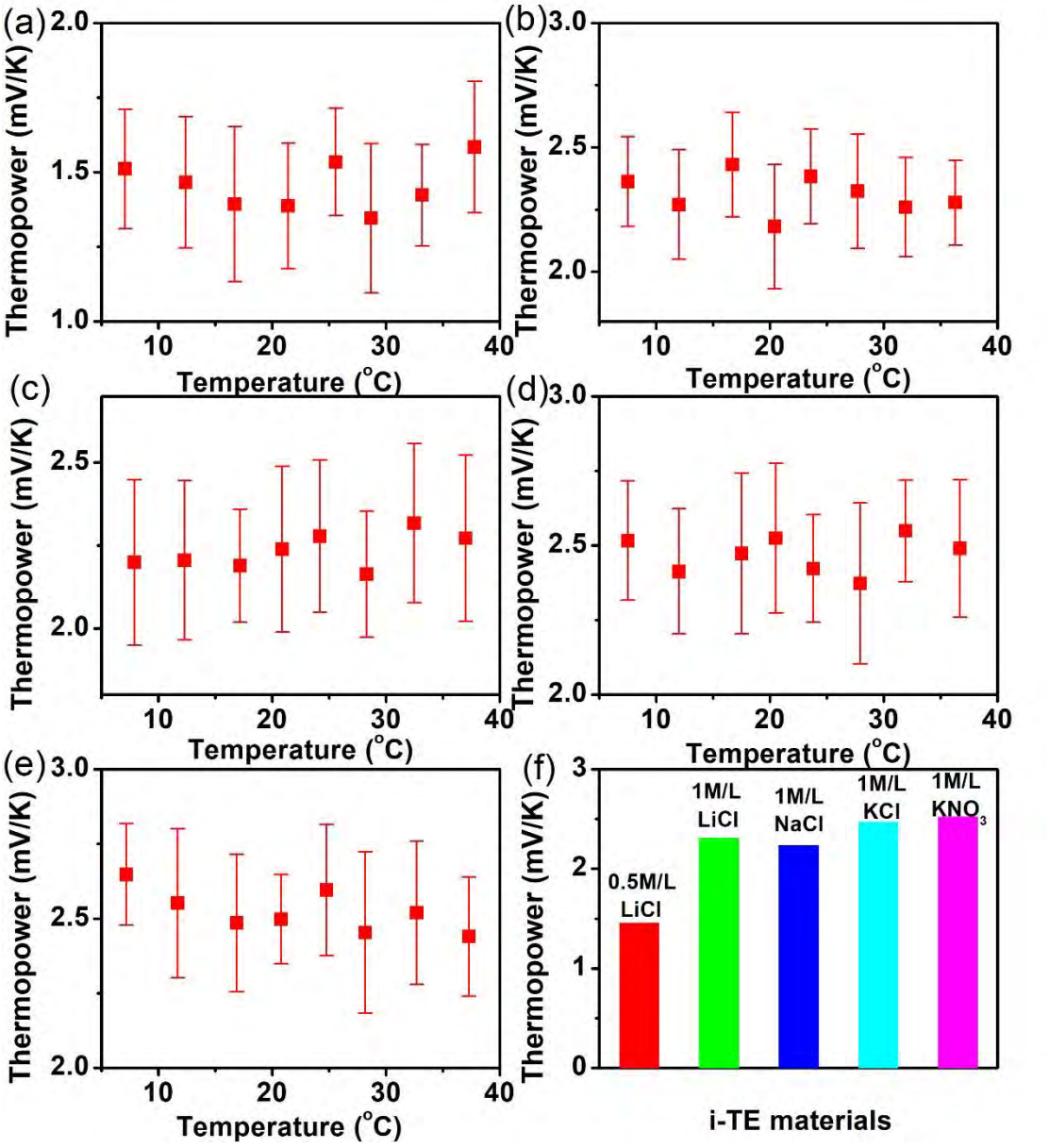

Figure 3.7 Thermopower-temperature relationship of the salt/10% (w/v) P407 systems. Temperature-dependent thermopower of **a.** 10% (w/v) P407-based 0.5 mol/L LiCl ionic solution. **b.** 10% (w/v) P407-based 1 mol/L LiCl ionic solution. **c.** 10% (w/v) P407-based 1 mol/L NaCl ionic solution. **d.** 10% (w/v) poloxamer 407-based 1 mol/L KCl ionic solution. **e.** 10% (w/v) poloxamer 407-based 1 mol/L KNO_3 ionic solution. **f.** Summary of the average thermopower from **Figure 3.7 a** to **e**.

Then i-TE material systems with phase change are studied. P407 water-based solutions with higher portion and various molal concentration of the Li ion were explored. Due to the limitations from the solubility of the ion providers and ability of phase change, the appropriate molal concentration of the ions in this work should be 1 M/L. Furthermore, the concentration of the P407 solution was chosen between 15 – 20% (w/v) to meet the constraints of phase change between liquid and gel under room temperature. Therefore, 1 M/L LiCl with 18% (w/v) P407 solution was chosen as target and 1 M/L LiCl with 20% (w/v) P407 solution was selected for contrast.

By shifting T_{cold} within the range of 5 ~ 35°C, the measured S_i of the ionic system fluctuates from 2 mV/K to more than 15 mV/K (**Figure 3.8a**). The S_i of the ionic system achieves a highest value of around 15.4 mV/K at around 17.4 °C, when the i-TE system change from liquid form to gel form (**Figure 3.8c**). However, when the temperature is lower than $T_{transition}$, the ionic system acts as a regular liquid and the thermopower of the system is relatively small (around 2-3 mV/K), which is comparable to the S_i of the i-TE system without transition behavior which consists of 10 % (w/v) P407 and 1 M/L LiCl.

After the phase transition, the appearance of i-TE system is similar with common hydrogels and the S_i of the gel system is also fairly small (around 2-3 mV/K), which is comparable to that of the system in liquid state. The S_i of the target materials appears to not have an apparent change in total liquid or gel form and seems to have no dependency on the portions of the P407 solution. Consequently, the massive improvement (6.5 folds) of the S_i of the i-TE system during the phase-transition may attribute to the change of ionic movements in various states of the electrolytes. For further verification this finding, similar i-TE system was selected but with higher portion of the P407 solution, which can modify the

temperature when the phase changes. **Figure 3.8b** shows the relations between S_i and temperature in the ionic system consists of 20% (w/v) P407 and 1 M/L LiCl. Likewise, the S_i of the 20% (w/v) P407 system displays a highest value of around 9.8 mV/K at around 16.9 °C, which is also the temperature for this system to experience the liquid-to-gel transition (**Figure 3.8d**).

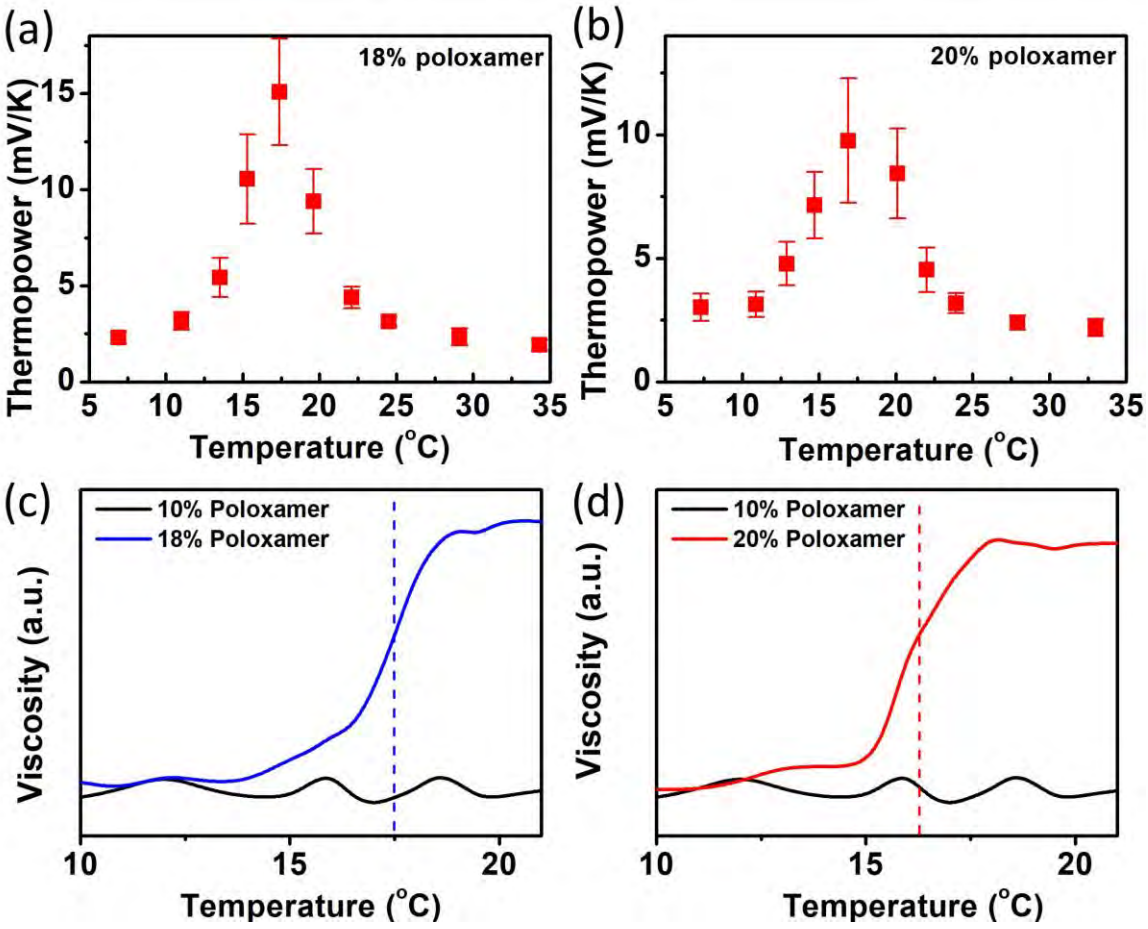

Figure 3.8 Thermopower and viscosity of the transitional i-TE materials. a. Thermopower-temperature relationship of the **a.** 18% (w/v) P407 + 1 M/L LiCl ionic **b.** 20% (w/v) P407 + 1 M/L LiCl ionic solution. Viscosity of the ionic system with **c.** 1 M/L LiCl in 10% and 18% (w/v) P407 aqueous solutions. **d**. 1 M/L LiCl in 10% and 20% (w/v) P407 aqueous solutions.

A question may arise that if it can be possible to switch the change route of phase transition and generate a giant decrease in S_i of a i-TE system with phase change behaviors? The response should be positive. The response can be realized in another type of i-TE system by using 1 M/L LiCl with 2% (w/v) Aga. aqueous solution. Different from P407, the Aga. water-based solution change from gel to liquid when the temperature increases, which is contrary to the path of phase change of poloxamer 407.[235] **Figure 3.9a** shows the relations between the S_i and temperature of the Aga.-based i-TE system. It is apparent that a rapid decrease of the S_i appears when the temperature is around 30 ℃, which is also within the range of temperature where phase starting to change (**Figure 3.9b**).

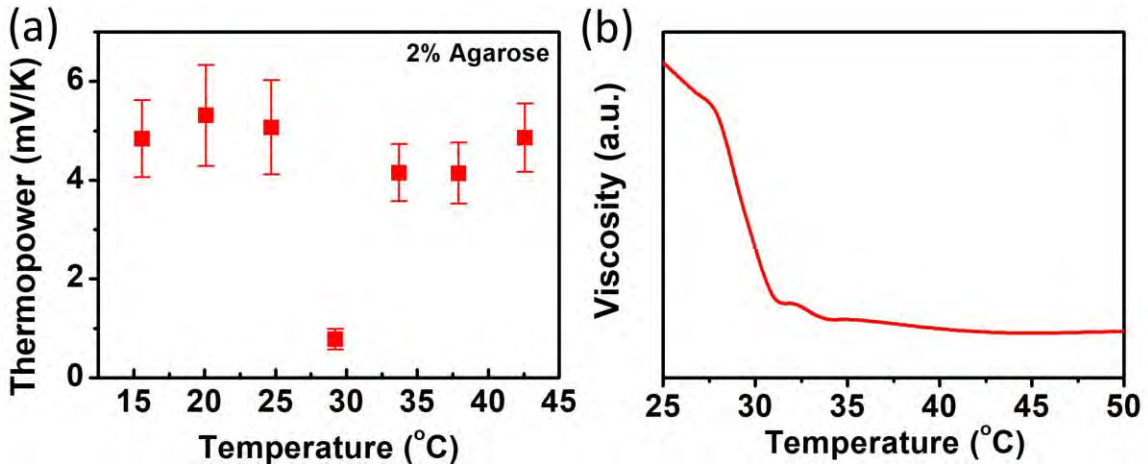

Figure 3.9 Characterization of a gel-to-liquid phase transition i-TE system. a. Thermopower-temperature relations of the 2% (w/v) Agarose + 1 mol/L LiCl ionic solution. **b.** Viscosity of the 2% (w/v) Agarose + 1 mol/L LiCl ionic solution. The viscosity test was conducted at the sequence from high T to low T.

3.3.3 Thermal, electrical conductivity and ZT values

Apart from thermopower, electrical conductivity and thermal conductivity are another two important factors that can affect ZT of the i-TE system. Therefore, next step should be measuring the thermal conductivity and electrical conductivity of the 1 mol/L LiCl/18% (w/v) P407 i-TE system to obtain the electrical outcomes and ZT. Traditional techniques to assess the σ of solid-state materials cannot be utilized to materials in liquid form. Consequently, the electrical impedance was evaluated in the beginning and relative σ was analyzed from the real part of the impedance from the quantity results from near zero phase angle region. **Figure 3.10** show the electrical impedance of the 1 mol/L LiCl with 18% (w/v) P407 i-TE system at near room-temperature.

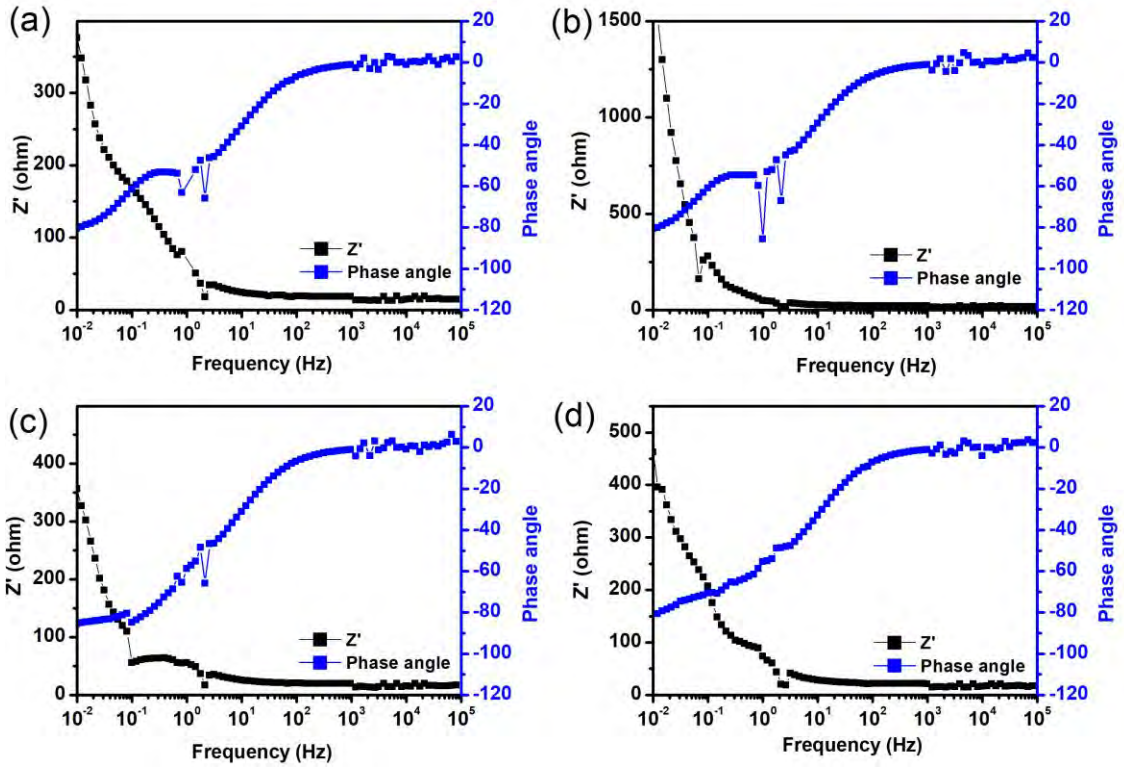

Figure 3.10 Bode's plot of 1 mol/L LiCl + 18% (w/v) P407 i-TE material at different temperature. a. EIS figure (Bode's plot) of the i-TE materials at 10 °C. **b.** EIS figure (Bode's plot) of the i-TE materials at 15 °C. **c.** EIS figure (Bode's plot) of the i-TE materials

at 20 °C. **d.** EIS figure (Bode's plot) of the i-TE materials at 30 °C. The electrical conductivity can be calculated from the impedance when phase angle is close to 0°. In this work, the impedances are chosen from high frequency regions.

When the temperature shifts, the electrical impedance of the i-TE systems seems have no obvious relation to the temperature, which means the phase-transition caused by the shift of temperature may not impact the impedance of the i-TE system. The electrical conductivity of the i-TE system, which can be directly assessed from the electrical impedance, nearly has no temperature dependency and the phase-transition has almost no effects on the electrical conductivity (**Figure 3.11a**). This result may attribute to the target material in this experiment shares the same working properties with a capacitor. **Figure 3.11b** displays the measured κ of the i-TE system at room temperature range. It is quite similar to the quantity of DI water (0.5 W/(m·K)) and almost experiences no change when temperature changes. Consequently, the S_i of the i-TE is the most important parameter to influence the TE properties when temperature changes.

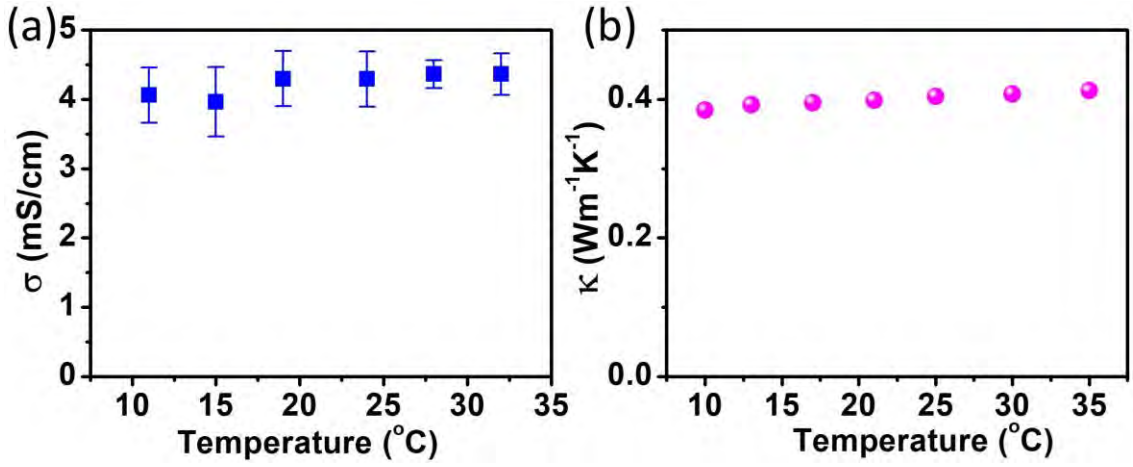

Figure 3.11 Electrical and thermal conductivity of the i-TE system. a. Electrical conductivity of 18% (w/v) P407 + 1 mol/L LiCl ionic solution. The electrical conductivity was attained from the EIS at high frequency region. **b.** Thermal conductivity of the 18% (w/v) P407 + 1 mol/L LiCl ionic solution.

However, distinct from the electronic TE materials, the output of the i-TE materials is not stable, which means the i-TE materials cannot generate a constant output current without decay. Normally, the i-TE systems based on thermodiffusion effect are working in capacitance mode, which is because the cations/anions cannot pass through the interfaces between the electrolyte and electrodes. **Figure 3.12** shows the cyclic voltammetry curves of the 18% (w/v) P407-based 1 mol/L LiCl ionic solution under room temperature. The rectangle shape of the curve indicates similar working properties of this material with capacitors.

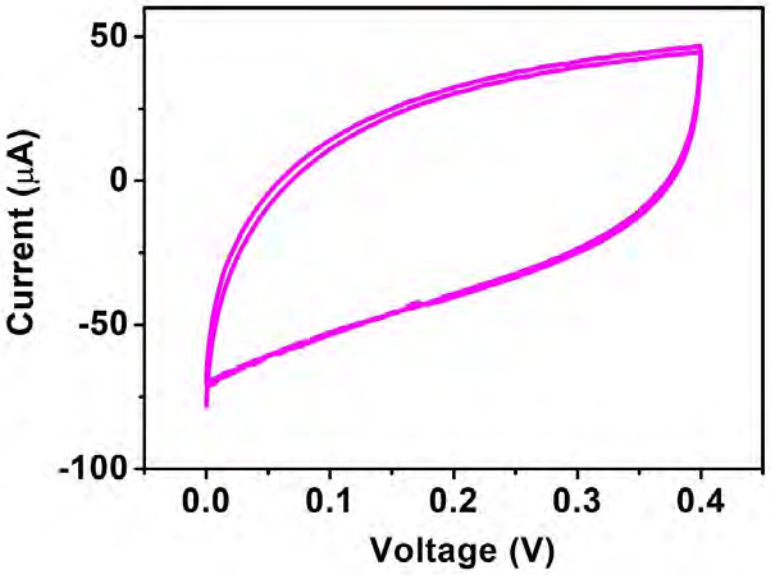

Figure 3.12 Cyclic voltammetry curves of the 18% (w/v) P407-based 1 mol/L LiCl ionic solution under room temperature. The scan rate is 50 mV/s. The rectangle shape of the curve proofs the i-TE system working in capacitance mode.

After measuring the required parameters of the i-TE systems, ZT_i can be calculated to illustrate the efficiency for energy conversion of the target materials (**Figure 3.13**). Similar with the ZT in electronic TEG, ZT_i can be calculated as $ZT_i = S^2\sigma T/\kappa$, where S, σ and κ represent the related parameters for ions. Nevertheless, the i-TE materials that have the identical ZT value of the conventional electronic TEGs will possess lower efficiency,[119] which is because the ionic thermodiffusive cells working as capacitors and power generated will decay with time. Even so, ZT_i can also be regarded as an essential parameter to illustrate the efficiency of the i-TE materials.[11] The relations between the converting efficiency and ZT_i will be illustrated in next chapters. The ZT_i experiences a sudden

increment of around 23 folds (less than 0.03 to 0.68) at the temperature for phase change of the i-TE material. Furthermore, the maximum converting efficiency can be calculated according to previous methods and the efficiency of the i-TE cells increases from 3.08×10^{-5} to around 6.18×10^{-4} (more than 20 times) during phase transition.[119]

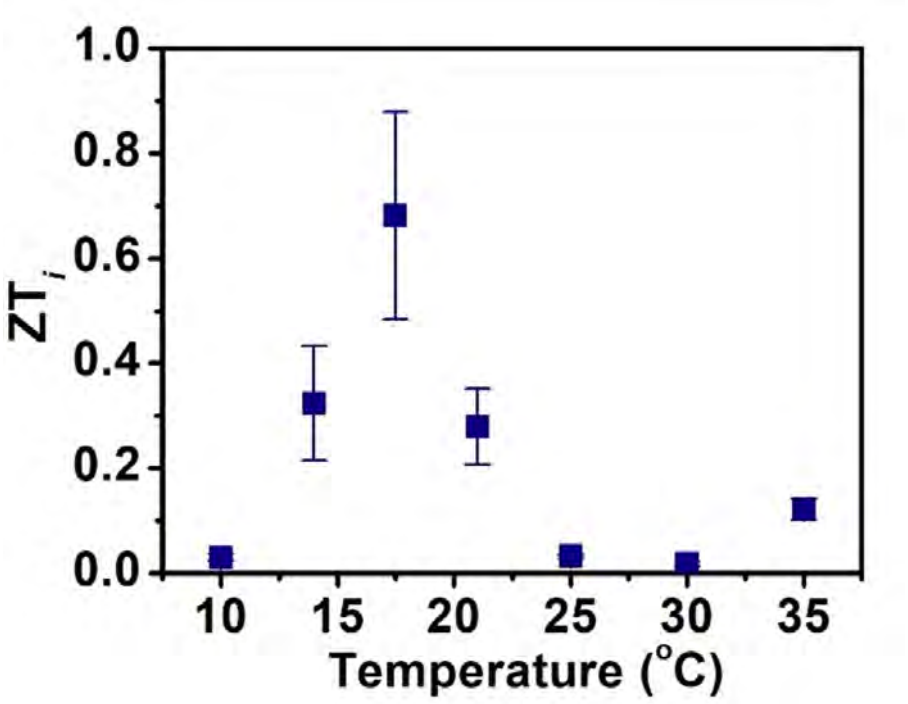

Figure 3.13 Temperature-ZT_i relations of 18% (w/v) P407-based 1 mol/L LiCl ionic solution.

3.4 Summary

A giant effect of phase change from liquid to gel on S_i can be achieved from three different kinds of i-TE systems. This is the first time that reporting the giant enhancement of thermopower (6.5 folds) and ZT_i (23 folds) in P407/LiCl i-TE system when experiencing

the phase change from liquid to gel. A positive S_i of around 15.4 mV/K has been attained at around 17.4 ℃ when the phase of the i-TE system started to change, comparing with a thermopower of around 2.5 mV/K at low temperature (before phase transition). The increase of thermopower can also be observed in i-TE systems with different concentrations of P407 which will result in phase change from liquid to gel at different temperature. On the contrary, the thermopower can drop rapidly in Agarose/LiCl i-TE system when it change from gel to liquid by increasing the temperature.

CHAPTER 4 Mechanisms and theoretical models

Chapter 3 has demonstrated the TE performances of different i-TE systems from different aspects and observed a quite interesting result. This chapter will explore this result and try to illustrate the reasons or mechanism behind these phenomena by establishing a theoretical analysis model.

4.1 TE performances of the i-TE cells

As mentioned from the previous chapter, the direct measurements of the TE performances for liquid-state TE materials are quite difficult. Therefore, all the measurements should be conducted after fabricating the liquid-state i-TE materials into test cells, which means the measured result should be the TE performances of the test cells but not that of i-TE materials. However, in previous chapter, the measured values of the i-TE cells, especially the output thermopower, were directly used as the parameter of the i-TE materials. This kind of substitution needs to be examined. So, in this part, I'll use a multiphysics simulation method (COMSOL) to examine the reliability of this substitution by comparing the S of TE composites with different components. The details of the simulation will be demonstrated in Appendix I. The result shows that when the size of the electrodes and framework are quite small (less than 0.1) when comparing with the volume of i-TE materials, the TE performances of the frameworks or electrodes can be neglectable, which

justified that the measured TE properties of the i-TE cells can be taken as the TE properties of the i-TE materials inside the cells.

4.2 Mechanisms of ionic thermodiffusion

4.2.1 Illustration of thermopower

Previous chapter introduced a very interesting increase of thermopower from the i-TE materials during phase-transition. The thermodiffusive thermopower can have an increase of 6.5 folds during phase transition. The key point to find out the reason behind this phenomenon is to derive the thermopower by the motions of ions. The thermodiffusive thermopower or ionic Seebeck coefficient is defined as

$$S_i = -\frac{V(T_H)-V(T_C)}{\Delta T} \tag{4.1}$$

where $V(T_H)$ and $V(T_C)$ represent the voltage at the hot temperature T_H and cold temperature T_c, respectively.

The sign of S in an i-TE system is defined by the kind of ion that possesses higher thermal mobility in the solution, which is quite different from the conventional TE materials whose sign is determined by the types of major carriers.[10] Hence, the ionic transportations that driven by temperature difference, which can also be called as the Soret effect, can be an important point to verify the thermopower of the i-TE system. The temperature difference can generate the movements of the ions from the hot side towards the cold side under most conditions while the mass diffusion process also pushes the ions from the region with high concentration to region with low one, which means a concentration difference will be

created under these two effects.[236] Furthermore, we can also separate the diffusive movements of ions as the result from two forces with opposite directions, namely the driving forces from the thermal source and concentration source, respectively. Finally, when steady, most of the ions with different signs should locate in the cold temperature region and the S_i is directly related to the concentration differences between the different ions at different sides.

Onsager's theory for irreversible processes can be a fundamental framework for knowledge of the ion's motions.[46,47] Onsager's theory can express the system with two current flow which both can affect each other, such as the heat and mass flow in this system. The ionic flux and the internal energy flux of the ions can be described by Onsager relations as:

$$J_i = L_{ii}X_i + L_{iq}X_q \tag{4.2}$$

$$J_q = L_{qi}X_i + L_{qq}X_q \tag{4.3}$$

where X_i and X_q can be taken as the driven force of the ion flux and heat flux while the $L_{ii}, L_{iq}, L_{qi}, L_{qq}$ are the transport coefficient, respectively. In this system, the driven force of the certain flux can be expressed as:

$$X_i = -\frac{1}{T}\nabla\mu \tag{4.4}$$

$$X_q = -\nabla\frac{1}{T} \tag{4.5}$$

where μ is chemical potential while T is temperature. The details about the Onsager relations and the expression of the transport coefficients will be listed in the Appendix II. Meanwhile, the Onsager relations should ensure that $L_{iq} = L_{qi}$. Note that, in this system,

the chemical potential should be taken as the electrochemical potential which consists of the chemical potential of the ions and the electric potential of the electric field formed by the ions. Therefore, the electrochemical potential in this system should be defined as:

$$\widetilde{\mu_i} = \mu_i[n_i(r), T(r)] + q_i V \tag{4.6}$$

where the chemical potential μ_i can be expressed as the functional of concentration $n_i(r)$ and temperature $T(r)$. Then based on equation 4.6, the gradient of the electrochemical potential can be expressed as:

$$\nabla\widetilde{\mu_i} = \frac{\partial \mu_i}{\partial n_i}\nabla n_i + \frac{\partial \mu_i}{\partial T}\nabla T + q_i \nabla V \tag{4.7}$$

By Maxwell's relations, the partial derivative of chemical potential over partial derivative of temperature should be expressed as:

$$\frac{\partial \mu_i}{\partial T} = -\frac{\partial S}{\partial n_i} = -s_i \tag{4.8}$$

where s_i is the partial entropy and S is the total entropy of the system. In ideal cases, the chemical potential can be expressed as:

$$\mu_i = {\mu_i}^{pure} + k_B T ln\frac{n_i}{N} \tag{4.9}$$

Therefore, the partial derivative can be expressed as:

$$\frac{\partial \mu_i}{\partial n_i} = \frac{k_B T}{n_i} \tag{4.10}$$

In this system, the parameter L_{ii} and L_{Qi} are be expressed as:

$$L_{ii} = \frac{n_i D_i}{k_B} \tag{4.11}$$

$$L_{iQ} = \frac{\overline{\overline{Q_i}}}{T} = \overline{\overline{s_i}} \tag{4.12}$$

where the $\overline{\overline{Q_i}}$ represents the heat of transport and $\overline{\overline{s_i}}$ represents the entropy of transport. Therefore, the ion flux from equation 4.2 can be written as:

$$J_i = -D_i\left[\nabla n_i + \frac{q_i n_i}{k_B T}\nabla V + \frac{(\overline{s_i} - s_i)n_i}{k_B T}\nabla T\right] \tag{4.13}$$

In open circuit conditions, there's no net current carried by ions, then:

$$\sum_i q_i J_i = 0 \tag{4.14}$$

If we assume the system is in near equilibrium, then the concentration profile can be expressed as:[10]

$$n_i(r) = n_i^0 + \delta n_i(r) \tag{4.15}$$

where $\delta n_i \ll n_i^0$. Besides, to analyze the mechanism in the system, some similarity conditions can be taken, which means the ΔV and ΔT across the device in near equilibrium state can be set a quite small value. Therefore, they can be expressed as:

$$\frac{q_i}{k_B T}\nabla V \ll \frac{n_i^0}{\delta n_i}, \tag{4.16}$$

$$\frac{(\overline{s_i} - s_i)n_i}{k_B T}\nabla T \ll \frac{n_i^0}{\delta n_i} \tag{4.17}$$

Then equation 3.14 can be expressed as:

$$-q_i D_i\left[\nabla \delta n_i + \frac{q_i n_i^0}{k_B T}\nabla V + \frac{(\overline{s_i} - s_i)n_i^0}{k_B T}\nabla T\right] = 0 \tag{4.18}$$

Besides, due to the previous approximation, the term $\nabla \delta n_i$ can also be neglected. Then the S_i can be expressed as thermodiffusive thermopower, which is:

$$S_{td} = -\frac{\nabla V}{\nabla T} = \frac{\sum q_i(\bar{\bar{s}}_i - s_i) n_i D_i}{\sum {q_i}^2 n_i D_i} \tag{4.19}$$

For symmetric electrolytes like LiCl, $q_+ = q_-$ and $n_+^0 = n_-^0$. Therefore, in non-phase-transition system (either total liquid or high viscosity gel system), equation 4.19 can be simplified into:

$$S_{td} = \frac{D_+ \hat{S}_+ - D_- \hat{S}_-}{e(D_+ + D_-)} \tag{4.20}$$

where $\hat{S}_i = \bar{\bar{s}}_i - s_i$ represents the Eastman entropy of transfer.[43] If expressing the ionic flux in form of $J_i = -n_i {v_i}^T$, where ${v_i}^T$ referred as the thermodiffusion velocity, the thermal mobility can be defined based on the Einstein's relation as:

$$\mu_i^T = \frac{D_i \hat{S}_i}{k_B T} \tag{4.21}$$

Besides, the ionic mobility is defined as:

$$\mu_i^I = \frac{D_i}{k_B T} \tag{4.22}$$

From equation 4.21 and 4.22, the Eastman entropy of transfer can also be taken as the ratio between thermal mobility and ionic mobility. In addition, equation 4.20 can be written in another form:

$$S_{td} = \frac{\mu_+^T - \mu_-^T}{q(\mu_+^I + \mu_-^I)} \tag{4.23}$$

Therefore, for ionic system with symmetric electrolytes, the sign of the thermopower is affected by the differences in thermal mobilities of different ions and the increasement of the differences in ionic mobility between different ions could also enhance the thermopower of the system.

Now go back to Equation 4.19. By taking the $\hat{S}_i$ into this equation, the S_{td} of the i-TE materials can be written as:

$$S_{td} = \frac{n_+ D_+ \hat{S}_+ - n_- D_- \hat{S}_-}{e(n_+ D_+ + n_- D_-)} \tag{4.24}$$

In the case of a symmetrical electrolyte like LiCl with ($n_+ = n_-$), equation 4.24 can be simplified as equation 4.20. From the equation 4.20 and 4.24, it can be found out that the diffusion coefficient and the Eastman entropy of transfer are the key points to determine the output thermopower of the i-TE system. **Table 4.1** illustrates the diffusion coefficients of some typical ions in water at 25°C. From the data of this table, H^+ and OH^- seem to be better choices for cations/anions comparing with other ions due to their rather high ionic diffusion coefficient.

Table 4.1 Diffusion coefficient of some different ions in water at 25°C.[3]

Ions	**D (x10^{-9} m^2/s)**	**Ions**	**D (x10^{-9} m^2/s)**
H^+	9.132	OH^-	5.192

Li^+	1.030	F^-	1.474
Na^+	1.333	Cl^-	1.970
K^+	1.893	Br^-	2.079
Rb^+	2.071	I^-	2.160
Cs^+	2.055	IO_3^-	1.041
Ag^+	1.647	IO_4^-	1.451
Mg^{2+}	1.411	HCO_3^-	1.118
Fe^{2+}	1.437	CO_3^{2-}	1.892
Fe^{3+}	1.810	SO_3^{2-}	1.916
Ba^{2+}	1.693	SO_4^{2-}	2.130
Cr^{3+}	1.783	ClO_3^-	1.719
Co^{3+}	0.905	ClO_4^-	1.791

4.2.2 Eastman entropy of transfer

Apart from diffusion coefficients, $\hat{S}_i$ is also another important factor to determine the output S_{td} of the i-TE system. This entropy can be calculated from the heat of transport Q^*, which is:

$$Q^* = -(\frac{\partial \mu}{\partial m})_{P,T} \frac{dm}{dlnT} \tag{4.25}$$

where m is molality of the solution.[43] Now consider the transfer of a single ion and take the ions as spherical ions. The ions will transport across the plane BB under the driven by the temperature gradient (**Figure 4.1**). For the calculation of heat of transport for a single ion, the heat of transport can be taken as the quantity of heat progressed to the right of this reference plane (plane B). To maintain steady state by a reverse process when the heat pass ahead of the ion, the heat should be absorbed behind the ion. Therefore, the same amount of heat should be extracted from the left of the reference plane B.

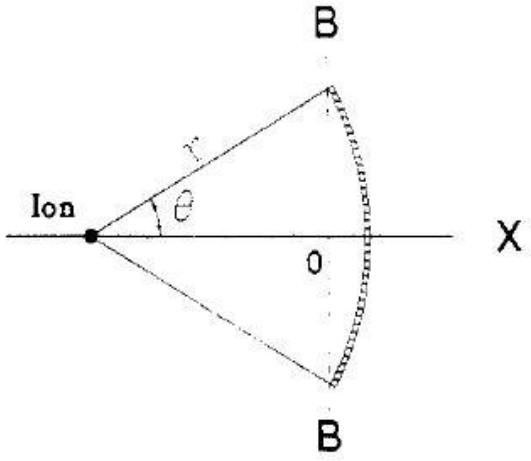

Figure 4.1 Hydrodynamic result of the single-ion heat of transport.[52] Q^* is the total amount of heat evolved to the right of plane B when the ion is transported across the plane B from the left side to the right side of the plane.

Now, suppose ions transporting in x direction with constant velocity **V** under a force **F**. The density of entropy of the solvent at distance r from ions is S and the velocity of the solvent relative to ion is $\mathbf{v_s}$.

Then,

$$\frac{dS}{dt} = \frac{\partial S}{\partial t} + \boldsymbol{v_s} \cdot \nabla S \tag{4.26}$$

The ion is assumed to be a sphere, so the irregularity of the entropy density owing to the ionic motion can be ignored and Equation 4.26 can be written into:

$$-T\frac{dS}{dt} = -\frac{dQ}{dt} = q = -Tv_s\frac{\partial S}{\partial r} \tag{4.27}$$

The radial velocity of the solvent $\mathbf{v_s}$ can be expressed as the value at $r = \infty$ as

$$v_s = v_\infty f(r)cos\theta \tag{4.28}$$

where θ is angle differences between the direction of **V** and **r**. By letting $f(r) = 1$ at $r = \infty$, $v_\infty = -V$, then q can be expressed as:

$$q = TVf(r)\left(\frac{\partial S}{\partial r}\right)cos\theta \tag{4.29}$$

Here, the *q* represents the local rate of heat evolution to the velocity. Therefore, the amount of heat evolved by the solvent lying inside the spherical structure between *r* and *r* + *dr* during the time interval *dt* can be written as:

$$dQ = 2\pi r^2 dr\left(\int_0^\theta qsin\theta d\theta\right)dt \tag{4.30}$$

Take Equation 4.29 into Equation 4.30,

$$dQ = 2\pi TVf(r)\frac{\partial S}{\partial r}r^2 dr\frac{sin^2\theta}{2}dt \tag{4.31}$$

When $\theta = \pi$, whole ion is located at the right side of the plane. Therefore, by taking $t = 0$ at $x = 0$, the time interval can be taken from *t = -r/V to t = r/V*. In Equation 4.31, $x =$

Vt and $sin^2\theta = \frac{r^2-x^2}{r^2}$. Therefore, the contribution from the ion shell to the heat of transport can be expressed as:

$$dQ^* = T(\frac{4\pi}{3})f(r)\frac{\partial S}{\partial r}r^3 dr \tag{4.32}$$

Then the total heat can be expressed as:

$$Q^* = T(\frac{4\pi}{3})\int f(r)\frac{\partial S}{\partial r}r^3 dr \tag{4.33}$$

Equation 4.33 can be taken as the fundamental hydrodynamic expression for the heat of transport of single ion at infinite solution. In analysis of real cases, Q is better to be written in terms of *S(r)* instead of partial form, which is:

$$Q^* = -T(\frac{4\pi}{3})\int_{R_i}^{\infty}[S(r)-S(\infty)]\frac{\partial}{\partial r}[r^3 f(r)]dr \tag{4.34}$$

At the limit, *f(r)* → 1. Equation 4.34 can be written as:

$$Q^* = -T\int_{R_i}^{\infty}[S(r)-S(\infty)]4\pi r^2 dr \tag{4.35}$$

In addition, from Born theory:

$$S(r)-S(\infty) = (\frac{e^2Z^2}{8\pi r^4\varepsilon^2})\frac{\partial\varepsilon}{\partial T} \tag{4.36}$$

Then the Eastman entropy can be expressed as:

$$\hat{S} = -\frac{(eZ)^2}{\varepsilon^2}\frac{\partial\varepsilon}{\partial T}\frac{1}{4R} \quad \text{(stick)} \tag{4.37a}$$

or

$$\hat{S} = -\frac{(eZ)^2}{\varepsilon^2}\frac{\partial \varepsilon}{\partial T}\frac{1}{3R} \quad \text{(slip)} \tag{4.37b}$$

From the Equation 4.37, it can be observed that the heat of transport from single ions is closely related to the radius of the ions and the dielectric constant of the solute. Therefore, the large differences between the radius of cations and anions can contribute greatly to enhance the S_i of the i-TE system. However, it should be marked that the radius here is not simply the radius of the atoms or ions. The radius in this analysis should be the radius of the ions with water molecules accompanied around them, including the region of immobilization of water molecules and the region of 'structure breaking'.[237] **Table 4.2** shows the calculated heat of transport (which can be used to calculate Eastman entropy) of different single ions at infinite aqueous solution.

Table 4.2 Q^* at infinite aqueous solution for single-ion.

Ions	Heat of transport (10^3 J/mol)	Ions	Heat of transport (10^3 J/mol)
H^+	13.3	Li^+	0.53
Na^+	3.46	K^+	2.59
Rb^+	3.91	Cs^+	4.01
NH_4^+	1.73	Ag^+	6.37
Tl^+	4.33	Mg^{2+}	9.04
Ca^{2+}	9.8	Sr^{2+}	11.1

Ba^{2+}	12.4	Ni^{2+}	9.3
OH^-	17.2	F^-	3.93
Cl^-	0.53	Br^-	0.60
I^-	-1.55	NO_3^-	-0.63
ClO_4^-	-0.31	IO_4^-	2.00

Similar with the result from **Table 4.1**, the Eastman entropy of transfer also indicates the choices of H^+/OH^- are superior compared with other counterparts.

4.3 Analysis of ionic transportations

Last part has demonstrated the illustrations of thermopower by Onsager's relations. In i-TE system with only one kind of cation and one kind of anion, the thermopower of the system can be expressed as:

$$S_{td} = \frac{n_+ D_+ \hat{S}_+ - n_- D_- \hat{S}_-}{e(n_+ D_+ + n_- D_-)} \tag{4.38}$$

where e is charge of electron, n is the concentration of the ion, D is mass diffusion coefficient, $\hat{S}$ is the Eastman entropy of transfer and the sign "+" and "-" represents for the cations and anions, respectively. This model can also be applied to analysis the i-TE systems introduced in **Chapter 3**, which include the phase-transition scenario. In this part, the scenario of the transportations of both cations and anions in an i-TE system should be

studied for different stages, that is, before, during and after the phase-transition, respectively.

4.3.1 Before phase-transition

Firstly, considering **the first scenario** of homogenous electrolyte solution without the phase transition under a temperature gradient is the starting step. **Figure 4.2** demonstrates the movements of different ions in a homogenous liquid-state electrolytes, which can be equivalent to describe the i-TE system before the change of phase.

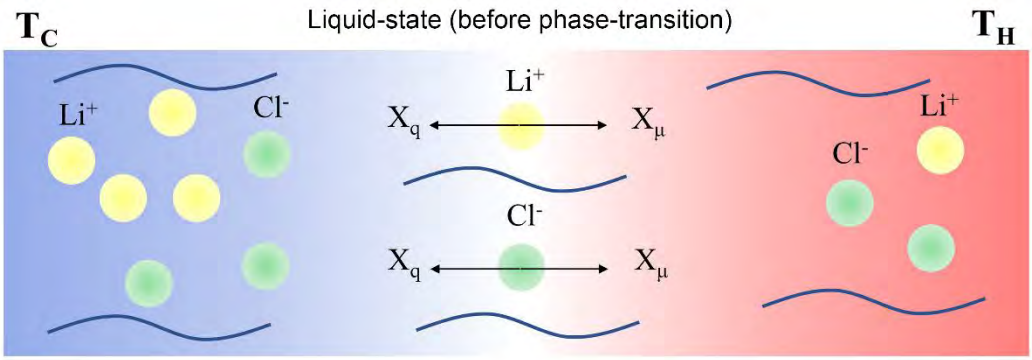

Figure 4.2 Schematic of the diffusion process of cations and anions under a temperature gradient within transitional i-TE system in liquid-state (before phase-transition).

The *D* of the different ions can be taken as a fixed value with the temperature change. In addition, all the ions can move fluently in water-based solution without change of phase, which means the variances between the *D* of different ions can be ignored when analysis the thermodiffusion effect in water-based solutions when comparing it with the thermodiffusion effect in solutions with high viscosity. These conditions can be described as:

$$n_+ = n_-$$

$$D_+ \approx D_-$$

Therefore, by considering these situations, the S_{td} of the i-TE materials for symmetrical electrolyte without phase change can be approximately written in simple form as:

$$S_{td} = \frac{\mathcal{S}_+ - \mathcal{S}_-}{2e} \tag{4.39}$$

From this equation, it can be obviously observed that in aqueous solutions, the thermopower of the symmetrical electrolyte is mostly determined by the heat of transport of the ions during the moving process, which has been verified from the previous works that the heat of transport of Li^+ is larger than that of Cl^- in aqueous solutions.[238] This result is also in good agreement with experiment results that the thermopower of this system is positive.

4.3.2 After phase-transition

The next step is to analysis the transportations of ions after phase transition. In **the second scenario**, competing with the liquid-state system, the transportations of ions in gel-state system or system with high viscosity are quite unique. **Figure 4.3** demonstrates the movements of different ions in a homogenous gel-state electrolytes, which conveys the i-TE materials after phase-transition.

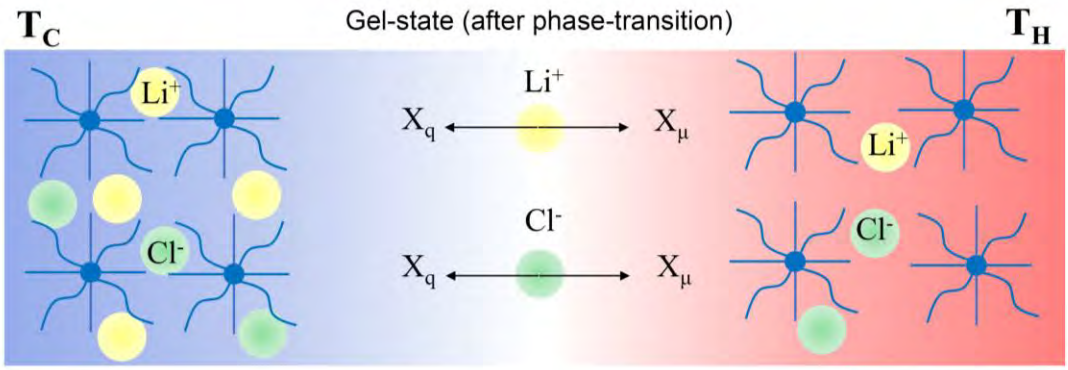

Figure 4.3 Schematic of the diffusion process of cations and anions under a temperature gradient within transitional i-TE system in gel-state (after phase-transition).

When increasing the temperature, the poloxamer 407 molecules have a tendency to create a net grid and form gels with higher viscosity. In viscous system, due to the variations of dimensions or shapes of different ions, the diffusion coefficient of the ions could be distinct from each other. The change of D under temperature gradient in homogenous system without phase transition can still be ignored and the situations in this case can be stated as:

$$n_+ = n_-$$

$$D_+ \neq D_-$$

Then the Equation 4.38 can be simplified into:

$$S_{td} = \frac{D_+ \hat{S}_+ - D_- \hat{S}_-}{e(D_+ + D_-)} \tag{4.40}$$

D of anions can be taken as a reference constant and the value of the cations as a specific ratio k to that of anions for simplification of the equation, which means Eq. 4.38 can be simplified into:

$$S_{td} = \frac{k\hat{S}_+ - \hat{S}_-}{(1+k)e} \quad (4.41)$$

Previous works indicated the proportional relationships between the Q^* and hydration energy[239–241], which means that apart from the heat of transport, the differences of diffusion coefficient between different ions could also be significant factors to affect the change of the S_{td} compared with value in liquid-state system. In this system, the differences between the D of different ions are slightly reduced as the appearances of the system change from liquid to gel, which makes the k value in gel-state greater than that in liquid-state. This forecast is also in good conformity with the consequences that the thermopower of the ionic system in high temperature (gel-state) is a little higher than that in low temperature (liquid-state).

4.3.3 During phase-transition

In **the third scenario**, during the phase-transition temperature range, the whole system displays a quasi-gel-liquid-state, in which the low temperature part is in liquid-state while the high temperature part in gel-state. **Figure 4.4** demonstrates the motions of different ions in quasi-liquid-gel-state electrolytes.

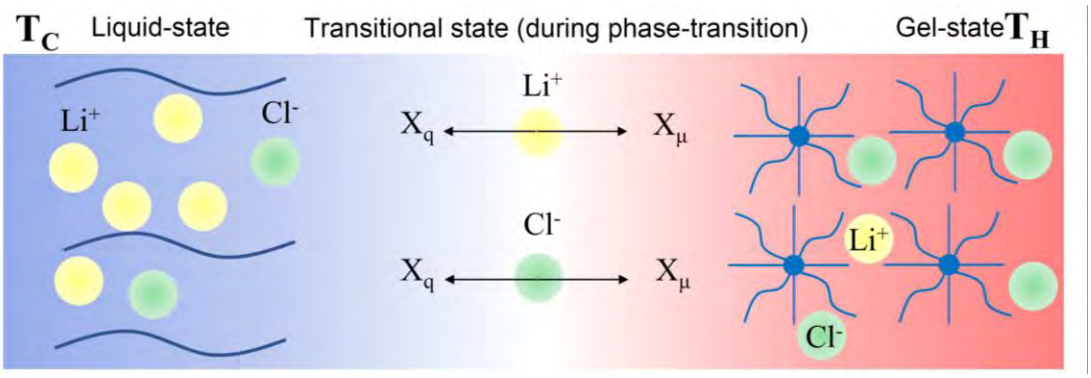

Figure 4.4 Schematic of the diffusion process of cations and anions under a temperature gradient within transitional i-TE system in quasi-state (during phase-transition).

Different from the cases that have been discussed, the D of different ions in this scenario is not a fixed value during phase transition. If still ignoring the change of D by change of temperature and considering ions in hot and cold regions (or ions with different D cause by phase-transition) as different ions with different D, Equation 4.38 can be revised into another form as:

$$S_{td} = \frac{\sum \hat{S}_+ n_+ D_+ - \sum \hat{S}_- n_- D_-}{e(\sum n_+ D_+ + \sum n_- D_-)} \tag{4.42}$$

However, geometrical description of phase change should be quite complicated since the phase transition should be a quite complex process. Hence, this project will not establish a model that can geometrically describe the boundaries of each phase and set a model to solve this difficulty by another aspect, which is by treating the ions moving in different phases as ions with different parameters (D and $\hat{S}$). Then sigma symbol in Eq. 4.42 can be expressed as the sum value of the different parameters of different ions. In hybrid-state system, the D of the ions will change as the environment changes. Nevertheless, it still be

quite complicated to numerically describe the D of each ion at different position in the phase-transitional system.

Therefore, the ratio of thermopower during and before the phase transition (γ) can be defined as a function of six dimensionless parameters, that is, ratios of concentrations of cations (a_+) and anions (a_-) at cold ends to total concentration, ratios of diffusion coefficients of cations (b_+) and anions (b_-) in gel-state to that in liquid-state, ratios of diffusion coefficients of cations to anions (k) in liquid-state and ratio of Eastman entropy of cations to anions (l).

4.3.4 Analysis model

The previous derivations about the thermopower in non-transitional and transitional states can be further explored for the possible explanation of the large variations of the thermopower of i-TE system during sol-gel phase-transition. Now is time to make the following assumptions based on some approximate conditions. If assuming that the size of the i-TE cell is quite small and almost all the ions are distributed at the ends (both hot and cold) of the cell, the concentrations of both cations and anions at different ends can be taken as $n_{+,hot}$, $n_{-,hot}$, $n_{+,cold}$, $n_{-,hot}$, respectively. As the salts are symmetric electrolytes, the total concentration of both cations and anions can be assumed as n_0. Therefore, the concentrations of ions at different ends of a cell can be expressed as:

$$n_{+,cold} = a_+ n_0 \,,$$

$$n_{+,hot} = (1 - a_+) n_0$$

$$n_{-,cold} = a_- n_0$$

$$n_{-,hot} = (1 - a_-) n_0 \tag{4.43}$$

where a_+, a_- represent the ratio of the concentrations for cations and anions at cold ends to the total concentration, respectively. We can take that both a_+ and a_- as constant when the ions transport to a stable state without output current (or open circuit)

During the phase change from liquid to gel of the LiCl/P407 system, the *D* of both cations and anions change significantly. If we ignore the temperature effects on diffusion coefficient and only consider the changes caused by the change of phase, it should be reasonable to assume that the diffusion coefficients of both cations and anions as constants. Meanwhile, during the sol-to-gel transition, the hot side of the i-TE system act as gel-state and cold side act as sol-state. Therefore, the diffusion coefficients of cations and anions at hot side, which can also be regarded as the diffusion coefficients of them in gel, can be expressed as:

$$D_{+,hot} = b_+ D_{+,cold} = b_+ D_+$$

$$D_{-,hot} = b_- D_{-,cold} = b_- D_- \tag{4.44}$$

where $D_{+,hot}, D_{+,cold}, D_{-,hot}, D_{-,cold}$ are diffusion coefficients of cations and anions at hot side and cold side, D_+, D_- are diffusion coefficients of cations and anions in liquid-state system and b_+, b_- are constants, respectively. Besides, by taking the k values into consideration and taking the ratio of Eastman entropy of cations to anions as l. The thermopower of the i-TE system before or after the phase-transition can be expressed as:

$$S_{td,before} = \frac{D_+\hat{S}_+ - D_-\hat{S}_-}{e(D_+ + D_-)} = \frac{(kl-1)\hat{S}_-}{e(k+1)} \tag{4.45}$$

Now taking Equation 4.43 and 4.44 into Equation 4.42, the thermopower of the i-TE system during the phase transition can be expressed as:

$$S_{td,transition} = \frac{\sum \hat{S}_+ n_+ D_+ - \sum \hat{S}_- n_- D_-}{e(\sum n_+ D_+ + \sum n_- D_-)} = \frac{(((1-a_+)b_+ + a_+)kl - ((1-a_-)b_- + a_-))\hat{S}_-}{e\left((1-a_+)b_+ + a_+\right)k + ((1-a_-)b_- + a_-)} \tag{4.46}$$

Then the ratio of the thermopower during phase-transition to the thermopower before phase transition (or the thermopower in liquid-state) can be expressed as:

$$\gamma = \frac{S_{td,transition}}{S_{td,before}} = \frac{(((1-a_+)b_+ + a_+)kl - ((1-a_-)b_- + a_-))(k+1)}{(\left((1-a_+)b_+ + a_+\right)k + ((1-a_-)b_- + a_-))(kl-1)} \tag{4.47}$$

Equation 4.47 is the above-mentioned ratio defined by six dimensionless parameters after doing normalizations. From Equation 4.47, it can be observed that a_+, b_+, a_-, b_-, k and l all can affect the ratio. However, there're some limitations for these parameters. For the i-TE system with positive thermopower and the phase-transition of the system is liquid-to-gel transition, the limitations of these parameters should be:

$$0.5 < a_- < a_+ < 1$$

$$b_+, b_- < 1$$

$$kl > 1$$

The next step is to analyze the effects of different parameters and find out which parameter can contribute more to the change of the ratio. Partial derivation can be a good solution to find out the relations. The partial derivation of the ratio γ with respect to each parameter can be calculated as:

$$\frac{\partial \gamma}{\partial a_+} =$$

$$\frac{(k+1)k(b_+-1)\Big(\big((1-a_+)b_++a_+\big)kl-\big((1-a_-)b_-+a_-\big)\Big)-kl(k+1)(b_+-1)\Big(\big((1-a_+)b_++a_+\big)k+(1-a_-)b_-+a_-\Big)}{(kl-1)\Big(\big((1-a_+)b_++a_+\big)k+(1-a_-)b_-+a_-\Big)^2} =$$

$$\frac{(k+1)k(l+1)(1-b_+)\big((1-a_-)b_-+a_-\big)}{(kl-1)\Big(\big((1-a_+)b_++a_+\big)k+(1-a_-)b_-+a_-\Big)^2}$$

$$\frac{\partial \gamma}{\partial a_-} =$$

$$\frac{(k+1)(b_--1)\Big(\big((1-a_+)b_++a_+\big)k+(1-a_-)b_-+a_-\Big)+(k+1)(b_--1)\Big(\big((1-a_+)b_++a_+\big)kl-\big((1-a_-)b_-+a_-\big)\Big)}{(kl-1)\Big(\big((1-a_+)b_++a_+\big)k+(1-a_-)b_-+a_-\Big)^2} =$$

$$\frac{(k+1)k(l+1)(b_--1)\big((1-a_-)b_-+a_-\big)}{(kl-1)\Big(\big((1-a_+)b_++a_+\big)k+(1-a_-)b_-+a_-\Big)^2}$$

$$\frac{\partial \gamma}{\partial b_+} =$$

$$\frac{(k+1)k(a_+-1)\Big(\big((1-a_+)b_++a_+\big)kl-\big((1-a_-)b_-+a_-\big)\Big)-kl(k+1)(a_+-1)\Big(\big((1-a_+)b_++a_+\big)k+(1-a_-)b_-+a_-\Big)}{(kl-1)\Big(\big((1-a_+)b_++a_+\big)k+(1-a_-)b_-+a_-\Big)^2} =$$

$$\frac{(k+1)k(l+1)(1-a_+)\big((1-a_-)b_-+a_-\big)}{(kl-1)\Big(\big((1-a_+)b_++a_+\big)k+(1-a_-)b_-+a_-\Big)^2}$$

$$\frac{\partial \gamma}{\partial b_-} =$$

$$\frac{(k+1)(a_--1)\Big(\big((1-a_+)b_++a_+\big)k+(1-a_-)b_-+a_-\Big)+(k+1)(a_--1)\Big(\big((1-a_+)b_++a_+\big)kl-\big((1-a_-)b_-+a_-\big)\Big)}{(kl-1)\Big(\big((1-a_+)b_++a_+\big)k+(1-a_-)b_-+a_-\Big)^2} =$$

$$\frac{(k+1)k(l+1)(a_--1)\big((1-a_-)b_-+a_-\big)}{(kl-1)\Big(\big((1-a_+)b_++a_+\big)k+(1-a_-)b_-+a_-\Big)^2}$$

$$\frac{\partial \gamma}{\partial l} = \frac{(k+1)(kl-1)k\big((1-a_+)b_++a_+\big)-(k+1)k\Big(\big((1-a_+)b_++a_+\big)kl-\big((1-a_-)b_-+a_-\big)\Big)}{(kl-1)^2\big(\big((1-a_+)b_++a_+\big)k+(1-a_-)b_-+a_-\big)} =$$

$$-\frac{(k+1)k\big((1-a_+)b_++a_+-\big((1-a_-)b_-+a_-\big)\big)}{(kl-1)^2\big(\big((1-a_+)b_++a_+\big)k+(1-a_-)b_-+a_-\big)}$$

$$\frac{\partial\gamma}{\partial k}=\frac{((((1-a_+)b_++a_+)kl-((1-a_-)b_-+a_-))+((1-a_+)b_++a_+)l(k+1))}{(kl-1)(((1-a_+)b_++a_+)k+(1-a_-)b_-+a_-)}-$$

$$\frac{(((1-a_+)b_++a_+)kl-((1-a_-)b_-+a_-))(k+1)(((1-a_+)b_++a_+)(kl-1)+l(((1-a_+)b_++a_+)k+((1-a_-)b_-+a_-))}{(kl-1)^2\left(((1-a_+)b_++a_+)k+(1-a_-)b_-+a_-\right)^2}=$$

$$-\frac{(((1-a_+)b_++a_+)(l-1)-((1-a_-)b_-+a_-)(l+1))(((1-a_+)b_++a_+)lk^2+(1-a_-)b_-+a_-)}{(kl-1)^2\left(((1-a_+)b_++a_+)k+(1-a_-)b_-+a_-\right)^2} \quad (4.48)$$

The signs of the partial derivations can be the issues to identify the relations between each factor and the ratio γ. By combining the limitations with Equation 4.48, the signs of the partial derivations can be summarized as:

$$\frac{\partial\gamma}{\partial a_+},\frac{\partial\gamma}{\partial b_+}>0$$

$$\frac{\partial\gamma}{\partial a_-},\frac{\partial\gamma}{\partial b_-},\frac{\partial\gamma}{\partial l}<0$$

$$\frac{\partial\gamma}{\partial k}\ may\ >,<or=0$$

The summary shows γ should have a positive correlation with a_+, b_+, a negative correlation with a_-, b_-, l and a complex relation with k. Therefore, large values of a_+, b_+ and small a_-, b_-, l should yield large values of γ.

The analysis should start in the simplest case, where $b_+ = b_- = b, k = 1$. In this case, if assuming the diffusion coefficients of cations and anions in liquid-state are equal and decrease to the same value in gel-state, there should be three parameters could affect the ratio, which are the value of a_- and a_+, b_+ (equals to b_-) and l, respectively. Now firstly set a_- and a_+ to be constant values and find out the effects of b and l. **Figure 4.5a** set a_+ =

0.9 and a_- = 0.6 and observe the effects of b and l. It can be clearly observed that γ could achieve a rather high value when l is close to 1 while b has weaker effects on γ than l does. In addition, set a_- = 0.55 and fix b = 0.1, when a_+ changes from 0.6 to 0.95, we can also observe that the larger the concentration differences are, the larger the ratio can achieve (**Figure 4.5b**). Based on the analysis, it can be assumed that liquid-to-gel phase-transition could generate a rather high increasement of thermopower in i-TE systems with small differences of Eastman entropy between anion and cation and proper diffusion coefficients and large variations exist in the concentration of cations and anions at different terminals. The previous analysis focuses on the i-TE systems where $D_+ = D_-$ in both gel-state and liquid-state system and both the cations and anions are thermophobic, which means both the cations and anions have higher concentrations in cold end. However, not all the ions in the i-TE system are thermophobic. The thermophilic ions or the thermophobic ions under strong internal electric field can have higher concentrations at hot ends than the cold ends. Meanwhile, the liquid-to-gel phase-transition can have different effects on cations and anions, which means the diffusion coefficients of cations and anions could be different from each other. Therefore, the conditions can be modified as:

$$0 < a_- < a_+ < 1$$

$$b_- < b_+ < 1$$

Here setting a_+ = 0.95, l = 1.1 and modify the value a_-, b_+ and b_- to find out the relations. **Figure 4.5c** shows the change of ratio with respect to the change of concentration difference of anions at different ends, which indicates the liquid-to-gel phase transition could also have a huge effect on thermopower when large variations exist in the

concentrations of cations and anions at different ends and the majority regions for cations and anions are at different ends. In addition, the D_+ and $D_$could be different in real cases and sometimes $D_+ < D\_$ even in i-TE system with positive thermopower. Therefore, the settings are modified as $l = 2$, $b_+ = b\_ = 0.1$ and change the value k from 0.6 to 2 and observe the ratio with different concentrations of cations and anions. The result shows a huge increase of thermopower can also be observed in system where cations have smaller diffusion coefficient than that of anions (**Figure 4.5d**).

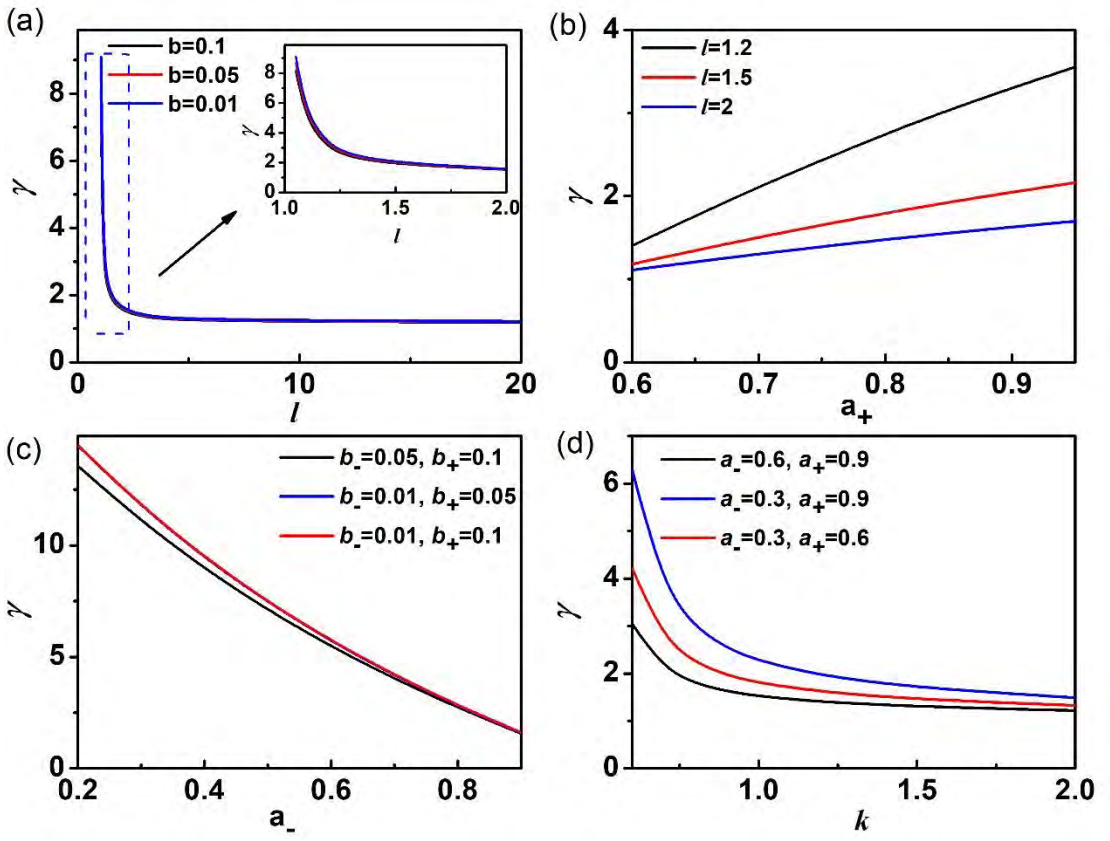

Figure 4.5 Analysis about the change of thermopower during phase-transition. The conditions and meaning of labels are discussed and illustrated in **Table 4.3**.

Table 4.3 Lists of conditions in Figure 4.5

4.5a	$a_+ = 0.9$, $a_- = 0.6$, $b_+ = b_- = b$, $k = 1$, change b and l
4.5b	$a_- = 0.55$, $b_+ = b_- = b = 0.1$, $k = 1$, change a_+ and l
4.5c	$a_+ = 0.95$, $l = 1.1$, $k = 1$, change b_-, b_+, a_-
4.5d	$l = 2$, $b_+ = b_- = 0.1$, change a_-, a_+, k

The equations and partial derivations can give a rough estimation about the relations between different factors and γ. The next step should be the analysis about the effect of factors. During the analysis, one parameter should be chosen as target while others should be maintained at a fixed value. By fixing other parameters but change the concentrations of ions, the relationships between γ and $a_\pm$ are shown in **Figure 4.6a**. When the phase changes, a rather high thermopower can be achieved since the majority of the ions with different signs distributed at different ends. In that case, ions with positive charge will concentrate at cold region while the ones with negative charge will be at the opposite region, thus it can give rise to the rise of thermopower in this system. **Figure 4.6b** shows the relationships between the ratio γ and $b_\pm$, which describe the drop of D for ions in gels. The movements of ions in gel parts are partially blocked which result in the drop of D. Nevertheless, γ is weakly impacted by the drop of D, especially when $b_\pm$ is low (less than 0.01). **Figure 4.6c** indicates that the ratio γ can attain rather high values of several thousand with proper choice of k and l values, which can be regarded as a massive enhancement of S_{td} for several thousand times. In addition, single positive or negative relations between γ and k/l pairs cannot be observed and this result verified the discussions in previous parts about the partial derivatives. The result demonstrates that the change of phase can enhance

the S_{td} for tens or even thousands of times if choosing suitable k and l values. **Figure 4.6d** further discuss the condition in **Figure 4.6c** and analyze the change of ratio detailly. The result indicates that the γ ratio can be distended in several orders when $kl \approx 1$, which shows the change of phase can strongly affect the TE performances of i-TE systems for the cases that the Eastman entropy of different ions are similar with each other or the majority of ions with different signs distribute in different ends.

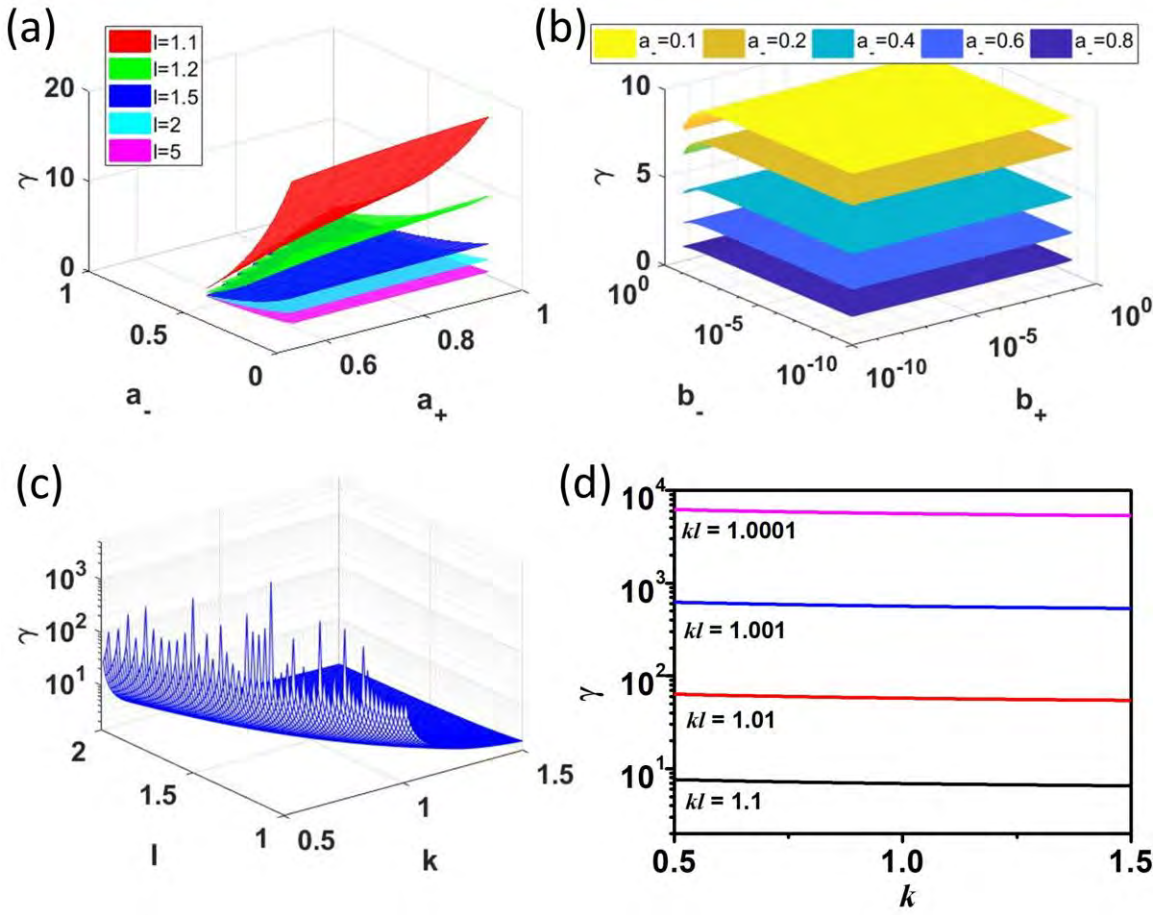

Figure 4.6 3D-plot relations between γ and other six parameters in the Equation 4.47. **a.** γ plotted as a function of a_+ , a_- and l with other fixed ($k = 1$, $b_- = b_+ = 0.01$). **b.** γ plotted as a function of b_+, b_- and a_- with others fixed ($a_+ = 0.9$, $k = 1$, $l = 1.2$). **c.** γ plotted against of k and l with others fixed ($b_+ = b_- = 0.01$, $a_+ = 0.9$, $a_- = 0.5$). **d.** γ plotted against

of k with others fixed ($b_+ = b_- = 0.01$, $a_+ = 0.9$, $a_- = 0.5$, kl equals to different constants as labeled in figure). Figures **a** to **c** are plotted by using Matlab. The codes will be shown in detail in **Appendix III**.

4.3.5 Experimental proofs

On the basis the analysis, the reason for the enhancement of the thermopower by around 6.5 times in the previous discussed P407/LiCl system can be identified. Even though the phase-transition will affect the diffusion coefficients of different ions, the large increment of thermopower might merely be due to the change of diffusion coefficient when the value is quite small (i.e., $b_+ < 0.1, b_- < 0.1$). In an i-TE system with fixed k and l values, especially in the system in which the differences between the thermal mobility of the different ions are small ($kl > 1$ and $kl \approx 1$), the rise or sometimes the drop of thermopower probably relies on the rearrangement of different ions by the movements of ions during phase-transition. The change of phase can strongly impact the moving velocity of different ions with different sizes, which thus affects the distribution of ions. During phase change from liquid to gel i-TE system with positive thermopower, the distribution of ions should change from both mainly distributed at cold side (before transition) to cations mainly at cold side and anions mainly at hot side (during transition), which means during the phase transition, $a_+ > 0.5$ and $a_- < 0.5$. Comparing the analysis with **Figure 4.6a**, it can be found out that the rearrangement of ions at different ends can probable be the reason of the strong enhancement of thermopower in LiCl/Poloxamer system. This assumption has also been roughly proved from the experiment result in **Figure 4.7**.

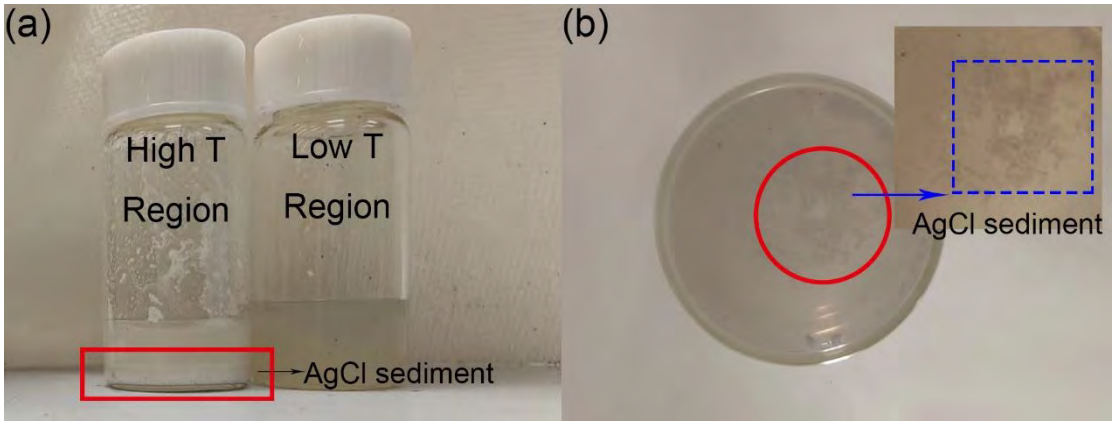

Figure 4.7 Proof of the concentration differences of Cl^- ions at different ends of the i-TE cell. 0.5 mL of the solutions from different sides of the cells were taken and added in excess amount of 1 M/L $AgNO_3$ solution. The amount of AgCl sediment can be the proof of existence of Cl^- ions. **(a)** Comparison about the concentrations of Cl^- ions at hot side and cold side by comparing the sediment amount. **(b)** An enlarge photo to clearly observe the sediment from solution in low temperature region by another angle.

Researchers have developed some in situ technologies to trace the motions of different ions (i.e., Li^+) by Raman mapping or Surface enhanced Raman spectroscopy (SERS).[242,243] However, due to the lack of the characterization methods and limitations of the experiment settings (the thermodiffusion should be driven by temperature gradient, which is not quite suitable for in situ Raman test), it is impossible for me to conduct the direct in situ measurements to trace the distributions of ions. Therefore, I decided to design an experiment which can indirectly indicate the distributions of ions at different ends by chemical methods.

This experiment decided to focus on Cl^- ion since it can react with Ag^+ and form sediments of AgCl. By setting the proper temperature at the hot ends (20℃) and cold ends (15℃), the i-TE cell exhibits in quasi-state, where the solution near hot end is in gel-state while the solution near cold end is in liquid-state. Then the glues are removed and the tested cell quickly can be opened after the experiment to separate the solutions with respect to the states. Then the solutions are collected into different containers and kept them in 5℃ to make them both exhibit in liquid-state. By taking 0.5 mL of the solutions from each sample and adding excess amount of 1 mol/L $AgNO_3$ solution into them both, it can be clearly observed that the sediment of AgCl from the solution picked from hot side but not very clear sign of sediment from the solution picked from cold side, which can be indirect evidence that Cl^- ions have higher concentrations at hot ends, which is inconsistent with the analysis from the theoretical prediction.

Similarly, a rapid reduce of the thermopower can be explained in the LiCl/Aga. System when phase change from gel to liquid. According to the evaluation of the LiCl/P407 system, the reduction of D also has small effect on the change of thermopower when D of different ions in gel-state region are relatively low ($b_+ < 0.1, b_- < 0.1$). In this system, the k and l values are fixed and the change of thermopower relies on the distribution of ions at different ends. However, the gel and liquid regions in this system are opposite to that in P407-based system, for example, the side with low temperature is in gel form and the ions in that region have lower D. Therefore, the Equation 4.47 can be modified to describe this system by changing the meaning of a_- and a_+ to the ratio of concentrations of anions and cations at hot ends to total concentration, respectively. In this system, the limits in this system should be modified as $0 < a_-, a_+ < 0.5$. Before transition, both the cations and anions have

higher concentrations at the low temperature region but the cations have larger concentration differences between different regions. The distribution will be the reason of the positive thermopower before phase change. During the phase change from gel to liquid, different ions tend to diffuse uniformly and result in the decrease of concentration differences of both ions at different ends, which means a_+ and a_- tend to be close to each other and finally change to a value quite close to 0.5. On the basis of this analysis, γ in this gel-to-liquid phase-transitional can be less than 1. Therefore, the positive thermopower should experience a rapid drop during the gel-to-sol phase-transition. Either the enhancement or decline of thermopower can be achieved in phase-transitional systems during phase change but the model predicts a rather massive increment of thermopower when the parameters of the i-TE system are appropriate. In summary, introducing the phase-transition into an i-TE system can adjust the thermopower and massive effects can be observed if the system is appropriate.

4.4 Generalization of the model

This model analyzed the transportations of ions in different conditions. From the analysis, it can be assumed that this model can be applied to transitional i-TE system. Because the model taking the phase transition as a process in which the diffusion coefficient and Eastman entropy of transfer of ions are changed with different position. Therefore, it can be generalized from this model that the reason for the phase-transition may not affect the result, which means the model can be applied to analysis of the transitional i-TE material

systems no matter which reason causes the phase transition. This assumption needs to be examined.

The previous analysis and illustrations about ionic transportations were conducted by taking the change of phase as different ions with different parameters. Therefore, it is acceptable to assume that the change of phase induced from no only temperature change but also other aspects (i.e., pH, light, electric field)[244] should also control or modify the thermopower. This project chooses the UV-light sensitive system consists of gels which are sensitive to UV light and LiCl. The i-TE materials change from liquid to gel at hot region when exposed to UV light and a rapid increase of thermopower was attained, which gave the evidence that the change of phase from liquid to gel in hot temperature region can generate the enhancement of positive thermopower by all means (**Figure 4.8**).

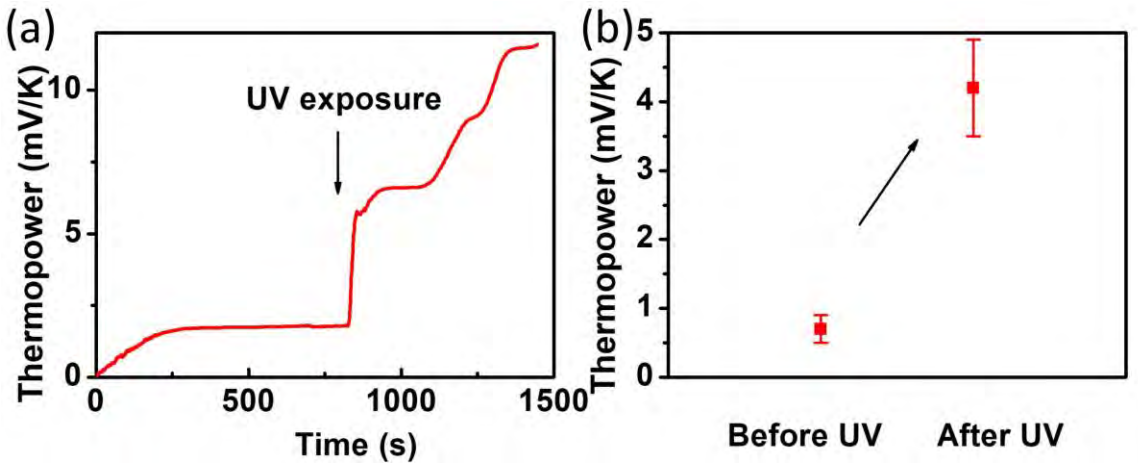

Figure 4.8 Output thermopower of UV-light induced sol-gel transitional i-TE materials. a. Output open-circuit voltage of the UV sensitive gel-based 0.3 M/L LiCl solution before and after UV exposure to the high-temperature region. The temperature is set for 15°C at cold side and 18°C at hot side. **b.** Output thermopower before and after UV light exposure for this system.

The result shows the huge thermopower arises from change of phase is widespread and is not affected by the reason for phase change from liquid to gel. Furthermore, if the polymer network where the ions are migrated can provide a selective transportation of different ions, it can also be applied to fabricate i-TE system and may demonstrate a gigantic output thermopower.

4.5 Summary

This chapter is about the theoretical analysis of the result from previous chapter. Based on the analysis, I've successfully established an analytical model that can link the thermopower with the ionic transportation during the whole phase change process. Using six-dimensional parameters, the relations between different parameters and the change of thermopower during phase change (described by ratio γ). From current theoretical result, it can be proved that the quite high value of thermopower arises from phase change that has demonstrated in Chapter 3 is a widespread phenomenon, which means the causes for phase change does not have effect on the phenomenon. This hypothesis has also been proved by the thermopower of the UV-induced liquid-to-gel transitional i-TE system. These discoveries open a unique and possible way to adjust the TE properties of i-TE systems by controlling the change of phase for next-stage adjustable ionic devices for applications that can harvest energy from low-grade thermal energy.

CHAPTER 5 Enhancement of output current and generation of continuous output

Chapter 3 has studied the effect of phase-transition on thermoelectric performances of the i-TE materials and chapter 4 has theoretically studied the transportations of ions at different states. This chapter will focus on one of the limitations of the previous studied i-TE materials, which is the i-TE systems are unable to generate a continuous current output. This chapter will demonstrate the effects of redox couples and asymmetrical electrodes on the previous studied i-TE systems and try to find out a possible solution to the problem of unstable output.

5.1 Figure of merit and efficiency of energy conversion

5.1.1 Figure of merit and efficiency of electronic TEGs

As introduced from the previous chapters, the thermoelectric energy conversion efficiency is normally described by the dimensionless figure of merit as $ZT = S^2\sigma T/\kappa$, where S, σ and κ are Seebeck coefficient, electrical conductivity and thermal conductivity, respectively. This term was firstly defined by the research on conventional TE materials and the carriers of these materials were electrons and holes. **Figure 5.1** shows a schematic figure of the transportation of holes and electrons in a conventional electronic TEG and the electrons/holes can pass through the interfaces between the material and electrodes. Therefore, the output current from electronic TE materials should be a constant current

with time. The energy conversion efficiency from thermal energy to electricity is directly related to $\sqrt{1+ZT}$ as:

$$\eta = \frac{T_H - T_C}{T_H} \frac{\sqrt{1+ZT}-1}{\sqrt{1+ZT}+\frac{T_C}{T_H}} \tag{5.1}$$

where T_H and T_C are temperature of high side and cold side, respectively.[245]

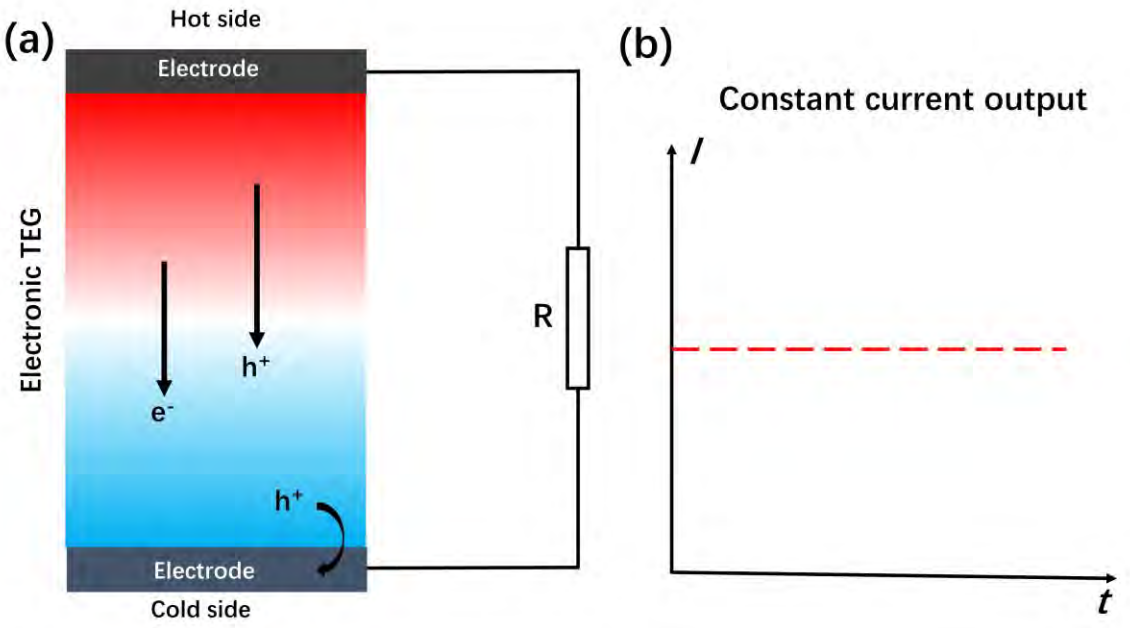

Figure 5.1 Schematic figures of the TE effect in electronic TEGs. (a) Schematically demonstration about the working of electronic TEGs with external load. (b) Output current of the electronic TEGs. The electronic TEGs can provide continuous and stable output current.

The first term in Equation 5.1 is also called Carnot efficiency, which represents the maximum efficiency that an ideal heat engine can have when operating between two

different temperatures. **Figure 5.2** shows the maximum efficiency that a TEG can have with different ZT values working at high temperature and room temperature range. A rather high converting efficiency can be achieved at high temperature range while a relatively low efficiency can be observed at room temperature range. However, if comparing with the Carnot efficiency, the converting efficiency that the TEGs with high ZT values can achieve at room temperature range should be compatible for applications. In addition, the rate of increase of the converting efficiency with respect to the ZT values decreases as the ZT value increases. In other words, the converting efficiency of the TEG will be doubled when ZT increases from 0.5 to 1.0 but the efficiency can be merely doubled when ZT increases from 1.0 to more than 2.0. Furthermore, the increases of ZT values at high values (i.e. ZT>2) can be quite difficult to achieve. Therefore, the possible solutions that may improve the ZT values of those TE materials with low ZT values can significantly enlarge their possibility for energy harvesting applications.

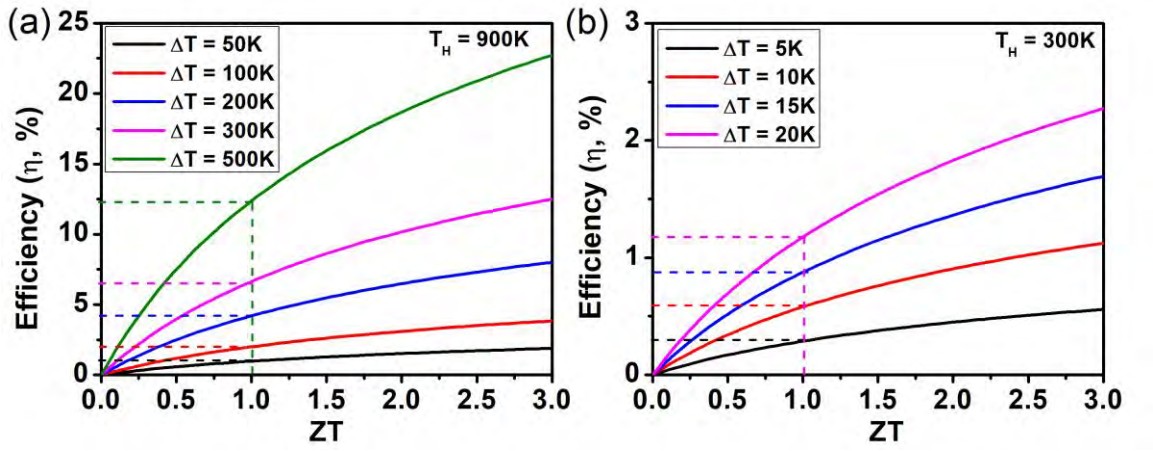

Figure 5.2 Calculated maximum conversion efficiency of TEGs. Calculated maximum conversion efficiency of TEGs at **a.** $T_H = 900K$ and **b.** $T_H = 300K$ with different temperature gradient and ZT values. Dash lines indicate the efficiencies at ZT = 1.

5.1.2 Figure of merit and efficiency of ionic TEGs

The relations between the efficiency and ZT of electronic TEGs have been discussed in previous part. It is time to find out the similar relations in ionic TEGs. Different from the working mode of electronic TEGs, where the carriers are electrons/holes which can migrate through the interfaces between materials and electrodes, the carriers in ionic TEGs are ions, which cannot pass through the interfaces between electrodes and ionic electrolytes. Therefore, the working mode of the ionic TEGs based on the transportations of ions (only thermodiffusion effect without redox couple or thermogalvanic effect) should be capacitance mode. **Figure 5.3** shows a schematic figure of the transportation of cations and anions in an ionic TEG and the ions cannot pass through the interfaces between the material and electrodes. Therefore, the output current of the ionic TEG when connected to external loads should drop to near zero over time.

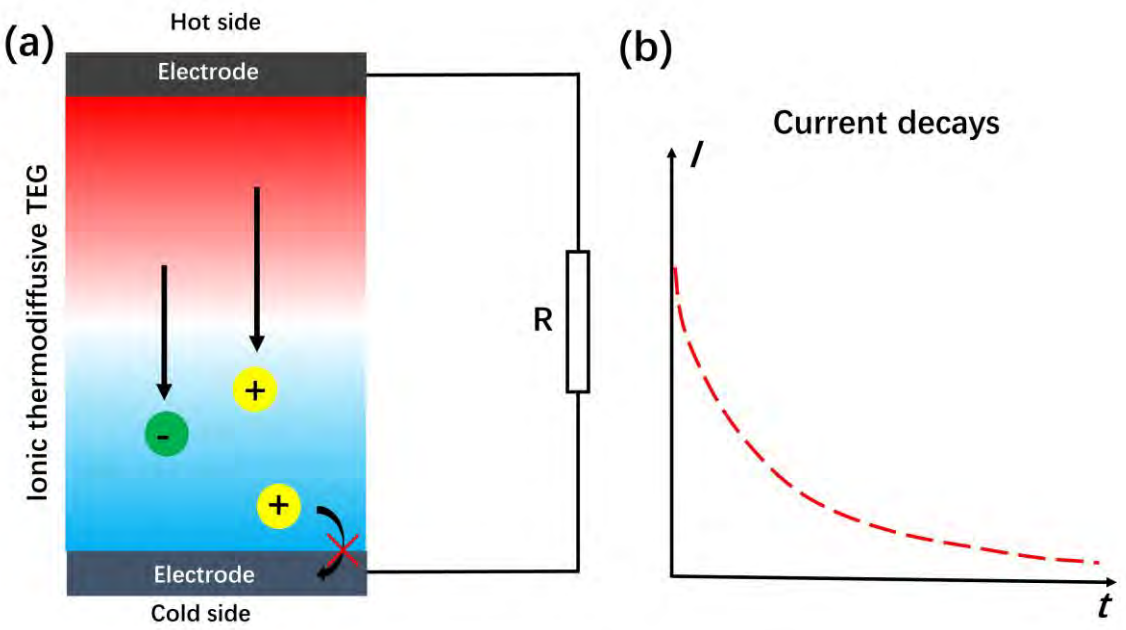

Figure 5.3 Schematic figures of the TE effect in ionic TEGs. (a) Schematically demonstration about the working of ionic TEGs with external load. (b) Output current of the ionic TEGs. The current will decrease to near zero over time.

The converting efficiency of the ionic TEGs should be estimated based on their working mode, which is the capacitance mode. Taking the whole ionic TEG as a capacitor, then after a compete charging cycle, the charge that stored on the electrodes should be:

$$Q_{ch} = CV_{TE} = CS_i\Delta T \tag{5.2}$$

where S_i is the ionic Seebeck coefficient (or thermopower) and C is the equivalent capacitance of the whole TEG. Then, the stored electrical energy can be written as:

$$E_{ch} = \frac{{Q_{ch}}^2}{2C} = \frac{1}{2}C(S_i\Delta T)^2 \tag{5.3}$$

This energy can be taken as the total harvested energy from the ionic TEG during the whole charging process. The input energy, which is also the thermal energy harvested by the TEG, should arise from three parts, which are the heat absorbed by the devices from Peltier effects and Joule heating and the heat flows through the whole device by temperature difference.[246] Each of these terms can be expressed as:

$$Q_{Peltier} = S_i T_H \int I_{ch} dt$$

$$Q_{Joule} = \frac{1}{2} \int {I_{ch}}^2 R_s dt$$

$$Q_{flow} = \kappa \frac{A}{L} \int \Delta T dt \tag{5.4}$$

where I_{ch} is the charging current, R_s is the equivalent resistance of the TEG ($R_s = \frac{L}{A\sigma_i}$, σ_i is the ionic electrical conductivity), κ is the thermal conductivity and A, L are the cross-sectional area and length at direction of temperature gradient of the TEG, respectively. Based on the properties of capacitance:

$$Q_{ch} = \int_0^{t_{ch}} I_{ch} dt$$

$$Q_{ch} = C V_{TE} \tag{5.5}$$

The total input thermal energy from Equation 5.4 can be expressed and modified as:

$$Q_{in} = {S_i}^2 T_H C \Delta T + \kappa \frac{A}{L} \Delta T t_{ch} - \frac{1}{4} C (S_i \Delta T)^2 \tag{5.6}$$

Using time constant for charging a capacitor ($\tau = CR_s$) and taking 5τ as the fully charging time when 99% of the charge has been transferred, Equation 5.6 can then be modified as:

$$Q_{in} = {S_i}^2 T_H C\Delta T + \frac{5C\kappa\Delta T}{\sigma_i} - \frac{1}{4}C(S_i\Delta T)^2 \quad (5.7)$$

By comparing Equation 5.7 with 5.3, it can be observed that the term C exists in both equation and the maximum converting efficiency can be expressed as:

$$\eta_{ionic} = \frac{E_{ch}}{Q_{in}} = \frac{\Delta T}{2T_H + \frac{10\kappa}{\sigma_i {S_i}^2} - \frac{1}{2}\Delta T} \quad (5.8)$$

It is quite interesting that the term C disappears in this equation, which means this equation is universal for all ionic TEG working in capacitance mode. Based on the definition of ionic figure of merit, the maximum converting efficiency of the ionic TEG can then be expressed as:

$$\eta_{ionic} = \frac{\Delta T}{T_H} \frac{ZT_i}{2ZT_i + 10 - \frac{1}{2}ZT_i\frac{\Delta T}{T_H}} \quad (5.9)$$

Comparing the Equation 5.9 with equation 5.1, it can be observed that the maximum converting efficiency of the ionic TEG should be lower than that of electronic TEG with the same ZT value. This is also due to the capacitance working mode of ionic TEG in which the output power is not constant and decreases with time.

5.2 Increase output current by thermogalvanic effect

As mentioned from the previous parts, the major limitation of the i-TE systems based on thermodiffusion effect is the output current will decay with time. This is because the i-TE systems based on thermodiffusion effects work in capacitance mode. **Figure 5.4a** shows the cyclic voltammetry (CV) curves of the P407/LiCl i-TE systems at room temperature

and the components are exact the same with the i-TE materials that used in Chapter 3. By setting the scan rate as 50 mV/s, the rectangle shape of the curve provides the proofs of capacitance working mode. The working mode can further be confirmed by measuring the output current and voltage when connected to an external resistance load. **Figure 5.4b** shows the maximum output power density of i-TE systems. The output power will decay suddenly when connected to the external load as shown in the current-time graph of the external resistance (**Figure 5.4c)**. In addition, the time constants of the i-TE system for different external resistances are also calculated and summarized in **Figure 5.4d**. These results show a similar phenomenon that the output of the i-TE materials introduced in Chapter 3 (working in capacitance mode) cannot generate a continuous current and power output which makes them not suitable for power supply of wearable electronic devices.

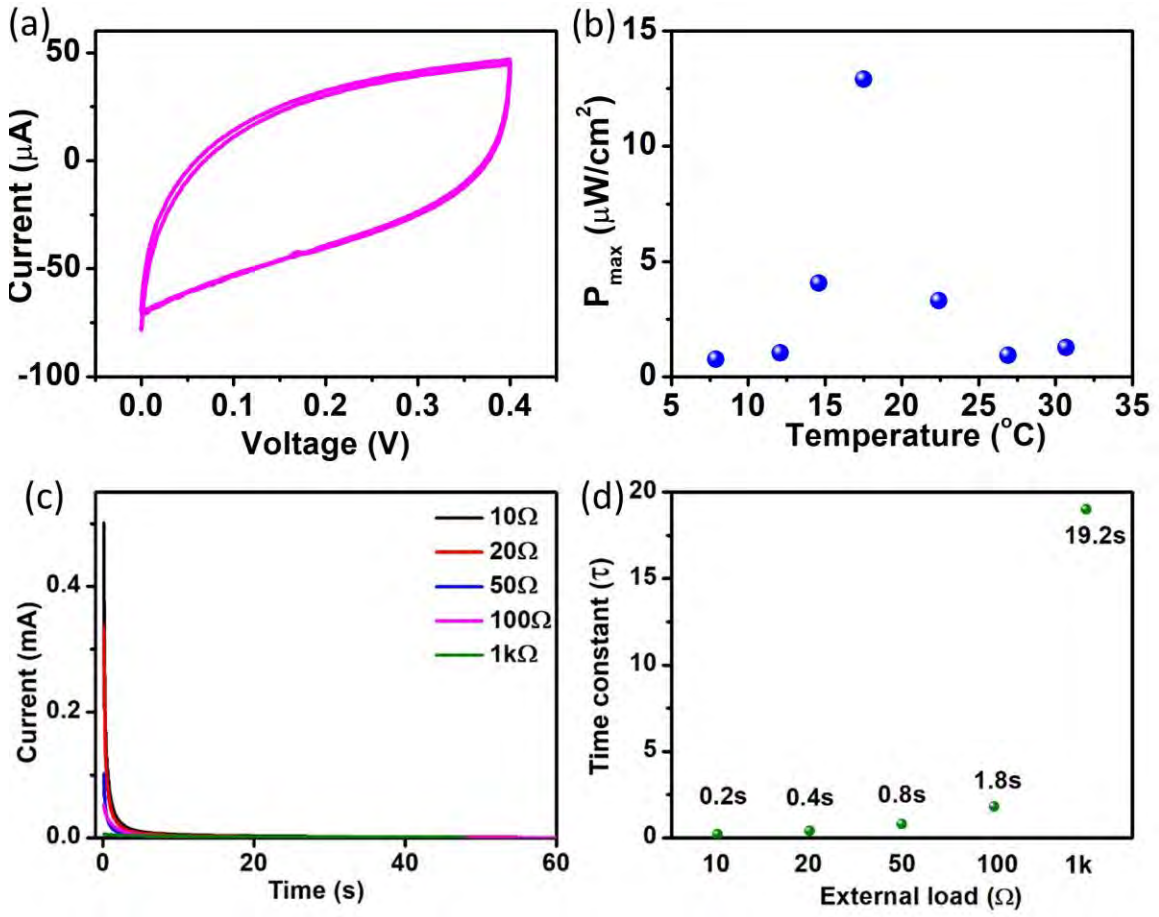

Figure 5.4 Evidences of capacitances working mode of the phase transitional i-TE materials. (a) Cyclic voltammetry curves i-TE materials in Chapter 3. This is exact the same figure with figure 3.12 for comparison. (b) Maximum of output power density on external resistance of 20Ω versus different cold side temperature with temperature differences between hot side and cold side $\Delta T = 3K$. (c) The relations between the current pass through the external load and time. (b) The time constant of the i-TE cell as a capacitor calculated by the time when output current decays to 37.3% (1/e) of its initial value. A single i-TE cell is applied a temperature gradient of 5K (hot side 20°C and cold side 15°C).

The main reason for the decay of the current with time is due to the working mode of the i-TE systems in which the ions as carriers cannot pass through the interfaces between the electrodes and the electrolyte. Therefore, if adding a tunnel for charges to pass through the interfaces and allow the interactions of charges between the inner circuit (the transportation of the charges inside the i-TE system) and the outer circuit (the circuit connected to the external load), a continuous current output can then be generated. One of the possible solutions is to add the thermogalvanic effect, which involves the redox reactions happen at different temperatures, into the i-TE systems. However, whether the synergetic effect can exist in the i-TE systems with both thermodiffusion effect and thermogalvanic effect needs to be explored. Previous research has demonstrated the possibility of the synergetic effect of thermodiffusion effect and thermogalvanic effect in gelatin-KCl-$Fe(CN)_6^{3-}/Fe(CN)_6^{4-}$ i-TE system.[10] However, whether this synergetic effect can be observed in phase-transitional i-TE systems is still a question. In order to examine this assumption, 0.25 M/L $K_4Fe(CN)_6/K_3Fe(CN)_6$ were added into i-TE materials in Chapter 3 (18%)..

The thermopower of this system during phase-transition was measured and compared with the thermopower of the i-TE system based on only thermodiffusion effect (**Figure 5.5a**). The S_i of the i-TE materials with redox couples is slightly larger than that of i-TE system without redox couples, indicating the synergetic effect of thermogalvanic effect and thermodiffusion effect exists in the phase-transitional i-TE system. However, the enhancement of the thermopower is quite low comparing with the previous research (more than 2 times), indicating the weak interactions of thermogalvanic effect and thermodiffusion effect in phase-transitional i-TE systems. The thermopower of the system arises from two aspects, which are the ionic Seebeck coefficient of all the cations and

anions and the contribution of thermopower from thermogalvanic effect, which is directly related to the entropy change of the redox reaction. The thermopower can be expressed as:

$$S_i = -\frac{s_R - s_O}{nF} + S_{td} \quad (5.10)$$

where $\Delta s_r = s_R - s_O$ is the entropy change in the standard reduction reaction $O + ne \leftrightharpoons R$ and F is the Faraday constant. The S_{td} can be expressed by Equation 4.19, which shows the thermopower of the i-TE systems based on thermodiffusion effect with different types of anions and cations. References have shown the sign of the entropy change and the positive contribution of the thermogalvanic effect to the thermopower. The key reason for the weak interactions may because the thermodiffusion of redox couples cannot be neglected during phase transition and partially reduced the whole thermopower of the i-TE system from the contribution of thermodiffusion effect. However, the increase of the output current indicates the change of the working mode from a single capacitance mode to hybrid mode (**Figure 5.5b**). Comparing the current pass through the external load after 5τ (19.2s) when i-TE capacitor can be taken as fully 'charged', the output current in i-TE systems with redox couple can increase by around 70 times (**Figure 5.5c**, from 0.001 to 0.07 mA), give rise to an output power increase by around 5000 times (**Figure 5.5d**, from 0.001 to 5.23 μW). Although the current still decays with time, which arises from the thermodiffusion of ions working in capacitance mode, the redox reactions happen at two different ends provide channels for the migration of electrons and thus induce a continuous current output, which can significantly enhance the output power and current of the i-TE systems when connected to the external load.

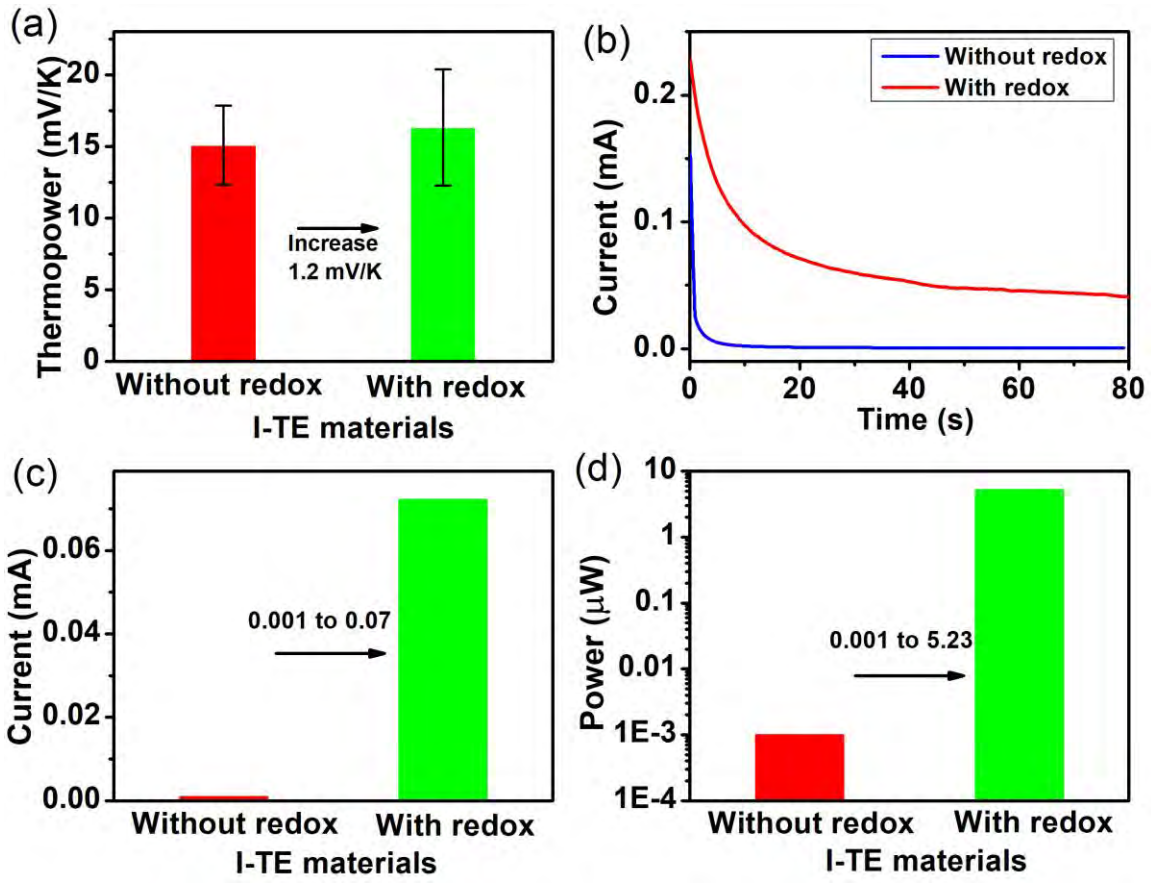

Figure 5.5 Comparison of the TE performances between the phase-transitional i-TE materials with/without redox couples. (a) Comparison of the output thermopower between the i-TE materials with and without redox couples ($K_4Fe(CN)_6/K_3Fe(CN)_6$) during phase transition. (b) Comparison of the current-time curves of i-TE materials with and without redox couples when connected to an external load of 1kΩ. All the measurements were conducted by setting temperature of hot ends and cold ends as 20°C and 15°C, respectively. Comparison of the (c) current and (d) output power on the 1kΩ external load after 5τ (19.2s) between the i-TE materials with and without redox couples ($K_4Fe(CN)_6/K_3Fe(CN)_6$) during phase transition.

5.3 Effects of active electrodes

Adding the thermogalvanic effect into the phase-transitional i-TE materials based on thermodiffusion effect can slightly increase the output thermopower but largely increase the output current and change the working mode of the i-TE systems which thus can generate continuous output. However, the i-TE systems including thermogalvanic effects may need a 'recovery' process to rebalance the concentrations of redox couple for a next working cycle. Normally, the redox couples can partially rebalance during the working process through mass diffusion process. However, this process is partially blocked due to the change of phase in the i-TE materials. Therefore, the long-term working of the phase-transitional i-TE systems with redox couples is questionable.

Apart from introducing redox couple into the i-TE systems, using active electrodes which can be involved in the redox reactions might be another possible solution for the decay of output current in phase-transitional i-TE systems. **Figure 5.6a** shows the output voltage of the phase transitional i-TE materials introduced in Chapter 3 by changing the electrodes from graphene to iron. Different from the i-TE materials based on only thermodiffusion effect, the active electrodes can join the redox reactions and provide the channel for electrons to pass through. The calculated thermopower of the i-TE cell is around 20.0 mV/K, which is slightly larger than that of i-TE cell with graphene electrodes, indicating the contribution of redox reactions from iron electrodes. In addition, the current across the external load is calculated to be 15μA , which means the i-TE cells with iron electrodes can generate a small but continuous current output. This is also the proof of changing of working mode. If changing one piece of the iron electrode with copper electrode, the output

voltage can be significantly enhanced (**Figure 5.6b**). At the starting time, a non-zero output voltage can be observed in i-TE cells without any temperature gradient, indicating the generation of the output voltage comes from standard electrode potentials.[247] With the help of electrode potential, the output voltage is increased by around 6 times. Meanwhile, the output current across the external load is around 20μA, indicating the continuous output in this i-TE system. Different from the i-TE systems with thermogalvanic effect, the i-TE cells with metal electrodes do not need the recovery process and the working life is just determined by the corrosion of the electrodes. Therefore, although the current in these i-TE cells are lower than those with redox couples, it may provide a longer working cycle compared with those with redox couples.

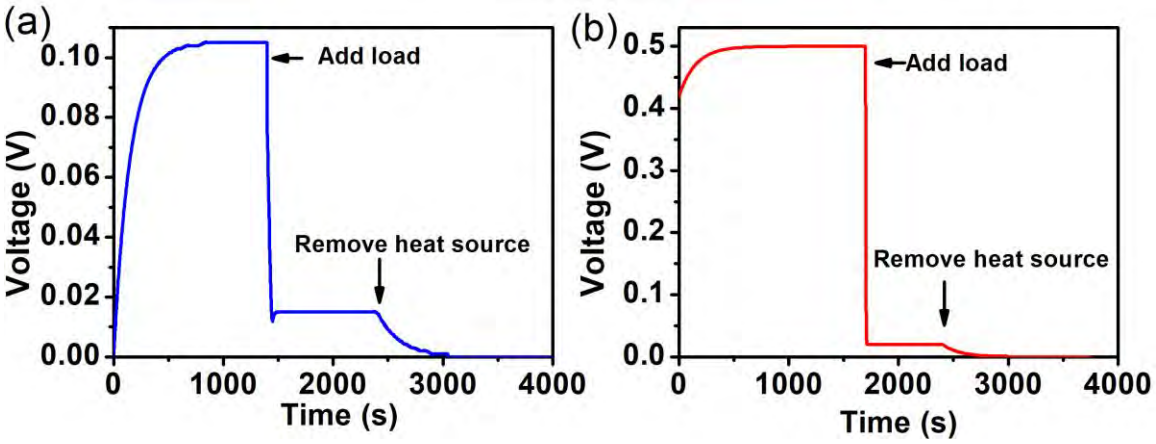

Figure 5.6 Output voltage from the i-TE materials using different electrodes. (a) Output voltage of the i-TE cell with both iron electrodes. (b) Output voltage of the i-TE cell with one piece of iron and copper electrode. All the measurements were conducted by setting temperature of hot ends and cold ends as 20°C and 15°C, respectively. The external resistance is 1kΩ.

Comparing with i-TE materials based on only thermodiffusion effect, the increase of thermopower by adding thermogalvanic effect or using metal electrodes (symmetry electrodes) is not quite satisfied. The increase of thermopower by these methods in phase transitional i-TE materials is normally quite small (less than 3 mV/K) comparing with the previous result in non-transitional i-TE gels. However, if judging these methods from the point view of current, the effects of these methods are satisfied. The current output when the i-TE cells are connected to the external load can be expressed as:

$$I_{load}(t) = I_{td}(t) + I_{re}(t) \tag{5.11}$$

where $I_{td}(t)$ and $I_{re}(t)$ represents the contribution of the current from thermodiffusion effect and redox reactions, respectively. The analysis from Chapter 3,4 and previous parts have shown that the ions cannot pass through the interfaces between electrodes and electrolytes. Therefore, the current from thermodiffusion effect should be similar with the charging current of a capacitor, which decays quickly with time. The current from redox reactions, however, is closely related to the chemical reaction rate of the redox reactions. Therefore, the decay of $I_{re}(t)$ can be quite small and even neglectable in short times. The capacitance can be taken as fully charged after 5τ, in which the current pass through can be taken as zero. As shown in **Figure 5.4d**, the current from thermodiffusion effect will decay to near zero after around 100s and then the continuous current should be generated by the redox reactions. The generation of the continuous current output should be the shining point for adding redox reactions into the phase-transitional i-TE systems.

5.4 Summary

This chapter dig out the working mode of the i-TE materials with only thermodiffusion effect and try to find out the possibility of the generation for continuous current output. A continuous current output requires redox reactions, which can either be provided by redox couples or electrodes. I-TE systems including thermogalvanic effect requires recovery process after a working cycle, which is not suitable in phase-transitional i-TE systems. The metal electrodes, especially the asymmetry electrodes, can provide a large output voltage due to electrochemical potential and considerable current output, but the corrosion of the electrodes should be considered carefully in applications.

CHAPTER 6 Conclusions and Suggestions for Future Research

6.1 Conclusions

This thesis presents a systematic study about phase-transitional i-TE materials. Firstly, the thermopower of different types of phase transitional i-TE materials are studied and studied. The thermopower and ionic ZT values of thermal-induced liquid-to-gel transitional i-TE materials before, after and during phase transition are measured and discussed. After that, theoretical analysis about the description of the motions of ions in phase-transitional i-TE systems is established. Based on the model, the increase of thermopower when phase changes is explained and a gigantic increase of thermopower when phase changes is also predicted. Finally, both thermogalvanic effect and metal electrodes are applied to enhance the output current of the i-TE systems and a continuous current output is successfully generated. Generally, the major conclusions are summarized as follows:

(1) A huge effect of phase transition from liquid to gel can be obtained in different i-TE systems from the change of thermopower. The different kinds of i-TE systems include the thermal-induced sol-to-gel, gel-to-sol and UV-induced sol-to-gel i-TE systems. A huge enhancement of thermopower (6.5 folds, from 2.5 mV/K to 15.4 mV/K) and ZT_i (23 folds, from less than 0.03 to around 0.70) can be observed in P407/LiCl water-based i-TE systems during the phase change from liquid to gel when temperature increases. The increase of thermopower can also be observed in other i-TE systems with different concentrations of poloxamer. On the contrast, the decrease of can be observed in Aga. /LiCl water-based i-TE system when phase

change from gel to liquid as temperature increases. This the study for the first time on TE performances phase-transitional i-TE materials during phase transition.

(2) In addition, a semi-quantitative model that can cover the whole phase transition stages, including different phase transition stages, is established based on the Onsager's relations and Eastman's entropy of transfer to find out the mechanism of ionic transportation in i-TE systems. The model can be further examined to derive the change of thermopower when phase changes as a function of different dimensionless parameters. The total number of influencing parameters is found out to be 6 and all the parameters are compared and examined by using partial derivations. The analysis predicts the possible massive enhancement of thermopower (i.e., several hundred or thousand times) in phase-transitional systems. On the basis of the analytical result, it can be speculated that the change of thermopower that attribute to phase change is widespread and does not rely on type of causes for the phase transition, which is further confirmed by the rise of thermopower in UV-induced phase-transitional system.

(3) The i-TE cells based on only thermodiffusion effects work in capacitance mode and the output current when connected to the external load will decay with time to a near zero value. The capacitance working mode of phase transitional i-TE systems are examined by the output performances with external load and cyclic voltammetry curve. Adding the thermogalvanic effect can slightly increase the output thermopower of the phase transitional i-TE system but significantly enhance the output current by changing the working mode from capacitance mode to hybrid mode. The current consists of two parts, which are the current from discharge of i-

TE capacitance and the current from redox reactions. The latter components can provide a continuous current output comparing with the phase transitional i-TE materials working in capacitance mode. The continous current output can further be improved by using metal electrodes, which can evolve into the redox reactions and provide a longer working cycle comparing with the i-TE systems with redox couples. Both of these methods can be applied to improve the output performances of the phase transitional i-TE systems and generate a continous current ouput.

(4) This thesis, for the first time, reveals a universal phenomenon of huge variation caused by the phase-transition in i-TE systems and its mechanism, sheds light on a novel and feasible venue to improve energy conversion performance of i-TE materials by controlled phase-transition, which may lead to a new perspective for future tunable i-TE devices for low-heat energy harvesting applications.

6.2 Limitations and outlooks

This thesis introduces a novel group of i-TE materials, which is the phase transitional i-TE materials. The above findings demonstrated progress towards i-TE materials for wearable applications. Still, owing to the insufficient time and resources, the research remains some limitations and it also needs further work. The following suggestions are of significant scientific and practical relevant for next-stage study. The main parts of the future work can be classified into three aspects:

(1) Experiment parts: The major limitation of the experiment parts in this thesis is that an in-situ measurement or tracing of ionic transportation is lack. The experiment result and theoretical analysis can provide a primary and fundamental proof for the

distributions of ions. If the ions can be traced in time by in-situ measurements, the transportation and distributions of ions can be further confirmed. These techniques can not only be used in the characterizations of i-TE materials, but also play important roles in studies of other area, including chemistry, biology and biomedical engineerings.

(2) Theoretical part: In this this, only some simple and basic explanations about the mechanisms or theory in this system have been introduced. However, the mechanisms behind the phenomenon of phase transition are still quite complicated. In this thesis, I treated the phase transition as a process in which the diffusion coefficients of ions are different, which means I can ignore the details about phase transition but taking the ions in solution at different phase as ions with different diffusion coefficients and Entropy. However, whether the structural change of the polymer networks can directly affect the thermopower and how to describe the phase transition in more clear ways are still the problems unsolved. Some further theoretically study about these phenomena should be conducted in detail.

(3) Device part: The final objective for the project is for applications on wearable electronics. Therefore, the fabrications of devices based on these TE materials should be an important task. In this report, the container or the cell which contains the i-TE materials for measurements and characterizations could be a good basement for the fabrication of devices. Based on the work have done in this project, the next-stage about device fabrication could mainly focus on how to use this kind of ionic-TE materials to fabricate devices and the evaluation about the performances of the devices.

At last, I would like to say, i-TE materials are a novel group of materials that has attracted research interests in recent years. At the first stage, researchers using i-TE materials just want to break the interrelations of Seebeck coefficient, electrical conductivity and thermal conductivity of the electronic TE materials by using ions as carriers. Nowadays, with the development of study in this area, the study about this area is becoming more and more comprehensive but the practical applications for wearable devices are still in poor progress. Therefore, I think, the outlook of this thesis, and maybe also in this area, can focus more on how to achieve practical applications of i-TE materials for wearable devices.

6.3 Recommendations on future work

The findings and works mentioned above have demonstrated a great significance of phase transition in ionic TE systems and provided a relative novel method to modify and control the TE properties of i-TE materials through a simple way. However, the limitations are still exist as mentioned in section 6.2. Based on these considerations, some recommendations for future works can be made as follows:

(1) The major limitation about the chapter 3 and 4 of this work is that I cannot find out the way to directly measure and monitor the transportations of ions in i-TE systems during phase transition. Therefore, the real-time in-situ techniques that can monitor the positions and concentrations of different ions in ionic system could improve not only the drawbacks of this work but also provide a significant technique for characterizations of ionic transportations in the study about i-TE or other ionic systems.

(2) The theoretical study about phase-transition from gel state to liquid or reversely has been provided in this thesis. However, this model is only an analytical model but not a quantitatively analysis model. Therefore, the theoretical study about the phase-transition of the i-TE, especially the study about the description of phase-transition and boundary condition between different phases can be an attractive direction for next-stage works.

(3) As far as I know, the practical applications based on i-TE materials have been demonstrated by previous studies but the result were not satisfied. Most of the works either lack of practical applications or the demonstrated applications cannot be used for wearable electronics. This thesis provides a novel routine for design of i-TE materials but the applications of this type of material are still deserved to be further explored. Therefore, the study about establishment of practical applications and improvement of the TE performances of i-TE materials to fulfill the requirements for wearable devices can be meaningful for future works.

In all, PhD study is not an end but a good beginning for research study. This thesis presents the works I've done at this stage. It possesses many novel ideas and bright points but still not perfect, which will encourage me to explore and work deeply in the future on the basis of this thesis and try to make some progresses that are meaningful for study in this area.

Appendix

Appendix I Simulations from COMSOL Multiphysics

This part demonstrates a simple simulation for TE performances of TE composites by using COMSOL Multiphysics. It's quite difficult to simulate the whole ionic transporation process by using COMSOL. Therefore, in this session, I'll treat the i-TE materials as a conventional TE material with the same parameters as measured in the previous chapters and take a rough simulation to find out the trend of different structures. The parameters and settings for simulations are shown below.

Materials	**Thermal conductivity W/(mK)**	**Electrical conductivity (S/m)**	**Seebeck (V/K)**
TE	0.4	4	0.02
PMMA	1.5	1×10^{-5}	1×10^{-6}
Electrodes	4000	8×10^{6}	1×10^{-6}

The study is firstly conducted in 2D structures. The domain is set as 1m×1m square and temperature are set as 400K and 300K for hot side and cold side, respectively. When the whole domain is filled with single type of materials, the output is shown as below.

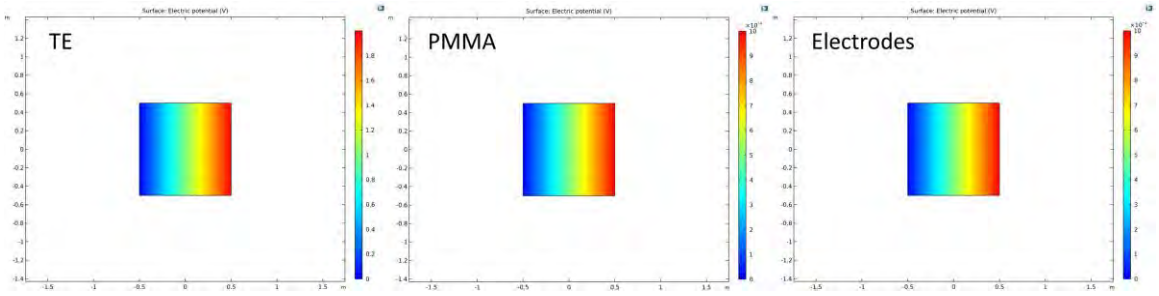

The output voltage of the TE materials is around 2V, with the output voltage of PMMA and electrodes as 1×10^{-4}V. Then the simulations come to different structures. Details are shown below.

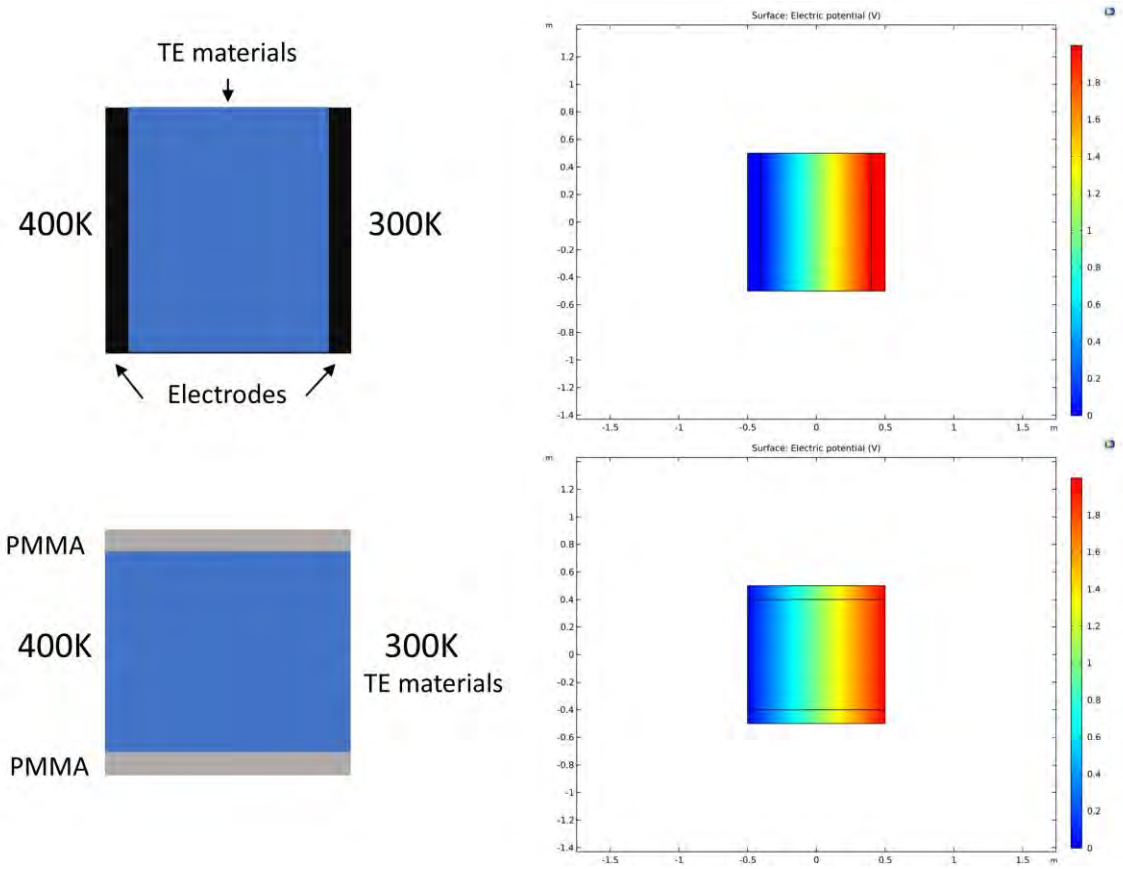

The thicknesses of the electrodes and PMMA frames are all set as 1mm. When the alignments of the electrodes and TE materials are parallel to the temperature gradient, the electrical potential difference between the hot end and the cold end of the structure is

almost the same value with that contains only TE materials. The electrical potential difference will drop as the proportion of the electrodes increase, but the drop can only be observed obviously when the proportion of electrodes are large than 90%, which means the main components in the TE cells are electrodes but not TE materials. Similar with the result of TE materials with electrodes, the electrical potential of TE materials with PMMA frames is also close to the same value that only contains TE materials. Now it's time to combine these two structures together and find out the relations between the output performances of a single TE material and the TE cell.

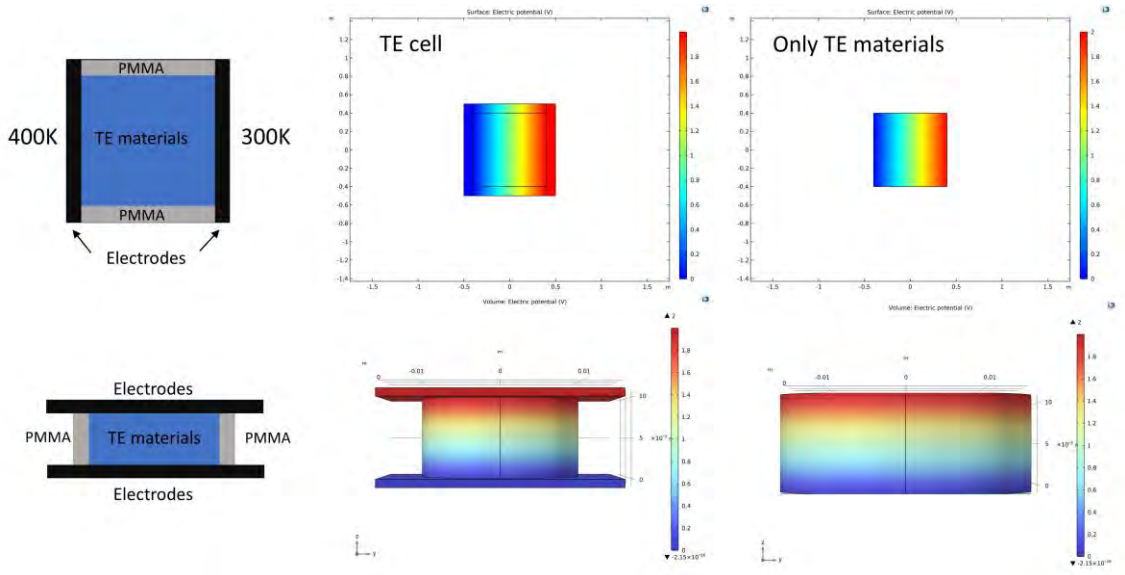

The result shows that, no matter which structures are applied, the output electrical potential between the hot ends and the cold ends of the TE cells will have the same value with that only contains TE materials. The result proofs that when the size of the frameworks and electrodes are quite small compared with the size of TE materials (i.e. less than 10% of the size of TE materials), the contribution of the output from unfunctional components (i.e. electrodes, frames) of the TE cells can be ignored. Therefore, the measured TE

performances of the whole cell can be taken as the TE properties of the TE materials inside the cell.

Appendix II Onsager relations

This part will demonstrate how to illustrate the equations 4.2 to 4.5 in Chapter 4.

Based on the energy conservation theory, the thermal transition through a system can be expressed as:

$$\frac{\partial u}{\partial t} = -\nabla \cdot J_q \tag{1}$$

where u is internal energy and J_q is density of heat flow.

Then, by the definition of entropy:

$$\frac{\partial s}{\partial t} = \frac{1}{T}\frac{\partial u}{\partial t} = -\frac{1}{T}\nabla \cdot J_q = -\nabla \cdot \frac{J_q}{T} + J_q \cdot \nabla \frac{1}{T} \tag{2}$$

where s represents the entropy. In local equilibrium state, the increasing rate of local partial entropy is:

$$\frac{\partial s}{\partial t} = -\nabla \cdot J_s + \Theta \tag{3}$$

where J_s is density of entropy flow, Θ is the local increasing rate of entropy. Comparing equation 2 and 3, we can get:

$$J_s = \frac{J_q}{\mathrm{T}},\ \Theta = J_q \cdot \nabla \frac{1}{T} \tag{4}$$

Θ can also be expressed in another way:

$$\Theta = J_q \cdot X_q \tag{5}$$

where X_q can be taken as the driven force for the transition of heat flow, which equals to $\nabla \frac{1}{T}$.

Now consider the mass diffusion process. Similar with the heat transition, the mass diffusion can also happen when chemical potential differences exist. Then, the mass diffusion can be expressed as:

$$\frac{\partial u}{\partial t} = -\nabla \cdot J_u = -\nabla \cdot J_q - \nabla \cdot (\mu J_n) \tag{6}$$

where μ is the chemical potential and J_n is the mass flux.

So the entropy can be expressed as:

$$\frac{\partial s}{\partial t} = \frac{1}{T}\frac{\partial u}{\partial t} - \frac{\mu}{T}\frac{\partial n}{\partial t} = -\frac{1}{T}\nabla \cdot J_q - \frac{1}{T}\nabla \cdot (\mu J_n) + \frac{\mu}{T}\nabla \cdot J_n$$

$$= -\nabla \cdot \frac{J_q}{T} + J_q \cdot \nabla \frac{1}{T} - \frac{J_n}{T} \cdot \nabla \mu \tag{7}$$

Then comparing equation 7 with 3, we can get:

$$J_s = \frac{J_q}{\mathrm{T}},\ \Theta = J_q \cdot \nabla \frac{1}{T} - \frac{J_n}{T} \cdot \nabla \mu \tag{8}$$

Similarly, Θ can also be expressed in:

$$\Theta = J_q \cdot X_q + J_n \cdot X_n \tag{9}$$

where X_q can be taken as the driven force for the transition of mass flow, which equals to $-\frac{1}{T}\nabla\mu$.

Then the Equation 4.4 and 4.5 can be derived.

Appendix III Matlab codes

This part lists the Matlab code for plotting the 3D figures.

File1: Thermopower_analysis.m (Analysis of data)

```
%clear all variables
clear variables;

%Define variables
syms a_ca;
syms a_an;
syms b_ca;
syms b_an;
syms k;
syms l;
syms x;

%Input function
f(a_ca, a_an, b_ca, b_an, k, l) = ((((1-a_ca)*b_ca + a_ca)*k*l-((1-
a_an)*b_an+a_an))*(k+1))/(((((1-a_ca)*b_ca+a_ca)*k+((1-
a_an)*b_an+a_an))*(k*l-1)));

%Find differential
da_ca = diff(f(a_ca, a_an, b_ca, b_an, k, l), a_ca);
da_an = diff(f(a_ca, a_an, b_ca, b_an, k, l), a_an);
db_ca = diff(f(a_ca, a_an, b_ca, b_an, k, l), b_ca);
db_an = diff(f(a_ca, a_an, b_ca, b_an, k, l), b_an);
dk = diff(f(a_ca, a_an, b_ca, b_an, k, l), k);
dl = diff(f(a_ca, a_an, b_ca, b_an, k, l), l);

%Solution to min/max points

xda_ca = solve(da_ca);
xda_an = solve(da_an);
xdb_ca = solve(db_ca);
xdb_an = solve(db_an);
xdk = solve(dk);
```

```
xdl = solve(dl);

x = [xda_ca, xda_an, xdb_ca, xdb_an, xdk, xdl];


%Display

disp(x);
disp(da_ca);
disp(da_an);
disp(db_ca);
disp(db_an);
disp(dk);
disp(dl);

save data.mat
```

File 2: Plot_analysis.m (Plot **Figure 4.6a**)

```
clear variables;
close all;

load data.mat

%plot the first figure
%set a_an, a_ca as variables, b_ca, b_an, k are constant. l also
variables

a_an_data = (0.05:0.05:0.95);
a_ca_data = (0.05:0.05:0.95);
[aca, aan] = meshgrid(a_ca_data, a_an_data);
index1 = aca-aan<=0;
aca(index1) = nan;
aan(index1) = nan;
index2 = aca<=0.5;
aca(index2) = nan;
aan(index2) = nan;
stdaf1 = (((1-aca)*0.01 + aca)*1.1-((1-aan)*0.01+aan))*2;
stdbe1 = (((1-aca)*0.01+aca)*1+((1-aan)*0.01+aan))*(1.1-1);
gamma1 = stdaf1./stdbe1;
mesh (aca, aan,
gamma1,'FaceColor','r','FaceAlpha','0.8','EdgeColor','r','EdgeAlpha','0
.8');

hold on

%Plot first figure second curve
%Set k = 1, l = 1.1

stdaf2 = (((1-aca)*0.01 + aca)*1.2-((1-aan)*0.01+aan))*2;
stdbe2 = (((1-aca)*0.01+aca)*1+((1-aan)*0.01+aan))*(1.2-1);
```

```
gamma2 = stdaf2./stdbe2;
mesh (aca, aan,
gamma2,'FaceColor','g','FaceAlpha','0.8','EdgeColor','g','EdgeAlpha','0
.8');

hold on

stdaf3 = (((1-aca)*0.01 + aca)*1.5-((1-aan)*0.01+aan))*2;
stdbe3 = (((1-aca)*0.01+aca)*1+((1-aan)*0.01+aan))*(1.5-1);
gamma3 = stdaf3./stdbe3;
mesh (aca, aan,
gamma3,'FaceColor','b','FaceAlpha','0.8','EdgeColor','b','EdgeAlpha','0
.8');

hold on

stdaf4 = (((1-aca)*0.01 + aca)*2-((1-aan)*0.01+aan))*2;
stdbe4 = (((1-aca)*0.01+aca)*1+((1-aan)*0.01+aan))*(2-1);
gamma4 = stdaf4./stdbe4;
mesh (aca, aan,
gamma4,'FaceColor','c','FaceAlpha','0.8','EdgeColor','c','EdgeAlpha','0
.58');

hold on

stdaf5 = (((1-aca)*0.01 + aca)*5-((1-aan)*0.01+aan))*2;
stdbe5 = (((1-aca)*0.01+aca)*1+((1-aan)*0.01+aan))*(5-1);
gamma5 = stdaf5./stdbe5;
mesh (aca, aan,
gamma5,'FaceColor','m','FaceAlpha','0.8','EdgeColor','m','EdgeAlpha','0
.8');

%str = ['Ratio \gamma with respect to the change of a_+ and a_-'
newline 'b_+ = b_- = 0.01, k = 1'];
%title(str);
xlabel('a_+');
ylabel('a_-');
zlabel('\gamma');
legend({'l=1.1','l=1.2','l=1.5','l=2','l=5'},'Location','northwest');
set(get(gca, 'xlabel'),'FontSize',20,'FontWeight','bold');
set(get(gca, 'ylabel'),'FontSize',20,'FontWeight','bold');
set(get(gca, 'zlabel'),'FontSize',20,'FontWeight','bold');
set(get(gca, 'xaxis'),'FontSize',20,'FontWeight','bold');
set(get(gca, 'yaxis'),'FontSize',20,'FontWeight','bold');
set(get(gca, 'zaxis'),'FontSize',20,'FontWeight','bold');
set(get(gca, 'legend'),'FontSize',15);

save analysis1.mat
```

File 3: Plot_analysis1.m (Plot **Figure 4.6b**)

```
clear variables;
close all;
load data.mat

%plot the first figure
%set a_an, a_ca as variables, b_ca, b_an, k are constant. l also
variables

ratio = (-10:0.1:-1);
b_an_data = 10.^ratio;
b_ca_data = 10.^ratio;
[bca, ban] = meshgrid(b_ca_data, b_an_data);
stdaf1 = (((1-0.9)*bca+0.9)*1.2-((1-0.1)*ban+0.1))*2;
stdbe1 = (((1-0.9)*bca+0.9)*1+((1-0.1)*ban+0.1))*(1.2-1);
gamma1 = stdaf1./stdbe1;
mesh1 = mesh (bca, ban, gamma1,'FaceColor','flat');

hold on

%Plot first figure second curve
%Set k = 1, l = 1.1

stdaf2 = (((1-0.9)*bca+0.9)*1.2-((1-0.2)*ban+0.2))*2;
stdbe2 = (((1-0.9)*bca+0.9)*1+((1-0.2)*ban+0.2))*(1.2-1);
gamma2 = stdaf2./stdbe2;
mesh2 = mesh (bca, ban, gamma2,'FaceColor','flat');

hold on

stdaf3 = (((1-0.9)*bca+0.9)*1.2-((1-0.4)*ban+0.4))*2;
stdbe3 = (((1-0.9)*bca+0.9)*1+((1-0.4)*ban+0.4))*(1.2-1);
gamma3 = stdaf3./stdbe3;
mesh3 = mesh (bca, ban, gamma3,'FaceColor','flat');

hold on

stdaf4 = (((1-0.9)*bca+0.9)*1.2-((1-0.6)*ban+0.6))*2;
stdbe4 = (((1-0.9)*bca+0.9)*1+((1-0.6)*ban+0.6))*(1.2-1);
gamma4 = stdaf4./stdbe4;
mesh4 = mesh (bca, ban, gamma4,'FaceColor','flat');

hold on

stdaf5 = (((1-0.9)*bca+0.9)*1.2-((1-0.8)*ban+0.8))*2;
stdbe5 = (((1-0.9)*bca+0.9)*1+((1-0.8)*ban+0.8))*(1.2-1);
gamma5 = stdaf5./stdbe5;
mesh5 = mesh (bca, ban, gamma5,'FaceColor','flat');

set(gca','xscale','log');
set(gca','yscale','log');
%str = ['Ratio \gamma with respect to the change of b_+ and b_-'
```

```
newline 'a_+ = 0.9, k = 1, l = 1.2'];
%title(str);
xlabel('b_+');
ylabel('b_-');
zlabel('\gamma');
legend({'a_-=0.1','a_-=0.2','a_-=0.4','a_-=0.6','a_-
=0.8'},'Orientation','Horizontal','Location','North');
set (get(gca, 'legend'),'FontSize',15);
axis([10^-10,1,10^-10,1,0,10]);
set(get(gca, 'xlabel'),'FontSize',20,'FontWeight','bold');
set(get(gca, 'ylabel'),'FontSize',20,'FontWeight','bold');
set(get(gca, 'zlabel'),'FontSize',20,'FontWeight','bold');
set(get(gca, 'xaxis'),'FontSize',20,'FontWeight','bold');
set(get(gca, 'yaxis'),'FontSize',20,'FontWeight','bold');
set(get(gca, 'zaxis'),'FontSize',20,'FontWeight','bold');

save analysis2.mat
```

File 4: Plot_analysis2.m (Plot **Figure 4.6c**)

```
clear variables;
close all;

load data.mat

%plot the first figure
%set a_an, a_ca as variables, b_ca, b_an, k are constant. l also
variables

k_data = (0.5:0.01:1.5);
l_data = (1:0.01:2);
[kk, ll] = meshgrid(k_data, l_data);
index1 = kk.*ll <= 1;
kk(index1) = nan;
ll(index1) = nan;
stdaf1 = (((1-0.9)*0.01+0.9).*(kk.*ll)-((1-0.55)*0.01+0.55)).*(kk+1);
stdbe1 = (((1-0.9)*0.01+0.9).*kk+((1-0.55)*0.01+0.55)).*(kk.*ll-1);
gamma1 = stdaf1./stdbe1;
mesh (kk, ll, gamma1,'EdgeColor','b');
set(gca','zscale','log');
zticks([0,10,100,1000]);
axis([0.5,1.5,1,2,0,5000]);
% str = ['Ratio \gamma with respect to the change of k and l' newline
'a_+ = 0.9, a_- = 0.5, b_+ = b_- = 0.01'];
% title(str);
xlabel('k');
ylabel('l');
zlabel('\gamma');
set(gca,'FontSize',20,'FontWeight','bold');

save analysis2.mat
```

References

(1) Bell, L. E. Cooling, Heating, Generating Power, and Recovering Waste Heat with Thermoelectric Systems. *Science (80-.).* **2008**, *321* (5895), 1457–1461. https://doi.org/10.1126/science.1158899.

(2) Wei, J.; Yang, L.; Ma, Z.; Song, P.; Zhang, M.; Ma, J.; Yang, F.; Wang, X. Review of Current High-ZT Thermoelectric Materials. *Journal of Materials Science*. Springer September 1, 2020, pp 12642–12704. https://doi.org/10.1007/s10853-020-04949-0.

(3) Wang, Y.; Yang, L.; Shi, X. L.; Shi, X.; Chen, L.; Dargusch, M. S.; Zou, J.; Chen, Z. G. Flexible Thermoelectric Materials and Generators: Challenges and Innovations. *Adv. Mater.* **2019**, *31* (29). https://doi.org/10.1002/adma.201807916.

(4) Zhang, L. S.; Lin, S. P.; Hua, T.; Huang, B. L.; Liu, S. R.; Tao, X. M. Fiber-Based Thermoelectric Generators: Materials, Device Structures, Fabrication, Characterization, and Applications. *Adv. Energy Mater.* **2018**, *8* (5). https://doi.org/ARTN 170052410.1002/aenm.201700524.

(5) Zhou, Y.; Zhao, L. D. Promising Thermoelectric Bulk Materials with 2D Structures. *Adv. Mater.* **2017**, *29* (45), 1–14. https://doi.org/10.1002/adma.201702676.

(6) Vieira, E. M. F.; Pires, A. L.; Silva, J. P. B.; Magalhães, V. H.; Grilo, J.; Brito, F. P.; Silva, M. F.; Pereira, A. M.; Goncalves, L. M. High-Performance μ-

Thermoelectric Device Based on Bi2Te3/Sb2Te3 p-n Junctions. *ACS Appl. Mater. Interfaces* **2019**, *11* (42), 38946–38954. https://doi.org/10.1021/acsami.9b13254.

(7) Shi, X. L.; Zou, J.; Chen, Z. G. Advanced Thermoelectric Design: From Materials and Structures to Devices. *Chem. Rev.* **2020**, *120* (15), 7399–7515. https://doi.org/10.1021/ACS.CHEMREV.0C00026/ASSET/IMAGES/LARGE/CR0C00026_0046.JPEG.

(8) Yu, B.; Duan, J.; Cong, H.; Xie, W.; Liu, R.; Zhuang, X.; Wang, H.; Qi, B.; Xu, M.; Wang, Z. L.; Zhou, J. Thermosensitive Crystallization-Boosted Liquid Thermocells for Low-Grade Heat Harvesting. *Science (80-.).* **2020**, *370* (6514), 342–346. https://doi.org/10.1126/science.abd6749.

(9) Zhao, D.; Wang, H.; Khan, Z. U.; Chen, J. C.; Gabrielsson, R.; Jonsson, M. P.; Berggren, M.; Crispin, X. Ionic Thermoelectric Supercapacitors. *Energy Environ. Sci.* **2016**, *9* (4), 1450–1457. https://doi.org/10.1039/c6ee00121a.

(10) Han, C. G.; Qian, X.; Li, Q.; Deng, B.; Zhu, Y.; Han, Z.; Zhang, W.; Wang, W.; Feng, S. P.; Chen, G.; Liu, W. Giant Thermopower of Ionic Gelatin near Room Temperature. *Science (80-.).* **2020**, *368* (6495), 1091–1098. https://doi.org/10.1126/science.aaz5045.

(11) Liu, Z.; Cheng, H.; Le, Q.; Chen, R.; Li, J.; Ouyang, J. Giant Thermoelectric Properties of Ionogels with Cationic Doping. *Adv. Energy Mater.* **2022**, *12* (22), 2200858. https://doi.org/10.1002/AENM.202200858.

(12) Fan, Z.; Zhang, Y.; Pan, L.; Ouyang, J.; Zhang, Q. Recent Developments in Flexible Thermoelectrics: From Materials to Devices. *Renew. Sustain. Energy Rev.* **2021**, *137*, 110448. https://doi.org/10.1016/J.RSER.2020.110448.

(13) Soleimani, Z.; Zoras, S.; Ceranic, B.; Cui, Y.; Shahzad, S. A Comprehensive Review on the Output Voltage/Power of Wearable Thermoelectric Generators Concerning Their Geometry and Thermoelectric Materials. *Nano Energy* **2021**, *89*, 106325. https://doi.org/10.1016/J.NANOEN.2021.106325.

(14) Park, Y. G.; Lee, S.; Park, J. U. Recent Progress in Wireless Sensors for Wearable Electronics. *Sensors (Switzerland)*. Multidisciplinary Digital Publishing Institute October 9, 2019, p 4353. https://doi.org/10.3390/s19204353.

(15) Nguyen, C. M.; Kota, P. K.; Nguyen, M. Q.; Dubey, S.; Rao, S.; Mays, J.; Chiao, J. C. Wireless Power Transfer for Autonomous Wearable Neurotransmitter Sensors. *Sensors (Switzerland)* **2015**, *15* (9), 24553–24572. https://doi.org/10.3390/s150924553.

(16) Shi, J.; Liu, S.; Zhang, L.; Yang, B.; Shu, L.; Yang, Y.; Ren, M.; Wang, Y.; Chen, J.; Chen, W.; Chai, Y.; Tao, X.; Shi, J.; Liu, S.; Zhang, L.; Yang, B.; Chen, W.; Chai, Y.; Tao, X.; Shu, L.; Yang, Y.; Ren, M.; Wang, Y.; Chen, J. Smart Textile-Integrated Microelectronic Systems for Wearable Applications. *Adv. Mater.* **2020**, *32* (5), 1901958. https://doi.org/10.1002/ADMA.201901958.

(17) Liu, S.; Zheng, W.; Yang, B.; Tao, X. Triboelectric Charge Density of Porous and Deformable Fabrics Made from Polymer Fibers. *Nano Energy* **2018**, *53*, 383–390. https://doi.org/10.1016/J.NANOEN.2018.08.071.

(18) Yang, B.; Xiong, Y.; Ma, K.; Liu, S.; Tao, X. Recent Advances in Wearable Textile-Based Triboelectric Generator Systems for Energy Harvesting from Human Motion. *EcoMat* **2020**, *2* (4), e12054. https://doi.org/10.1002/EOM2.12054.

(19) Li, L.; Zhao, Y.; Shi, C.; Zeng, W.; Liao, B.; Zhang, M.; Tao, X. Facile Synthesis of Copper Selenides with Different Stoichiometric Compositions and Their Thermoelectric Performance at a Low Temperature Range. *RSC Adv.* **2021**, *11* (42), 25955–25960. https://doi.org/10.1039/D1RA04626H.

(20) Chen, J.; Zhang, L.; Tu, Y.; Zhang, Q.; Peng, F.; Zeng, W.; Zhang, M.; Tao, X. Wearable Self-Powered Human Motion Sensors Based on Highly Stretchable Quasi-Solid State Hydrogel. *Nano Energy* **2021**, *88*, 106272. https://doi.org/10.1016/J.NANOEN.2021.106272.

(21) Chen, Y.; Shi, C.; Zhang, J.; Dai, Y.; Su, Y.; Liao, B.; Zhang, M.; Tao, X.; Zeng, W. Ionic Thermoelectric Effect Inducing Cation-Enriched Surface of Hydrogel to Enhance Output Performance of Triboelectric Nanogenerator. *Energy Technol.* **2022**, *10* (5), 2200070. https://doi.org/10.1002/ENTE.202200070.

(22) Anatychuk, L. I.; Kobylianskyi, R. R. Electronic Medical Thermometer with Thermoelectric Power Supply. *Mater. Today Proc.* **2015**, *2* (2), 849–857. https://doi.org/10.1016/J.MATPR.2015.05.109.

(23) Zeng, W.; Shu, L.; Li, Q.; Chen, S.; Wang, F.; Tao, X.-M.; Zeng, W.; Shu, L.; Li, Q.; Chen, S.; Wang, F.; Tao, X.-M. Fiber-Based Wearable Electronics: A Review

of Materials, Fabrication, Devices, and Applications. *Adv. Mater.* **2014**, *26* (31), 5310–5336. https://doi.org/10.1002/ADMA.201400633.

(24) Chen, J.; Shi, C.; Wu, L.; Deng, Y.; Wang, Y.; Zhang, L.; Zhang, Q.; Peng, F.; Tao, X. M.; Zhang, M.; Zeng, W. Environmentally Tolerant Ionic Hydrogel with High Power Density for Low-Grade Heat Harvesting. *ACS Appl. Mater. Interfaces* **2022**, *14* (30), 34714–34721. https://doi.org/10.1021/ACSAMI.2C07423/ASSET/IMAGES/LARGE/AM2C07423_0007.JPEG.

(25) Ma, W.; Xu, Y.; Zeng, W.; Zhu, Z.; Liu, J. Thermal Degradation Kinetics of Transparent Fluorinated Poly(Imide Siloxane) Copolymers. *High Perform. Polym.* **2021**, *33* (5), 479–487. https://doi.org/10.1177/0954008320969777/ASSET/IMAGES/LARGE/10.1177_0954008320969777-FIG2.JPEG.

(26) Zou, Q.; Shang, H.; Huang, D.; Xie, B.; Zhang, L.; Wang, K.; Dong, H.; Li, C.; Gu, H.; Ding, F. Bi2Te3-Based Flexible Thermoelectric Generator for Wearable Electronics. *Appl. Phys. Lett.* **2022**, *120* (2), 023903. https://doi.org/10.1063/5.0078389.

(27) Jin, H.; Li, J.; Iocozzia, J.; Zeng, X.; Wei, P. C.; Yang, C.; Li, N.; Liu, Z.; He, J. H.; Zhu, T.; Wang, J.; Lin, Z.; Wang, S. Hybrid Organic–Inorganic Thermoelectric Materials and Devices. *Angew. Chemie Int. Ed.* **2019**, *58* (43), 15206–15226. https://doi.org/10.1002/ANIE.201901106.

(28) Park, H.; Lee, D.; Kim, D.; Cho, H.; Eom, Y.; Hwang, J.; Kim, H.; Kim, J.; Han, S.; Kim, W. High Power Output from Body Heat Harvesting Based on Flexible Thermoelectric System with Low Thermal Contact Resistance. *J. Phys. D. Appl. Phys.* **2018**, *51* (36), 365501. https://doi.org/10.1088/1361-6463/AAD270.

(29) Yang, S.; Qiu, P.; Chen, L.; Shi, X. Recent Developments in Flexible Thermoelectric Devices. *Small Sci.* **2021**, *1* (7), 2100005. https://doi.org/10.1002/SMSC.202100005.

(30) Pei, Y.; Lalonde, A. D.; Wang, H.; Snyder, G. J. Low Effective Mass Leading to High Thermoelectric Performance. *Energy Environ. Sci.* **2012**, *5* (7), 7963–7969. https://doi.org/10.1039/C2EE21536E.

(31) Xie, H.; Su, X.; Bailey, T. P.; Zhang, C.; Liu, W.; Uher, C.; Tang, X.; Kanatzidis, M. G. Anomalously Large Seebeck Coefficient of CuFeS2 Derives from Large Asymmetry in the Energy Dependence of Carrier Relaxation Time. *ACS Appl. Mater. Interfaces* **2020**. https://doi.org/10.1021/ACS.CHEMMATER.0C00388/ASSET/IMAGES/LARGE/CM0C00388_0005.JPEG.

(32) Zhang, L.; Lin, S.; Hua, T.; Huang, B.; Liu, S.; Tao, X. Fiber-Based Thermoelectric Generators: Materials, Device Structures, Fabrication, Characterization, and Applications. *Adv. Energy Mater.* **2018**, *8* (5), 1–18. https://doi.org/10.1002/aenm.201700524.

(33) Sun, J.; Yeh, M. L.; Jung, B. J.; Zhang, B.; Feser, J.; Majumdar, A.; Katz, H. E. Simultaneous Increase in Seebeck Coefficient and Conductivity in a Doped

Poly(Alkylthiophene) Blend with Defined Density of States. *Macromolecules* **2010**, *43* (6), 2897–2903. https://doi.org/10.1021/MA902467K/ASSET/IMAGES/LARGE/MA-2009-02467K_0002.JPEG.

(34) Watanabe, S.; Ohno, M.; Yamashita, Y.; Terashige, T.; Okamoto, H.; Takeya, J. Validity of the Mott Formula and the Origin of Thermopower in π-Conjugated Semicrystalline Polymers. *Phys. Rev. B* **2019**, *10* (24), 241201. https://doi.org/10.1103/PhysRevB.100.241201.

(35) Cutler, M.; Mott, N. F. Observation of Anderson Localization in an Electron Gas. *Phys. Rev.* **1969**, *181* (3), 1336–1340. https://doi.org/10.1103/PhysRev.181.1336.

(36) Patel, S. N.; Glaudell, A. M.; Peterson, K. A.; Thomas, E. M.; O'Hara, K. A.; Lim, E.; Chabinyc, M. L. Morphology Controls the Thermoelectric Power Factor of a Doped Semiconducting Polymer. *Sci. Adv.* **2017**, *3* (6). https://doi.org/10.1126/sciadv.1700434.

(37) Moshwan, R.; Yang, L.; Zou, J.; Chen, Z. G. Eco-Friendly SnTe Thermoelectric Materials: Progress and Future Challenges. *Advanced Functional Materials*. Wiley-VCH Verlag November 17, 2017, p 1703278. https://doi.org/10.1002/adfm.201703278.

(38) Wu, H.; Huang, Y. A.; Xu, F.; Duan, Y.; Yin, Z. Energy Harvesters for Wearable and Stretchable Electronics: From Flexibility to Stretchability. *Adv. Mater.* **2016**, *28* (45), 9881–9919. https://doi.org/10.1002/adma.201602251.

(39) Kim, H. S.; Gibbs, Z. M.; Tang, Y.; Wang, H.; Snyder, G. J. Characterization of Lorenz Number with Seebeck Coefficient Measurement. *APL Mater.* **2015**, *3* (4), 1–6. https://doi.org/10.1063/1.4908244.

(40) Snyder, G. J.; Toberer, E. S. Complex Thermoelectric Materials. *Nature Materials*. February 2008, pp 105–114. https://doi.org/10.1038/nmat2090.

(41) Zhao, D.; Würger, A.; Crispin, X. Ionic Thermoelectric Materials and Devices. *J. Energy Chem.* **2021**, *61*, 88–103. https://doi.org/10.1016/J.JECHEM.2021.02.022.

(42) Cheng, H.; Le, Q.; Liu, Z.; Qian, Q.; Zhao, Y.; Ouyang, J. Ionic Thermoelectrics: Principles, Materials and Applications. *J. Mater. Chem. C* **2022**, *10* (2), 433–450. https://doi.org/10.1039/D1TC05242J.

(43) Eastman, E. D. Theory of the Soret Effect. *J. Am. Chem. Soc.* **1928**, *50* (2), 283–291. https://doi.org/10.1021/ja01389a007.

(44) Quickenden, T. I.; Mua, Y. A Review of Power Generation in Aqueous Thermogalvanic Cells. *J. Electrochem. Soc.* **1995**, *142* (11), 3985–3994. https://doi.org/10.1149/1.2048446/XML.

(45) Dhont, J. K. G. Thermodiffusion of Interacting Colloids. II. A Microscopic Approach. *J. Chem. Phys.* **2004**, *120* (3), 1642. https://doi.org/10.1063/1.1633547.

(46) Onsager, L. Reciprocal Relations in Irreversible Processes. I. *Phys. Rev.* **1931**, *37* (4), 405. https://doi.org/10.1103/PhysRev.37.405.

(47) Onsager, L. Reciprocal Relations in Irreversible Processes. II. *Phys. Rev.* **1931**, *38* (12), 2265. https://doi.org/10.1103/PhysRev.38.2265.

(48) Liu, W.; Qian, X.; Han, C. G.; Li, Q.; Chen, G. Ionic Thermoelectric Materials for near Ambient Temperature Energy Harvesting. *Applied Physics Letters*. American Institute of Physics Inc. January 11, 2021, p 20501. https://doi.org/10.1063/5.0032119.

(49) Liu, J.; Zeng, W.; Tao, X. Gigantic Effect Due to Phase Transition on Thermoelectric Properties of Ionic Sol–Gel Materials. *Adv. Funct. Mater.* **2022**, 2208286. https://doi.org/10.1002/ADFM.202208286.

(50) Huang, B. T.; Roger, M.; Bonetti, M.; Salez, T. J.; Wiertel-Gasquet, C.; Dubois, E.; Cabreira Gomes, R.; Demouchy, G.; Mériguet, G.; Peyre, V.; Kouyaté, M.; Filomeno, C. L.; Depeyrot, J.; Tourinho, F. A.; Perzynski, R.; Nakamae, S. Thermoelectricity and Thermodiffusion in Charged Colloids. *J. Chem. Phys.* **2015**, *143* (5), 054902. https://doi.org/10.1063/1.4927665.

(51) Liu, J.; Zeng, W.; Tao, X. Gigantic Effect Due to Phase Transition on Thermoelectric Properties of Ionic Sol–Gel Materials. *Adv. Funct. Mater.* **2022**, 2208286. https://doi.org/10.1002/ADFM.202208286.

(52) Agar, J. N.; Mou, C. Y.; Lin, J. L. Single-Ion Heat of Transport in Electrolyte Solutions: A Hydrodynamic Theory. *J. Phys. Chem.* **2002**, *93* (5), 2079–2082. https://doi.org/10.1021/J100342A073.

(53) Eastman, E. D.; 48, Y. THERMODYNAMICS OF NON-ISOTHERMAL SYSTEMS. *J. Am. Chem. Soc.* **2002**, *48* (6), 1482–1493. https://doi.org/10.1021/JA01417A004.

(54) Hu, R.; Cola, B. A.; Haram, N.; Barisci, J. N.; Lee, S.; Stoughton, S.; Wallace, G.; Too, C.; Thomas, M.; Gestos, A.; Dela Cruz, M. E.; Ferraris, J. P.; Zakhidov, A. A.; Baughman, R. H. Harvesting Waste Thermal Energy Using a Carbon-Nanotube-Based Thermo-Electrochemical Cell. *Nano Lett.* **2010**, *10* (3), 838–846. https://doi.org/10.1021/nl903267n.

(55) Zeng, W.; Tao, X. M.; Lin, S. P.; Lee, C.; Shi, D. L.; Lam, K. H.; Huang, B. L.; Wang, Q. M.; Zhao, Y. Defect-Engineered Reduced Graphene Oxide Sheets with High Electric Conductivity and Controlled Thermal Conductivity for Soft and Flexible Wearable Thermoelectric Generators. *Nano Energy* **2018**, *54*, 163–174. https://doi.org/10.1016/j.nanoen.2018.10.015.

(56) Yeo, M. ; Sattar, M.; Yeo, W.-H.; Woodruff, G. W. Recent Advances in Materials for Wearable Thermoelectric Generators and Biosensing Devices. *Mater. 2022, Vol. 15, Page 4315* **2022**, *15* (12), 4315. https://doi.org/10.3390/MA15124315.

(57) Zhou, Z.; Han, G.; Lu, X.; Wang, G.; Zhou, X. High-Performance Magnesium-Based Thermoelectric Materials: Progress and Challenges. *J. Magnes. Alloy.* **2022**, *10* (7), 1719–1736. https://doi.org/10.1016/J.JMA.2022.05.021.

(58) Giri, K.; Wang, Y. L.; Chen, T. H.; Chen, C. H. Challenges and Strategies to Optimize the Figure of Merit: Keeping Eyes on Thermoelectric Metamaterials. *Mater. Sci. Semicond. Process.* **2022**, *150*, 106944. https://doi.org/10.1016/J.MSSP.2022.106944.

(59) Liu, W.; Hu, J.; Zhang, S.; Deng, M.; Han, C. G.; Liu, Y. New Trends, Strategies and Opportunities in Thermoelectric Materials: A Perspective. *Materials Today*

Physics. Elsevier Ltd June 1, 2017, pp 50–60. https://doi.org/10.1016/j.mtphys.2017.06.001.

(60) Acharya, M.; Jana, S. S.; Ranjan, M.; Maiti, T. High Performance (ZT>1) n-Type Oxide Thermoelectric Composites from Earth Abundant Materials. *Nano Energy* **2021**, *84*, 105905. https://doi.org/10.1016/J.NANOEN.2021.105905.

(61) Rahman, J. U.; Van Du, N.; Rahman, G.; García-Suárez, V. M.; Seo, W. S.; Kim, M. H.; Lee, S. Localized Double Phonon Scattering and DOS Induced Thermoelectric Enhancement of Degenerate Nonstoichiometric Li 1−x NbO 2 Compounds. *RSC Adv.* **2017**, *7* (84), 53255–53264. https://doi.org/10.1039/C7RA10557F.

(62) Zhang, X.; Zhang, Y.; Wu, L.; Tsuruta, A.; Mikami, M.; Cho, H. J.; Ohta, H. Ba1/3CoO2: A Thermoelectric Oxide Showing a Reliable ZT of ∼0.55 at 600 °C in Air. *ACS Appl. Mater. Interfaces* **2022**, *14* (29), 33355–33360. https://doi.org/10.1021/ACSAMI.2C08555.

(63) Gu, Y.; Shi, X. L.; Pan, L.; Liu, W. Di; Sun, Q.; Tang, X.; Kou, L. Z.; Liu, Q. F.; Wang, Y. F.; Chen, Z. G. Rational Electronic and Structural Designs Advance BiCuSeO Thermoelectrics. *Adv. Funct. Mater.* **2021**, *31* (25), 2101289. https://doi.org/10.1002/ADFM.202101289.

(64) Tang, D.; Zhu, W.; Wei, P.; Zhou, H.; Liu, Z.; Yu, J.; Zhao, W. Preparation and Properties of Zn4Sb2.94In0.06/ZnO Composite Thermoelectric Materials. *J. Electron. Mater. 2014 446* **2015**, *44* (6), 1902–1908. https://doi.org/10.1007/S11664-014-3590-7.

(65) Fu, C.; Bai, S.; Liu, Y.; Tang, Y.; Chen, L.; Zhao, X.; Zhu, T. Realizing High Figure of Merit in Heavy-Band p-Type Half-Heusler Thermoelectric Materials. *Nat. Commun. 2015 61* **2015**, *6* (1), 1–7. https://doi.org/10.1038/ncomms9144.

(66) Xing, Y.; Liu, R.; Liao, J.; Zhang, Q.; Xia, X.; Wang, C.; Huang, H.; Chu, J.; Gu, M.; Zhu, T.; Zhu, C.; Xu, F.; Yao, D.; Zeng, Y.; Bai, S.; Uher, C.; Chen, L. High-Efficiency Half-Heusler Thermoelectric Modules Enabled by Self-Propagating Synthesis and Topologic Structure Optimization. *Energy Environ. Sci.* **2019**, *12* (11), 3390–3399. https://doi.org/10.1039/C9EE02228G.

(67) Rogl, G.; Ghosh, S.; Renk, O.; Yubuta, K.; Grytsiv, A.; Schafler, E.; Zehetbauer, M.; Mallik, R. C.; Bauer, E.; Rogl, P. Influence of Shear Strain on HPT-Processed n-Type Skutterudites Yielding ZT=2.1. *J. Alloys Compd.* **2021**, *855*, 157409. https://doi.org/10.1016/J.JALLCOM.2020.157409.

(68) Zhang, J.; Zhang, L.; Ren, W.; Gou, W.; Zhang, J.; Geng, H. Multiple-Filling-Induced Full-Spectrum Phonon Scattering and Band Convergence Leading to High-Performance n-Type Skutterudites. *ACS Appl. Mater. Interfaces* **2021**, *13* (25), 29809–29819. https://doi.org/10.1021/ACSAMI.1C06267/ASSET/IMAGES/LARGE/AM1C06267_0008.JPEG.

(69) Qin, D.; Shi, W.; Lu, Y.; Cai, W.; Sui, J. Efficient Si Doping Promoting Thermoelectric Performance of Yb-Filled CoSb3-Based Skutterudites. *ACS Appl. Mater. Interfaces* **2022**, *14*, 30906.

https://doi.org/10.1021/ACSAMI.2C07044/SUPPL_FILE/AM2C07044_SI_001.PDF.

(70) Jiang, Y.; Na, L.; Ma, H. HPHT Synthesis and Enhanced Thermoelectric Transport Properties of Double-Doped Co4Sb11TexSn1-x Skutterudites. *J. Alloys Compd.* **2022**, *894*, 162426. https://doi.org/10.1016/J.JALLCOM.2021.162426.

(71) Zhang, J.; Wang, L.; Liu, M.; Wang, J.; Sun, K.; Yang, Y.; Hu, B.; Xu, J.; Su, T.; Du, B. Preparation and Thermoelectric Performance of Tetrahedrite-like Cubic Cu3SbS3 Compound. *J. Mater. Sci. Mater. Electron.* **2021**, *32* (8), 10789–10802. https://doi.org/10.1007/S10854-021-05737-5/FIGURES/10.

(72) Hu, H.; Zhuang, H.-L.; Jiang, Y.; Shi, J.; Li, J.-W.; Cai, B.; Han, Z.; Pei, J.; Su, B.; Ge, Z.-H.; Zhang, B.-P.; Li, J.-F.; Hu, H.; Zhuang, H.-L.; Jiang, Y.; Li, J.-W.; Cai, B.; Han, Z.; Pei, J.; Su, B.; Li, J.-F.; Shi, J.; Zhang, B.-P.; Ge, Z.-H. Thermoelectric Cu12Sb4S13-Based Synthetic Minerals with a Sublimation-Derived Porous Network. *Adv. Mater.* **2021**, *33* (43), 2103633. https://doi.org/10.1002/ADMA.202103633.

(73) Lu, X.; Morelli, D. T.; Xia, Y.; Zhou, F.; Ozolins, V.; Chi, H.; Zhou, X.; Uher, C.; Lu, X.; Morelli, D. T.; Xia, Y.; Zhou, F.; Ozolins, V.; Chi, H.; Zhou, X.; Uher, C. High Performance Thermoelectricity in Earth-Abundant Compounds Based on Natural Mineral Tetrahedrites. *Adv. Energy Mater.* **2013**, *3* (3), 342–348. https://doi.org/10.1002/AENM.201200650.

(74) Heo, J.; Laurita, G.; Muir, S.; Subramanian, M. A.; Keszler, D. A. Enhanced Thermoelectric Performance of Synthetic Tetrahedrites. *Chem. Mater.* **2014**, *26*

(6), 2047–2051. https://doi.org/10.1021/CM404026K/SUPPL_FILE/CM404026K_SI_001.PDF.

(75) Zhao, K.; Qiu, P.; Song, Q.; Blichfeld, A. B.; Eikeland, E.; Ren, D.; Ge, B.; Iversen, B. B.; Shi, X.; Chen, L. Ultrahigh Thermoelectric Performance in Cu2−ySe0.5S0.5 Liquid-like Materials. *Mater. Today Phys.* **2017**, *1*, 14–23. https://doi.org/10.1016/J.MTPHYS.2017.04.003.

(76) Zhao, K.; Blichfeld, A. B.; Chen, H.; Song, Q.; Zhang, T.; Zhu, C.; Ren, D.; Hanus, R.; Qiu, P.; Iversen, B. B.; Xu, F.; Snyder, G. J.; Shi, X.; Chen, L. Enhanced Thermoelectric Performance through Tuning Bonding Energy in Cu2Se1-XSx Liquid-like Materials. *Chem. Mater.* **2017**, *29* (15), 6367–6377. https://doi.org/10.1021/ACS.CHEMMATER.7B01687/ASSET/IMAGES/CM-2017-01687F_M006.GIF.

(77) He, Y.; Day, T.; Zhang, T.; Liu, H.; Shi, X.; Chen, L.; Jeffrey Snyder, G.; He, Y.; Zhang, T.; Liu, H.; Shi, X.; Chen, L.; Day, T.; Snyder, G. J. High Thermoelectric Performance in Non-Toxic Earth-Abundant Copper Sulfide. *Adv. Mater.* **2014**, *26* (23), 3974–3978. https://doi.org/10.1002/ADMA.201400515.

(78) Zhao, L.; Wang, X.; Fei, F. Y.; Wang, J.; Cheng, Z.; Dou, S.; Wang, J.; Snyder, G. J. High Thermoelectric and Mechanical Performance in Highly Dense Cu 2−x S Bulks Prepared by a Melt-Solidification Technique. *J. Mater. Chem. A* **2015**, *3* (18), 9432–9437. https://doi.org/10.1039/C5TA01667C.

(79) Zhao, K.; Blichfeld, A. B.; Eikeland, E.; Qiu, P.; Ren, D.; Iversen, B. B.; Shi, X.; Chen, L. Extremely Low Thermal Conductivity and High Thermoelectric

Performance in Liquid-like Cu2Se1−xSx Polymorphic Materials. *J. Mater. Chem. A* **2017**, *5* (34), 18148–18156. https://doi.org/10.1039/C7TA05788A.

(80) Zhao, L. D.; Lo, S. H.; Zhang, Y.; Sun, H.; Tan, G.; Uher, C.; Wolverton, C.; Dravid, V. P.; Kanatzidis, M. G. Ultralow Thermal Conductivity and High Thermoelectric Figure of Merit in SnSe Crystals. *Nature* **2014**, *508* (7496), 373–377. https://doi.org/10.1038/nature13184.

(81) Kong, S.; Wu, T.; Yuan, M.; Huang, Z.; Meng, Q. L.; Jiang, Q.; Zhuang, W.; Jiang, P.; Bao, X. Dramatically Enhanced Thermoelectric Performance of MoS2 by Introducing MoO2 Nanoinclusions. *J. Mater. Chem. A* **2017**, *5* (5), 2004–2011. https://doi.org/10.1039/C6TA10219K.

(82) Wang, J.; Xie, F.; Cao, X. H.; An, S. C.; Zhou, W. X.; Tang, L. M.; Chen, K. Q. Excellent Thermoelectric Properties in Monolayer WSe2 Nanoribbons Due to Ultralow Phonon Thermal Conductivity. *Sci. Reports 2017 71* **2017**, *7* (1), 1–8. https://doi.org/10.1038/srep41418.

(83) Hu, Z. Y.; Li, K. Y.; Lu, Y.; Huang, Y.; Shao, X. H. High Thermoelectric Performances of Monolayer SnSe Allotropes. *Nanoscale* **2017**, *9* (41), 16093–16100. https://doi.org/10.1039/C7NR04766E.

(84) Gelbstein, Y.; Dashevsky, Z.; Dariel, M. P. High Performance N-Type PbTe-Based Materials for Thermoelectric Applications. *Phys. B Condens. Matter* **2005**, *363* (1–4), 196–205. https://doi.org/10.1016/J.PHYSB.2005.03.022.

(85) Fu, J.; Song, S.; Zhang, X.; Cao, F.; Zhou, L.; Li, X.; Zhang, H. Bi2Te3 Nanoplates and Nanoflowers: Synthesized by Hydrothermal Process and Their Enhanced Thermoelectric Properties. *CrystEngComm* **2012**, *14* (6), 2159–2165. https://doi.org/10.1039/C2CE06348D.

(86) Wu, F.; Song, H.; Gao, F.; Shi, W.; Jia, J.; Hu, X. Effects of Different Morphologies of Bi2Te3 Nanopowders on Thermoelectric Properties. *J. Electron. Mater. 2013 426* **2013**, *42* (6), 1140–1145. https://doi.org/10.1007/S11664-013-2541-Z.

(87) Venkatasubramanian, R.; Siivola, E.; Colpitts, T.; O'Quinn, B. Thin-Film Thermoelectric Devices with High Room-Temperature Figures of Merit. *Nat. 2001 4136856* **2001**, *413* (6856), 597–602. https://doi.org/10.1038/35098012.

(88) Kim, S. J.; We, J. H.; Cho, B. J. A Wearable Thermoelectric Generator Fabricated on a Glass Fabric. *Energy Environ. Sci.* **2014**, *7* (6), 1959–1965. https://doi.org/10.1039/c4ee00242c.

(89) Ohta, H.; Seo, W. S.; Koumoto, K. Thermoelectric Properties of Homologous Compounds in the ZnO–In2O3 System. *J. Am. Ceram. Soc.* **1996**, *79* (8), 2193–2196. https://doi.org/10.1111/J.1151-2916.1996.TB08958.X.

(90) Muta, H.; Kurosaki, K.; Uno, M.; Yamanaka, S. Thermoelectric Properties of Ti- and Sn-Doped α-Fe2O3. *J. Alloys Compd.* **2002**, *335* (1–2), 200–202. https://doi.org/10.1016/S0925-8388(01)01804-7.

(91) Ohtaki, M.; Koga, H.; Tokunaga, T.; Eguchi, K.; Arai, H. Electrical Transport Properties and High-Temperature Thermoelectric Performance of (Ca0.9M0.1)MnO3 (M = Y, La, Ce, Sm, In, Sn, Sb, Pb, Bi). *J. Solid State Chem.* **1995**, *120* (1), 105–111. https://doi.org/10.1006/JSSC.1995.1384.

(92) Koumoto, K.; Seo, W. S.; Ozawa, S. Huge Thermopower of Porous Y2O3. *Appl. Phys. Lett.* **1998**, *71* (11), 1475. https://doi.org/10.1063/1.119941.

(93) Ji, L. Metal Oxide-Based Thermoelectric Materials. *Met. Oxides Energy Technol.* **2018**, 49–72. https://doi.org/10.1016/B978-0-12-811167-3.00003-1.

(94) Huang, L.; Zhang, Q.; Yuan, B.; Lai, X.; Yan, X.; Ren, Z. Recent Progress in Half-Heusler Thermoelectric Materials. *Mater. Res. Bull.* **2016**, *76*, 107–112. https://doi.org/10.1016/J.MATERRESBULL.2015.11.032.

(95) Nolas, G. S.; Morelli, D. T.; Tritt, T. M. SKUTTERUDITES: A Phonon-Glass-Electron Crystal Approach to Advanced Thermoelectric Energy Conversion Applications. *http://dx.doi.org/10.1146/annurev.matsci.29.1.89* **2003**, *29*, 89–116. https://doi.org/10.1146/ANNUREV.MATSCI.29.1.89.

(96) Olvera, A. A.; Moroz, N. A.; Sahoo, P.; Ren, P.; Bailey, T. P.; Page, A. A.; Uher, C.; Poudeu, P. F. P. Partial Indium Solubility Induces Chemical Stability and Colossal Thermoelectric Figure of Merit in Cu2Se. *Energy Environ. Sci.* **2017**, *10* (7), 1668–1676. https://doi.org/10.1039/C7EE01193H.

(97) Xie, W.; Liu, F.; Zheng, Y.; Ge, N.; Dai, B.; Zhang, X. Thermoelectric Performance Enhancement of Eco-Friendly Cu 2 Se through Incorporating CB 4. *RSC Adv.* **2022**, *12* (22), 14112–14118. https://doi.org/10.1039/D2RA01546C.

(98) Ding, Y.; Qiu, Y.; Cai, K.; Yao, Q.; Chen, S.; Chen, L.; He, J. High Performance N-Type Ag2Se Film on Nylon Membrane for Flexible Thermoelectric Power Generator. *Nat. Commun. 2019 101* **2019**, *10* (1), 1–7. https://doi.org/10.1038/s41467-019-08835-5.

(99) Yang, D.; Su, X.; Li, J.; Bai, H.; Wang, S.; Li, Z.; Tang, H.; Tang, K.; Luo, T.; Yan, Y.; Wu, J.; Yang, J.; Zhang, Q.; Uher, C.; Kanatzidis, M. G.; Tang, X. Blocking Ion Migration Stabilizes the High Thermoelectric Performance in Cu2Se Composites. *Adv. Mater.* **2020**, *32* (40), 2003730. https://doi.org/10.1002/ADMA.202003730.

(100) Shi, X.; Chen, H.; Hao, F.; Liu, R.; Wang, T.; Qiu, P.; Burkhardt, U.; Grin, Y.; Chen, L. Room-Temperature Ductile Inorganic Semiconductor. *Nat. Mater. 2018 175* **2018**, *17* (5), 421–426. https://doi.org/10.1038/s41563-018-0047-z.

(101) Liu, H.; Shi, X.; Xu, F.; Zhang, L.; Zhang, W.; Chen, L.; Li, Q.; Uher, C.; Day, T.; Snyder Jeffrey, G. Copper Ion Liquid-like Thermoelectrics. *Nat. Mater.* **2012**, *11* (5), 422–425. https://doi.org/10.1038/nmat3273.

(102) Byeon, D.; Sobota, R.; Delime-Codrin, K.; Choi, S.; Hirata, K.; Adachi, M.; Kiyama, M.; Matsuura, T.; Yamamoto, Y.; Matsunami, M.; Takeuchi, T. Discovery of Colossal Seebeck Effect in Metallic Cu2Se. *Nat. Commun. 2019 101* **2019**, *10* (1), 1–7. https://doi.org/10.1038/s41467-018-07877-5.

(103) Bai, H.; Su, X.; Yang, D.; Zhang, Q.; Tan, G.; Uher, C.; Tang, X.; Wu, J. An Instant Change of Elastic Lattice Strain during Cu2Se Phase Transition: Origin of Abnormal Thermoelectric Properties. *Adv. Funct. Mater.* **2021**, *31* (20). https://doi.org/10.1002/adfm.202100431.

(104) Lalonde, A. D.; Pei, Y.; Wang, H.; Jeffrey Snyder, G. Lead Telluride Alloy Thermoelectrics. *Mater. Today* **2011**, *14* (11), 526–532. https://doi.org/10.1016/S1369-7021(11)70278-4.

(105) Xiao, Y.; Zhao, L. D. Charge and Phonon Transport in PbTe-Based Thermoelectric Materials. *npj Quantum Mater. 2018 31* **2018**, *3* (1), 1–12. https://doi.org/10.1038/s41535-018-0127-y.

(106) Il Kim, S.; Lee, K. H.; Mun, H. A.; Kim, H. S.; Hwang, S. W.; Roh, J. W.; Yang, D. J.; Shin, W. H.; Li, X. S.; Lee, Y. H.; Snyder, G. J.; Kim, S. W. Dense Dislocation Arrays Embedded in Grain Boundaries for High-Performance Bulk Thermoelectrics. *Science (80-.).* **2015**, *348* (6230), 109–114. https://doi.org/10.1126/science.aaa4166.

(107) Huang, B. L.; Kaviany, M. Ab Initio and Molecular Dynamics Predictions for Electron and Phonon Transport in Bismuth Telluride. *Phys. Rev. B - Condens. Matter Mater. Phys.* **2008**, *77* (12), 125209. https://doi.org/10.1103/PHYSREVB.77.125209/FIGURES/16/MEDIUM.

(108) Zhao, L. D.; Lo, S. H.; Zhang, Y.; Sun, H.; Tan, G.; Uher, C.; Wolverton, C.; Dravid, V. P.; Kanatzidis, M. G. Ultralow Thermal Conductivity and High

Thermoelectric Figure of Merit in SnSe Crystals. *Nature* **2014**, *508* (7496), 373–377. https://doi.org/10.1038/nature13184.

(109) Park, Y. W.; Yoon, C. O.; Lee, C. H.; Shirakawa, H.; Suezaki, Y.; Akagi, K. Conductivity and Thermoelectric Power of the Newly Processed Polyacetylene. *Synth. Met.* **1989**, *28* (3), D27–D34. https://doi.org/10.1016/0379-6779(89)90670-X.

(110) Zuzok, R.; Kaiser, A. B.; Pukacki, W.; Roth, S. Thermoelectric Power and Conductivity of Iodine-Doped "New" Polyacetylene. *J. Chem. Phys.* **1991**, *95* (2), 1270–1275. https://doi.org/10.1063/1.461107.

(111) Moses, D.; Denenstein, A. Experimental Determination of the Thermal Conductivity of a Conducting Polymer: Pure and Heavily Doped Polyacetylene. *Phys. Rev. B* **1984**, *30* (4), 2090–2097. https://doi.org/10.1103/PhysRevB.30.2090.

(112) Maddison, D. S.; Unsworth, J.; Roberts, R. B. Electrical Conductivity and Thermoelectric Power of Polypyrrole with Different Doping Levels. *Synth. Met.* **1988**, *26* (1), 99–108. https://doi.org/10.1016/0379-6779(88)90339-6.

(113) Holland, E. R.; Pomfret, S. J.; Adams, P. N.; Abell, L.; Monkman, A. P. Doping Dependent Transport Properties of Polyaniline-CSA Films. *Synth. Met.* **1997**, *84* (1–3), 777–778. https://doi.org/10.1016/s0379-6779(96)04141-0.

(114) Anno, H.; Hokazono, M.; Akagi, F.; Hojo, M.; Toshima, N. Thermoelectric Properties of Polyaniline Films with Different Doping Concentrations of (±)-10-

Camphorsulfonic Acid. *J. Electron. Mater.* **2013**, *42* (7), 1346–1351. https://doi.org/10.1007/s11664-012-2368-z.

(115) [a]bert[o] Groenendaal, L.; Jonas, F.; Freitag, D.; Pielartzik, H.; Reynolds, J. R. *Poly(3,4-Ethylenedioxythiophene) and Its Derivatives: Past, Present, and Future***. https://doi.org/10.1002/(SICI)1521-4095(200004)12:7.

(116) Taroni, P. J.; Hoces, I.; Stingelin, N.; Heeney, M.; Bilotti, E. Thermoelectric Materials: A Brief Historical Survey from Metal Junctions and Inorganic Semiconductors to Organic Polymers. *Israel Journal of Chemistry*. Wiley-VCH Verlag June 1, 2014, pp 534–552. https://doi.org/10.1002/ijch.201400037.

(117) Kim, G. H.; Shao, L.; Zhang, K.; Pipe, K. P. Engineered Doping of Organic Semiconductors for Enhanced Thermoelectric Efficiency. *Nat. Mater.* **2013**, *12* (8), 719–723. https://doi.org/10.1038/nmat3635.

(118) Zhao, D.; Wang, H.; Khan, Z. U.; Chen, J. C.; Gabrielsson, R.; Jonsson, M. P.; Berggren, M.; Crispin, X. Ionic Thermoelectric Supercapacitors. *Energy Environ. Sci.* **2016**, *9* (4), 1450–1457. https://doi.org/10.1039/c6ee00121a.

(119) Wang, H.; Zhao, D.; Khan, Z. U.; Puzinas, S.; Jonsson, M. P.; Berggren, M.; Crispin, X. Ionic Thermoelectric Figure of Merit for Charging of Supercapacitors. *Adv. Electron. Mater.* **2017**, *3* (4), 1700013. https://doi.org/10.1002/AELM.201700013.

(120) Bonetti, M.; Nakamae, S.; Roger, M.; Guenoun, P. Huge Seebeck Coefficients in Nonaqueous Electrolytes. *J. Chem. Phys.* **2011**, *134* (11), 114513. https://doi.org/10.1063/1.3561735.

(121) Bonetti, M.; Nakamae, S.; Roger, M.; Guenoun, P. Huge Seebeck Coefficients in Nonaqueous Electrolytes. *J. Chem. Phys.* **2011**, *134* (11), 114513. https://doi.org/10.1063/1.3561735.

(122) Zhao, D.; Martinelli, A.; Willfahrt, A.; Fischer, T.; Bernin, D.; Khan, Z. U.; Shahi, M.; Brill, J.; Jonsson, M. P.; Fabiano, S.; Crispin, X. Polymer Gels with Tunable Ionic Seebeck Coefficient for Ultra-Sensitive Printed Thermopiles. *Nat. Commun. 2019 101* **2019**, *10* (1), 1–8. https://doi.org/10.1038/s41467-019-08930-7.

(123) Cheng, H.; He, X.; Fan, Z.; Ouyang, J. Flexible Quasi-Solid State Ionogels with Remarkable Seebeck Coefficient and High Thermoelectric Properties. *Adv. Energy Mater.* **2019**, *9* (32), 1901085. https://doi.org/10.1002/AENM.201901085.

(124) Abraham, T. J.; Macfarlane, D. R.; Pringle, J. M. High Seebeck Coefficient Redox Ionic Liquid Electrolytes for Thermal Energy Harvesting. *Energy Environ. Sci.* **2013**, *6* (9), 2639–2645. https://doi.org/10.1039/c3ee41608a.

(125) Buckingham, M. A.; Marken, F.; Aldous, L. The Thermoelectrochemistry of the Aqueous Iron(Ii)/Iron(Iii) Redox Couple: Significance of the Anion and PH in Thermogalvanic Thermal-to-Electrical Energy Conversion. *Sustain. Energy Fuels* **2018**, *2* (12), 2717–2726. https://doi.org/10.1039/c8se00416a.

(126) Abraham, T. J.; Macfarlane, D. R.; Baughman, R. H.; Jin, L.; Li, N.; Pringle, J. M. Towards Ionic Liquid-Based Thermoelectrochemical Cells for the Harvesting of Thermal Energy. *Electrochim. Acta* **2013**, *113*, 87–93. https://doi.org/10.1016/J.ELECTACTA.2013.08.087.

(127) Im, H.; Kim, T.; Song, H.; Choi, J.; Park, J. S.; Ovalle-Robles, R.; Yang, H. D.; Kihm, K. D.; Baughman, R. H.; Lee, H. H.; Kang, T. J.; Kim, Y. H. High-Efficiency Electrochemical Thermal Energy Harvester Using Carbon Nanotube Aerogel Sheet Electrodes. *Nat. Commun. 2016 71* **2016**, *7* (1), 1–9. https://doi.org/10.1038/ncomms10600.

(128) Duan, J.; Feng, G.; Yu, B.; Li, J.; Chen, M.; Yang, P.; Feng, J.; Liu, K.; Zhou, J. Aqueous Thermogalvanic Cells with a High Seebeck Coefficient for Low-Grade Heat Harvest. *Nat. Commun.* **2018**, *9* (1), 1–8. https://doi.org/10.1038/s41467-018-07625-9.

(129) Yu, B.; Duan, J.; Cong, H.; Xie, W.; Liu, R.; Zhuang, X.; Wang, H.; Qi, B.; Xu, M.; Wang, Z. L.; Zhou, J. Thermosensitive Crystallization-Boosted Liquid Thermocells for Low-Grade Heat Harvesting. *Science (80-.).* **2020**, *370* (6514), 342–346. https://doi.org/10.1126/science.abd6749.

(130) Moshwan, R.; Liu, W. Di; Shi, X. L.; Wang, Y. P.; Zou, J.; Chen, Z. G. Realizing High Thermoelectric Properties of SnTe via Synergistic Band Engineering and Structure Engineering. *Nano Energy* **2019**, *65*, 104056. https://doi.org/10.1016/j.nanoen.2019.104056.

(131) Zheng, Z.; Su, X.; Deng, R.; Stoumpos, C.; Xie, H.; Liu, W.; Yan, Y.; Hao, S.; Uher, C.; Wolverton, C.; Kanatzidis, M. G.; Tang, X. Rhombohedral to Cubic Conversion of GeTe via MnTe Alloying Leads to Ultralow Thermal Conductivity, Electronic Band Convergence, and High Thermoelectric Performance. *J. Am. Chem. Soc.* **2018**, *140* (7), 2673–2686. https://doi.org/10.1021/jacs.7b13611.

(132) He, M.; Ge, J.; Lin, Z.; Feng, X.; Wang, X.; Lu, H.; Yang, Y.; Qiu, F. Thermopower Enhancement in Conducting Polymer Nanocomposites via Carrier Energy Scattering at the Organic-Inorganic Semiconductor Interface. *Energy Environ. Sci.* **2012**, *5* (8), 8351–8358. https://doi.org/10.1039/c2ee21803h.

(133) Ko, D. K.; Kang, Y.; Murray, C. B. Enhanced Thermopower via Carrier Energy Filtering in Solution-Processable Pt-Sb2Te3 Nanocomposites. *Nano Lett.* **2011**, *11* (7), 2841–2844. https://doi.org/10.1021/nl2012246.

(134) Yang, L.; Chen, Z. G.; Han, G.; Hong, M.; Zou, Y.; Zou, J. High-Performance Thermoelectric Cu2Se Nanoplates through Nanostructure Engineering. *Nano Energy* **2015**, *16*, 367–374. https://doi.org/10.1016/j.nanoen.2015.07.012.

(135) Lan, J. Le; Liu, Y.; Lin, Y. H.; Nan, C. W.; Cai, Q.; Yang, X. Enhanced Thermoelectric Performance of In2O3-Based Ceramics via Nanostructuring and Point Defect Engineering. *Sci. Reports 2015 51* **2015**, *5* (1), 1–6. https://doi.org/10.1038/srep07783.

(136) Suarez, F.; Parekh, D. P.; Ladd, C.; Vashaee, D.; Dickey, M. D.; Ozturk, M. C. Flexible Thermoelectric Generator Using Bulk Legs and Liquid Metal

Interconnects for Wearable Electronics. *Appl. Energy* **2017**, *202*, 736–745. https://doi.org/10.1016/j.apenergy.2017.05.181.

(137) Reddy, B. V. K.; Barry, M.; Li, J.; Chyu, M. K. Convective Heat Transfer and Contact Resistances Effects on Performance of Conventional and Composite Thermoelectric Devices. *J. Heat Transfer* **2014**, *136* (10). https://doi.org/10.1115/1.4028021/373219.

(138) Hu, X. K.; Yamamoto, A.; Ohta, M.; Nishiate, H. Measurement and Simulation of Thermoelectric Efficiency for Single Leg. *Rev. Sci. Instrum.* **2015**, *86* (4). https://doi.org/Artn 04510310.1063/1.4916545.

(139) LeBlanc, S. Thermoelectric Generators: Linking Material Properties and Systems Engineering for Waste Heat Recovery Applications. *Sustain. Mater. Technol.* **2014**, *1–2*, 26–35. https://doi.org/10.1016/J.SUSMAT.2014.11.002.

(140) Zhang, Z.; Zhao, K.; Wei, T. R.; Qiu, P.; Chen, L.; Shi, X. Cu2Se-Based Liquid-like Thermoelectric Materials: Looking Back and Stepping Forward. *Energy and Environmental Science*. Royal Society of Chemistry October 1, 2020, pp 3307–3329. https://doi.org/10.1039/d0ee02072a.

(141) Mehdizadeh Dehkordi, A.; Zebarjadi, M.; He, J.; Tritt, T. M. Thermoelectric Power Factor: Enhancement Mechanisms and Strategies for Higher Performance Thermoelectric Materials. *Materials Science and Engineering R: Reports*. Elsevier Ltd November 1, 2015, pp 1–22. https://doi.org/10.1016/j.mser.2015.08.001.

(142) Hong, M.; Chen, Z. G.; Yang, L.; Zou, Y. C.; Dargusch, M. S.; Wang, H.; Zou, J. Realizing ZT of 2.3 in Ge1−x−ySbxInyTe via Reducing the Phase-Transition Temperature and Introducing Resonant Energy Doping. *Adv. Mater.* **2018**, *30* (11), 1705942. https://doi.org/10.1002/adma.201705942.

(143) Chen, Z.; Ge, B.; Li, W.; Lin, S.; Shen, J.; Chang, Y.; Hanus, R.; Snyder, G. J.; Pei, Y. Vacancy-Induced Dislocations within Grains for High-Performance PbSe Thermoelectrics. *Nat. Commun.* **2017**, *8* (1), 1–8. https://doi.org/10.1038/ncomms13828.

(144) Hu, L.; Zhu, T.; Liu, X.; Zhao, X. Point Defect Engineering of High-Performance Bismuth-Telluride-Based Thermoelectric Materials. *Adv. Funct. Mater.* **2014**, *24* (33), 5211–5218. https://doi.org/10.1002/adfm.201400474.

(145) Principles of the Theory of Solids - J. M. Ziman - Google Books https://books.google.com.hk/books?hl=en&lr=&id=o4woMNO-C3sC&oi=fnd&pg=PA1&ots=IOImd27Bfb&sig=r8cGpZEEvR8U590e_fZB8MOYhlM&redir_esc=y#v=onepage&q&f=false (accessed May 17, 2021).

(146) Recent Trends in Thermoelectric Materials Research, Part Two, Volume 70 - 1st Edition https://www.elsevier.com/books/recent-trends-in-thermoelectric-materials-research-part-two/tritt/978-0-12-752179-4 (accessed May 17, 2021).

(147) Solid State Physics, Volume 51 - 1st Edition https://www.elsevier.com/books/solid-state-physics/ehrenreich/978-0-12-607751-3 (accessed May 17, 2021).

(148) Toberer, E. S.; Zevalkink, A.; Snyder, G. J. Phonon Engineering through Crystal Chemistry. *J. Mater. Chem.* **2011**, *21* (40), 15843–15852. https://doi.org/10.1039/c1jm11754h.

(149) Dresselhaus, M. S.; Chen, G.; Tang, M. Y.; Yang, R.; Lee, H.; Wang, D.; Ren, Z.; Fleurial, J. P.; Gogna, P. New Directions for Low-Dimensional Thermoelectric Materials. *Adv. Mater.* **2007**, *19* (8), 1043–1053. https://doi.org/10.1002/adma.200600527.

(150) Poudel, B.; Hao, Q.; Ma, Y.; Lan, Y.; Minnich, A.; Yu, B.; Yan, X.; Wang, D.; Muto, A.; Vashaee, D.; Chen, X.; Liu, J.; Dresselhaus, M. S.; Chen, G.; Ren, Z. High-Thermoelectric Performance of Nanostructured Bismuth Antimony Telluride Bulk Alloys. *Science (80-.).* **2008**, *320* (5876), 634–638. https://doi.org/10.1126/science.1156446.

(151) Kim, S. Il; Lee, K. H.; Mun, H. A.; Kim, H. S.; Hwang, S. W.; Roh, J. W.; Yang, D. J.; Shin, W. H.; Li, X. S.; Lee, Y. H.; Snyder, G. J.; Kim, S. W. Dense Dislocation Arrays Embedded in Grain Boundaries for High-Performance Bulk Thermoelectrics. *Science (80-.).* **2015**, *348* (6230), 109–114. https://doi.org/10.1126/science.aaa4166.

(152) Mu, E.; Wu, Z.; Wu, Z.; Chen, X.; Liu, Y.; Fu, X.; Hu, Z. A Novel Self-Powering Ultrathin TEG Device Based on Micro/Nano Emitter for Radiative Cooling. *Nano Energy* **2019**, *55*, 494–500. https://doi.org/10.1016/j.nanoen.2018.10.057.

(153) Gao, Q.; Wang, W.; Lu, Y.; Cai, K. F.; Li, Y. T.; Wang, Z. X.; Wu, M. M.; Huang, C. J.; He, J. Q. High Power Factor Ag/Ag2Se Composite Films for Flexible

Thermoelectric Generators. *ACS Appl. Mater. Interfaces* **2021**, *13* (12), 14340–14346. https://doi.org/10.1021/acsami.1c02194.

(154) Zeng, W.; Tao, X. M.; Lin, S.; Lee, C.; Shi, D.; Lam, K. ho; Huang, B.; Wang, Q.; Zhao, Y. Defect-Engineered Reduced Graphene Oxide Sheets with High Electric Conductivity and Controlled Thermal Conductivity for Soft and Flexible Wearable Thermoelectric Generators. *Nano Energy* **2018**, *54*, 163–174. https://doi.org/10.1016/J.NANOEN.2018.10.015.

(155) Kim, S. J.; Lee, H. E.; Choi, H.; Kim, Y.; We, J. H.; Shin, J. S.; Lee, K. J.; Cho, B. J. High-Performance Flexible Thermoelectric Power Generator Using Laser Multiscanning Lift-Off Process. *ACS Nano* **2016**, *10* (12), 10851–10857. https://doi.org/10.1021/ACSNANO.6B05004/ASSET/IMAGES/NN-2016-05004Z_M001.GIF.

(156) Park, S. H.; Jo, S.; Kwon, B.; Kim, F.; Ban, H. W.; Lee, J. E.; Gu, D. H.; Lee, S. H.; Hwang, Y.; Kim, J. S.; Hyun, D. B.; Lee, S.; Choi, K. J.; Jo, W.; Son, J. S. High-Performance Shape-Engineerable Thermoelectric Painting. *Nat. Commun.* **2016**, *7*. https://doi.org/ARTN 1340310.1038/ncomms13403.

(157) Kim, F.; Kwon, B.; Eom, Y.; Lee, J. E.; Park, S.; Jo, S.; Park, S. H.; Kim, B. S.; Im, H. J.; Lee, M. H.; Min, T. S.; Kim, K. T.; Chae, H. G.; King, W. P.; Son, J. S. 3D Printing of Shape-Conformable Thermoelectric Materials Using All-Inorganic Bi2Te3-Based Inks. *Nat. Energy* **2018**, *3* (4), 301–309. https://doi.org/10.1038/s41560-017-0071-2.

(158) Fan, W. S.; Shen, Z. Y.; Zhang, Q.; Liu, F.; Fu, C. G.; Zhu, T. J.; Zhao, X. B. High-Power-Density Wearable Thermoelectric Generators for Human Body Heat Harvesting. *ACS Appl. Mater. Interfaces* **2022**, *14* (18), 21224–21231. https://doi.org/10.1021/acsami.2c03431.

(159) Hong, S.; Gu, Y.; Seo, J. K.; Wang, J.; Liu, P.; Meng, Y. S.; Xu, S.; Chen, R. K. Wearable Thermoelectrics for Personalized Thermoregulation. *Sci. Adv.* **2019**, *5* (5). https://doi.org/ARTN eaaw053610.1126/sciadv.aaw0536.

(160) Zheng, Y. Y.; Han, X.; Yang, J. W.; Jing, Y. Y.; Chen, X. Y.; Li, Q. Q.; Zhang, T.; Li, G. D.; Zhu, H. T.; Zhao, H. Z.; Snyder, G. J.; Zhang, K. Durable, Stretchable and Washable Inorganic-Based Woven Thermoelectric Textiles for Power Generation and Solid-State Cooling. *Energy Environ. Sci.* **2022**, *15* (6), 2374–2385. https://doi.org/10.1039/d1ee03633e.

(161) Lee, J. A.; Aliev, A. E.; Bykova, J. S.; de Andrade, M. J.; Kim, D.; Sim, H. J.; Lepro, X.; Zakhidov, A. A.; Lee, J. B.; Spinks, G. M.; Roth, S.; Kim, S. J.; Baughman, R. H. Woven-Yarn Thermoelectric Textiles. *Adv. Mater.* **2016**, *28* (25), 5038–5044. https://doi.org/10.1002/adma.201600709.

(162) Tian, Z. T.; Lee, S.; Chen, G. Heat Transfer in Thermoelectric Materials and Devices. *J. Heat Transf. Asme* **2013**, *135* (6). https://doi.org/Artn 06160510.1115/1.4023585.

(163) Suter, C.; Tomes, P.; Weidenkaff, A.; Steinfeld, A. Heat Transfer and Geometrical Analysis of Thermoelectric Converters Driven by Concentrated Solar Radiation. *Materials (Basel).* **2010**, *3* (4), 2735–2752. https://doi.org/10.3390/ma3042735.

(164) Chen, L. G.; Gong, J. Z.; Sun, F. R.; Wu, C. Effect of Heat Transfer on the Performance of Thermoelectric Generators. *Int. J. Therm. Sci.* **2002**, *41* (1), 95–99. https://doi.org/Pii S1290-0729(01)01307-2Doi 10.1016/S1290-0729(01)01307-2.

(165) Stevens, J. W. Optimal Design of Small Delta T Thermoelectric Generation Systems. *Energy Convers. Manag.* **2001**, *42* (6), 709–720. https://doi.org/Doi 10.1016/S0196-8904(00)00099-6.

(166) Tan, G.; Zhao, D. L. Study of a Thermoelectric Space Cooling System Integrated with Phase Change Material. *Appl. Therm. Eng.* **2015**, *86*, 187–198. https://doi.org/10.1016/j.applthermaleng.2015.04.054.

(167) Xu, Q.; Deng, B.; Zhang, L.; Lin, S.; Han, Z.; Zhou, Q.; Li, J.; Zhu, Y.; Jiang, F.; Li, Q.; Zhang, P.; Zhang, X.; Chen, G.; Liu, W. High-Performance, Flexible Thermoelectric Generator Based on Bulk Materials. *Cell Reports Phys. Sci.* **2022**, *3* (3), 100780. https://doi.org/10.1016/J.XCRP.2022.100780.

(168) Lin, S.; Zhang, L.; Zeng, W.; Shi, D.; Liu, S.; Ding, X.; Yang, B.; Liu, J.; Lam, K. ho; Huang, B.; Tao, X. Flexible Thermoelectric Generator with High Seebeck Coefficients Made from Polymer Composites and Heat-Sink Fabrics. *Commun. Mater. 2022 31* **2022**, *3* (1), 1–13. https://doi.org/10.1038/s43246-022-00263-1.

(169) Hyland, M.; Hunter, H.; Liu, J.; Veety, E.; Vashaee, D. Wearable Thermoelectric Generators for Human Body Heat Harvesting. *Appl. Energy* **2016**, *182*, 518–524. https://doi.org/10.1016/J.APENERGY.2016.08.150.

(170) Kim, C. S.; Lee, G. S.; Choi, H.; Kim, Y. J.; Yang, H. M.; Lim, S. H.; Lee, S. G.; Cho, B. J. Structural Design of a Flexible Thermoelectric Power Generator for Wearable Applications. *Appl. Energy* **2018**, *214*, 131–138. https://doi.org/10.1016/j.apenergy.2018.01.074.

(171) He, M.; Zhao, Y.; Wang, B.; Xi, Q.; Zhou, J.; Liang, Z.; He, M.; Zhao, Y.; Liang, Z.; Wang, B.; Xi, Q.; Zhou, J. 3D Printing Fabrication of Amorphous Thermoelectric Materials with Ultralow Thermal Conductivity. *Small* **2015**, *11* (44), 5889–5894. https://doi.org/10.1002/SMLL.201502153.

(172) Qiu, J.; Yan, Y.; Luo, T.; Tang, K.; Yao, L.; Zhang, J.; Zhang, M.; Su, X.; Tan, G.; Xie, H.; Kanatzidis, M. G.; Uher, C.; Tang, X. 3D Printing of Highly Textured Bulk Thermoelectric Materials: Mechanically Robust BiSbTe Alloys with Superior Performance. *Energy Environ. Sci.* **2019**, *12* (10), 3106–3117. https://doi.org/10.1039/C9EE02044F.

(173) Kim, F.; Kwon, B.; Eom, Y.; Lee, J. E.; Park, S.; Jo, S.; Park, S. H.; Kim, B. S.; Im, H. J.; Lee, M. H.; Min, T. S.; Kim, K. T.; Chae, H. G.; King, W. P.; Son, J. S. 3D Printing of Shape-Conformable Thermoelectric Materials Using All-Inorganic Bi2Te3-Based Inks. *Nat. Energy 2017 34* **2018**, *3* (4), 301–309. https://doi.org/10.1038/s41560-017-0071-2.

(174) Burton, M. R.; Mehraban, S.; Beynon, D.; McGettrick, J.; Watson, T.; Lavery, N. P.; Carnie, M. J. 3D Printed SnSe Thermoelectric Generators with High Figure of Merit. *Adv. Energy Mater.* **2019**, *9* (26), 1900201. https://doi.org/10.1002/AENM.201900201.

(175) Kee, S.; Haque, M. A.; Corzo, D.; Alshareef, H. N.; Baran, D. Self-Healing and Stretchable 3D-Printed Organic Thermoelectrics. *Adv. Funct. Mater.* **2019**, *29* (51), 1905426. https://doi.org/10.1002/ADFM.201905426.

(176) Jiang, B.; Muddemann, T.; Kunz, U.; -, al; Jung, J.; Bark, H.; Byun, D.; Patil, B.; Bernini, C.; Marré, D.; Pellegrino, L.; Pallecchi, I. Ink-Jet Printing and Drop-Casting Deposition of 2H-Phase SnSe2 and WSe2 Nanoflake Assemblies for Thermoelectric Applications. *Nanotechnology* **2021**, *33* (3), 035302. https://doi.org/10.1088/1361-6528/AC2F26.

(177) Park, D.; Kim, M.; Kim, J. Conductive PEDOT:PSS-Based Organic/Inorganic Flexible Thermoelectric Films and Power Generators. *Polymers (Basel).* **2021**, *13* (2), 1–12. https://doi.org/10.3390/POLYM13020210.

(178) Wang, Y. Y.; Cai, K. F.; Yao, X. Facile Synthesis of Thermoelectric Films via Spin-Coating Metastable Precursors. *Ceram. Int.* **2012**, *38* (SUPPL. 1), S535–S538. https://doi.org/10.1016/J.CERAMINT.2011.05.070.

(179) Nugraha, M. I.; Kim, H.; Sun, B.; Azimul Haque, M.; Pelayo Garcia de Arquer, F.; Rosas Villalva, D.; El-Labban, A.; Sargent, E. H.; Alshareef, H. N.; Baran, D.; Nugraha, M. I.; Haque, M. A.; Villalva, D. R.; El-Labban, A.; Baran, D.; Kim, H.; Alshareef, H. N.; Sun, B.; G de Arquer, F. P.; Sargent, E. H. Low-Temperature-Processed Colloidal Quantum Dots as Building Blocks for Thermoelectrics. *Adv. Energy Mater.* **2019**, *9* (13), 1803049. https://doi.org/10.1002/AENM.201803049.

(180) Wu, Q.; Hu, J. Thermoelectric Textile Materials. *Bringing Thermoelectr. into Real.* **2018**. https://doi.org/10.5772/INTECHOPEN.75474.

(181) Kim, D. H.; Byon, E.; Lee, G. H.; Cho, S. Effect of Deposition Temperature on the Structural and Thermoelectric Properties of Bismuth Telluride Thin Films Grown by Co-Sputtering. *Thin Solid Films* **2006**, *510* (1–2), 148–153. https://doi.org/10.1016/J.TSF.2005.12.306.

(182) Santos, R.; Loureiro, J.; Nogueira, A.; Elangovan, E.; Pinto, J. V.; Veiga, J. P.; Busani, T.; Fortunato, E.; Martins, R.; Ferreira, I. Thermoelectric Properties of V2O5 Thin Films Deposited by Thermal Evaporation. *Appl. Surf. Sci.* **2013**, *282*, 590–594. https://doi.org/10.1016/J.APSUSC.2013.06.016.

(183) Bashir, A.; Awan, T. I.; Tehseen, A.; Tahir, M. B.; Ijaz, M. Interfaces and Surfaces. *Chem. Nanomater.* **2020**, 51–87. https://doi.org/10.1016/B978-0-12-818908-5.00003-2.

(184) Shin, S.; Kumar, R.; Roh, J. W.; Ko, D. S.; Kim, H. S.; Kim, S. Il; Yin, L.; Schlossberg, S. M.; Cui, S.; You, J. M.; Kwon, S.; Zheng, J.; Wang, J.; Chen, R. High-Performance Screen-Printed Thermoelectric Films on Fabrics. *Sci. Reports 2017 71* **2017**, *7* (1), 1–9. https://doi.org/10.1038/s41598-017-07654-2.

(185) Shin, S.; Kumar, R.; Roh, J. W.; Ko, D. S.; Kim, H. S.; Kim, S. Il; Yin, L.; Schlossberg, S. M.; Cui, S.; You, J. M.; Kwon, S.; Zheng, J.; Wang, J.; Chen, R. High-Performance Screen-Printed Thermoelectric Films on Fabrics. *Sci. Reports 2017 71* **2017**, *7* (1), 1–9. https://doi.org/10.1038/s41598-017-07654-2.

(186) Kim, S. J.; We, J. H.; Cho, B. J. A Wearable Thermoelectric Generator Fabricated on a Glass Fabric. *Energy Environ. Sci.* **2014**, *7* (6), 1959–1965. https://doi.org/10.1039/C4EE00242C.

(187) Nugraha, M. I.; Kim, H.; Sun, B.; Azimul Haque, M.; Pelayo Garcia de Arquer, F.; Rosas Villalva, D.; El-Labban, A.; Sargent, E. H.; Alshareef, H. N.; Baran, D.; Nugraha, M. I.; Haque, M. A.; Villalva, D. R.; El-Labban, A.; Baran, D.; Kim, H.; Alshareef, H. N.; Sun, B.; G de Arquer, F. P.; Sargent, E. H. Low-Temperature-Processed Colloidal Quantum Dots as Building Blocks for Thermoelectrics. *Adv. Energy Mater.* **2019**, *9* (13), 1803049. https://doi.org/10.1002/AENM.201803049.

(188) Wu, Q.; Hu, J. Thermoelectric Textile Materials. *Bringing Thermoelectr. into Real.* **2018**. https://doi.org/10.5772/INTECHOPEN.75474.

(189) Kim, D. H.; Byon, E.; Lee, G. H.; Cho, S. Effect of Deposition Temperature on the Structural and Thermoelectric Properties of Bismuth Telluride Thin Films Grown by Co-Sputtering. *Thin Solid Films* **2006**, *510* (1–2), 148–153. https://doi.org/10.1016/J.TSF.2005.12.306.

(190) Bashir, A.; Awan, T. I.; Tehseen, A.; Tahir, M. B.; Ijaz, M. Interfaces and Surfaces. *Chem. Nanomater.* **2020**, 51–87. https://doi.org/10.1016/B978-0-12-818908-5.00003-2.

(191) Riemer, R.; Shapiro, A. Biomechanical Energy Harvesting from Human Motion: Theory, State of the Art, Design Guidelines, and Future Directions. *J. Neuroeng. Rehabil.* **2011**, *8* (1), 22. https://doi.org/10.1186/1743-0003-8-22.

(192) Wang, J. Fundamentals of Classical Thermodynamics; Springer Berlin Heidelberg, 2011; pp 53–88. https://doi.org/10.1007/978-3-642-11349-9_3.

(193) Snyder, G. J. Small Thermoelectric Generators. *Electrochem. Soc. interface* **2008**, *17* (3), 54.

(194) Qi, Y.; McAlpine, M. C. Nanotechnology-Enabled Flexible and Biocompatible Energy Harvesting. *Energy Environ. Sci.* **2010**, *3* (9), 1275–1285. https://doi.org/10.1039/C0EE00137F.

(195) Sue, C.-Y.; Tsai, N.-C. Human Powered MEMS-Based Energy Harvest Devices. *Appl. Energy* **2012**, *93*, 390–403. https://doi.org/https://doi.org/10.1016/j.apenergy.2011.12.037.

(196) Kishi, M.; Nemoto, H.; Hamao, T.; Yamamoto, M.; Sudou, S.; Mandai, M.; Yamamoto, S. Micro-Thermoelectric Modules and Their Application to Wristwatches as an Energy Source. *Int. Conf. Thermoelectr. ICT, Proc.* **1999**, 301–307. https://doi.org/10.1109/ICT.1999.843389.

(197) Dyson energy bracelet a good call https://newatlas.com/dyson-energy-bracelet/12040/ (accessed Sep 28, 2022).

(198) Torfs, T.; Leonov, V.; Vullers, R. J. M. Pulse Oximeter Fully Powered by Human Body Heat; 2007.

(199) Leonov, V.; Vullers, R. J. M. Wearable Electronics Self-Powered by Using Human Body Heat: The State of the Art and the Perspective. *J. Renew. Sustain. Energy* **2009**, *1* (6), 62701.

(200) Leonov, V.; Torfs, T.; Van Hoof, C.; Vullers, R. Smart Wireless Sensors Integrated in Clothing: An Electrocardiography System in a Shirt Powered Using Human Body Heat. *Sensors and Transducers* **2009**, *107*, 165–176.

(201) Lay-Ekuakille, A.; Vendramin, G.; Trotta, A.; Mazzotta, G. Thermoelectric Generator Design Based on Power from Body Heat for Biomedical Autonomous Devices; 2009 IEEE International Workshop on Medical Measurements and Applications, MeMeA 2009 (2009) 1-4. https://doi.org/10.1109/memea.2009.5167942.

(202) Leonov, V. Thermoelectric Energy Harvesting of Human Body Heat for Wearable Sensors. *IEEE Sens. J.* **2013**, *13* (6), 2284–2291. https://doi.org/10.1109/jsen.2013.2252526.

(203) Leonov, V. Human Heat Generator for Energy Scavenging with Wearable Thermopiles. *Sensors and Transducers* **2011**, *126*, 1–10.

(204) Kim, C. S.; Yang, H. M.; Lee, J.; Lee, G. S.; Choi, H.; Kim, Y. J.; Lim, S. H.; Cho, S. H.; Cho, B. J. Self-Powered Wearable Electrocardiography Using a Wearable Thermoelectric Power Generator. *ACS Energy Lett.* **2018**, *3* (3), 501–507. https://doi.org/10.1021/acsenergylett.7b01237.

(205) Kim, M. K.; Kim, M. S.; Lee, S.; Kim, C.; Kim, Y. J. Wearable Thermoelectric Generator for Harvesting Human Body Heat Energy. *Smart Mater. Struct.* **2014**, *23* (10), 105002. https://doi.org/10.1088/0964-1726/23/10/105002.

(206) Champier, D. Thermoelectric Generators: A Review of Applications. *Energy Convers. Manag.* **2017**, *140*, 167–181. https://doi.org/10.1016/J.ENCONMAN.2017.02.070.

(207) Yuan, J.; Zhu, R.; Li, G. Self-Powered Electronic Skin with Multisensory Functions Based on Thermoelectric Conversion. *Adv. Mater. Technol.* **2020**, 2000419. https://doi.org/10.1002/admt.202000419.

(208) Wang, Y.; Shi, Y.; Mei, D.; Chen, Z. Wearable Thermoelectric Generator to Harvest Body Heat for Powering a Miniaturized Accelerometer. *Appl. Energy* **2018**, *215*, 690–698. https://doi.org/10.1016/J.APENERGY.2018.02.062.

(209) Zoui, M. A.; Bentouba, S.; Stocholm, J. G.; Bourouis, M. A Review on Thermoelectric Generators: Progress and Applications. *Energies 2020, Vol. 13, Page 3606* **2020**, *13* (14), 3606. https://doi.org/10.3390/EN13143606.

(210) Liu, Y.; Yin, L.; Zhang, W.; Wang, J.; Hou, S.; Wu, Z.; Zhang, Z.; Chen, C.; Li, X.; Ji, H.; Zhang, Q.; Liu, Z.; Cao, F. A Wearable Real-Time Power supplywith a Mg 3Bi 2 -Based Thermoelectric Module. *Cell Reports Phys. Sci.* **2021**. https://doi.org/10.1016/j.xcrp.2021.100412.

(211) Wang, Y.; Yang, L.; Shi, X. L.; Shi, X.; Chen, L.; Dargusch, M. S.; Zou, J.; Chen, Z. G. Flexible Thermoelectric Materials and Generators: Challenges and Innovations. *Advanced Materials*. Wiley-VCH Verlag July 19, 2019, p 1807916. https://doi.org/10.1002/adma.201807916.

(212) Ebrahimi, K.; Jones, G. F.; Fleischer, A. S. A Review of Data Center Cooling Technology, Operating Conditions and the Corresponding Low-Grade Waste Heat Recovery Opportunities. *Renew. Sustain. Energy Rev.* **2014**, *31*, 622–638. https://doi.org/10.1016/J.RSER.2013.12.007.

(213) Li, X.; Cai, K.; Gao, M.; Du, Y.; Shen, S. Recent Advances in Flexible Thermoelectric Films and Devices. *Nano Energy* **2021**, *89*, 106309. https://doi.org/10.1016/J.NANOEN.2021.106309.

(214) Haras, M.; Skotnicki, T. Thermoelectricity for IoT – A Review. *Nano Energy* **2018**, *54*, 461–476. https://doi.org/10.1016/J.NANOEN.2018.10.013.

(215) He, J.; Tritt, T. M. Advances in Thermoelectric Materials Research: Looking Back and Moving Forward. *Science (80-.).* **2017**, *357* (6358). https://doi.org/10.1126/SCIENCE.AAK9997/ASSET/8273CBC8-7739-44FF-A41C-5530E2BBF995/ASSETS/GRAPHIC/357_AAK9997_F6.JPEG.

(216) Vining, C. B. An Inconvenient Truth about Thermoelectrics. *Nat. Mater. 2009 82* **2009**, *8* (2), 83–85. https://doi.org/10.1038/nmat2361.

(217) Zhang, Q.; Liao, B.; Lan, Y.; Lukas, K.; Liu, W.; Esfarjani, K.; Opeil, C.; Broido, D.; Chen, G.; Ren, Z. High Thermoelectric Performance by Resonant Dopant Indium in Nanostructured SnTe. *Proc. Natl. Acad. Sci. U. S. A.* **2013**, *110* (33), 13261–13266. https://doi.org/10.1073/PNAS.1305735110/SUPPL_FILE/PNAS.201305735SI.PDF.

(218) Heremans, J. P.; Jovovic, V.; Toberer, E. S.; Saramat, A.; Kurosaki, K.; Charoenphakdee, A.; Yamanaka, S.; Snyder, G. J. Enhancement of Thermoelectric Efficiency in PbTe by Distortion of the Electronic Density of States. *Science (80-.).* **2008**, *321* (5888), 554–557. https://doi.org/10.1126/SCIENCE.1159725/SUPPL_FILE/HEREMANS_SOM.PDF.

(219) Chen, C.; Feng, Z.; Yao, H.; Cao, F.; Lei, B. H.; Wang, Y.; Chen, Y.; Singh, D. J.; Zhang, Q. Intrinsic Nanostructure Induced Ultralow Thermal Conductivity Yields Enhanced Thermoelectric Performance in Zintl Phase Eu2ZnSb2. *Nat. Commun. 2021 121* **2021**, *12* (1), 1–9. https://doi.org/10.1038/s41467-021-25483-w.

(220) Jaziri, N.; Boughamoura, A.; Müller, J.; Mezghani, B.; Tounsi, F.; Ismail, M. A Comprehensive Review of Thermoelectric Generators: Technologies and Common Applications. *Energy Reports* **2020**, *6*, 264–287. https://doi.org/10.1016/j.egyr.2019.12.011.

(221) Iezzi, B.; Ankireddy, K.; Twiddy, J.; Losego, M. D.; Jur, J. S. Printed, Metallic Thermoelectric Generators Integrated with Pipe Insulation for Powering Wireless Sensors. *Appl. Energy* **2017**, *208*, 758–765. https://doi.org/10.1016/j.apenergy.2017.09.073.

(222) Liu, W.; Tan, X.; Yin, K.; Liu, H.; Tang, X.; Shi, J.; Zhang, Q.; Uher, C. Convergence of Conduction Bands as a Means of Enhancing Thermoelectric Performance of N-Type Mg 2Si 1-XSn x Solid Solutions. *Phys. Rev. Lett.* **2012**,

108 (16), 166601. https://doi.org/10.1103/PHYSREVLETT.108.166601/FIGURES/3/MEDIUM.

(223) Xiao, Y.; Wu, H.; Cui, J.; Wang, D.; Fu, L.; Zhang, Y.; Chen, Y.; He, J.; Pennycook, S. J.; Zhao, L. D. Realizing High Performance N-Type PbTe by Synergistically Optimizing Effective Mass and Carrier Mobility and Suppressing Bipolar Thermal Conductivity. *Energy Environ. Sci.* **2018**, *11* (9), 2486–2495. https://doi.org/10.1039/C8EE01151F.

(224) Lae Kim, S.; Taisun Lin, H.; Yu, C.; Kim, S. L.; Yu, C.; Lin, H. T. Thermally Chargeable Solid-State Supercapacitor. *Adv. Energy Mater.* **2016**, *6* (18), 1600546. https://doi.org/10.1002/AENM.201600546.

(225) Li, T.; Zhang, X.; Lacey, S. D.; Mi, R.; Zhao, X.; Jiang, F.; Song, J.; Liu, Z.; Chen, G.; Dai, J.; Yao, Y.; Das, S.; Yang, R.; Briber, R. M.; Hu, L. Cellulose Ionic Conductors with High Differential Thermal Voltage for Low-Grade Heat Harvesting. *Nat. Mater.* **2019**, *18* (6), 608–613. https://doi.org/10.1038/s41563-019-0315-6.

(226) Kunitski, M.; Eicke, N.; Huber, P.; Köhler, J.; Zeller, S.; Voigtsberger, J.; Schlott, N.; Henrichs, K.; Sann, H.; Trinter, F.; Schmidt, L. P. H.; Kalinin, A.; Schöffler, M. S.; Jahnke, T.; Lein, M.; Dörner, R. Double-Slit Photoelectron Interference in Strong-Field Ionization of the Neon Dimer. *Nat. Commun. 2019 101* **2019**, *10* (1), 1–7. https://doi.org/10.1038/s41467-018-07882-8.

(227) Leighton, C. Electrolyte-Based Ionic Control of Functional Oxides. *Nat. Mater. 2018 181* **2018**, *18* (1), 13–18. https://doi.org/10.1038/s41563-018-0246-7.

(228) Li, X.; Li, M.; Yang, Q.; Li, H.; Xu, H.; Chai, Z.; Chen, K.; Liu, Z.; Tang, Z.; Ma, L.; Huang, Z.; Dong, B.; Yin, X.; Huang, Q.; Zhi, C. Phase Transition Induced Unusual Electrochemical Performance of V2CTX MXene for Aqueous Zinc Hybrid-Ion Battery. *ACS Nano* **2020**, *14* (1), 541–551. https://doi.org/10.1021/ACSNANO.9B06866/ASSET/IMAGES/MEDIUM/NN9B06866_M001.GIF.

(229) Akgöl, Y.; Cramer, C.; Hofmann, C.; Karatas, Y.; Wiemhöfer, H. D.; Schönhoff, M. Humidity-Dependent Dc Conductivity of Polyelectrolyte Multilayers: Protons or Other Small Ions as Charge Carriers? *Macromolecules* **2010**, *43* (17), 7282–7287. https://doi.org/10.1021/MA1012489/ASSET/IMAGES/MEDIUM/MA-2010-012489_0004.GIF.

(230) Fakhari, A.; Corcoran, M.; Schwarz, A. Thermogelling Properties of Purified Poloxamer 407. *Heliyon* **2017**, *3* (8), e00390. https://doi.org/10.1016/j.heliyon.2017.e00390.

(231) Dumortier, G.; Grossiord, J. L.; Agnely, F.; Chaumeil, J. C. A Review of Poloxamer 407 Pharmaceutical and Pharmacological Characteristics. *Pharm. Res. 2006 2312* **2006**, *23* (12), 2709–2728. https://doi.org/10.1007/S11095-006-9104-4.

(232) Choi, B. M.; Hwang, C. S.; Yoon, Y. S.; Park, I. J.; Yoo, M. W.; Kim, B. S. Novel Temperature-Responsive Hydrogel Injected to the Incision Site for Postoperative Pain Relief in Laparoscopic Abdominal Surgery: A Single-Blind, Randomized, Pivotal Clinical Trial. *Surg. Endosc.* **2022**, *36* (8), 5794–5802. https://doi.org/10.1007/S00464-022-09252-4/TABLES/3.

(233) Li, G.; Dong, D.; Hong, G.; Yan, L.; Zhang, X.; Song, W.; Li, G.; Dong, D.; Zhang, X.; Hong, G.; Yan, L.; Song, W. High-Efficiency Cryo-Thermocells Assembled with Anisotropic Holey Graphene Aerogel Electrodes and a Eutectic Redox Electrolyte. *Adv. Mater.* **2019**, *31* (25), 1901403. https://doi.org/10.1002/ADMA.201901403.

(234) Kim, K.; Lee, H. Thermoelectrochemical Cells Based on Li+/Li Redox Couples in LiFSI Glyme Electrolytes. *Phys. Chem. Chem. Phys.* **2018**, *20* (36), 23433–23440. https://doi.org/10.1039/C8CP03155J.

(235) Morita, T.; Narita, T.; Mukai, S. A.; Yanagisawa, M.; Tokita, M. Phase Behaviors of Agarose Gel. *AIP Adv.* **2013**, *3* (4), 042128. https://doi.org/10.1063/1.4802968.

(236) Hemmat Esfe, M.; Esfandeh, S.; Kamyab, M. H. History and Introduction. *Hybrid Nanofluids Convect. Heat Transf.* **2020**, 1–48. https://doi.org/10.1016/B978-0-12-819280-1.00001-X.

(237) Frank, H. S.; Wen, W. Y. Ion-Solvent Interaction. Structural Aspects of Ion-Solvent Interaction in Aqueous Solutions: A Suggested Picture of Water Structure. *Discuss. Faraday Soc.* **1957**, *24* (0), 133–140. https://doi.org/10.1039/DF9572400133.

(238) Di Lecce, S.; Albrecht, T.; Bresme, F. A Computational Approach to Calculate the Heat of Transport of Aqueous Solutions. *Sci. Reports 2017 71* **2017**, *7* (1), 1–10. https://doi.org/10.1038/srep44833.

(239) Rezende Franco, L.; Sehnem, A. L.; Figueiredo Neto, A. M.; Coutinho, K. Molecular Dynamics Approach to Calculate the Thermodiffusion (Soret and Seebeck) Coefficients of Salts in Aqueous Solutions. *J. Chem. Theory Comput.* **2021**, *17* (6), 3539–3553. https://doi.org/10.1021/ACS.JCTC.1C00116/SUPPL_FILE/CT1C00116_SI_001.PDF.

(240) Takeyama, N.; Nakashima, K. Proportionality of Intrinsic Heat of Transport to Standard Entropy of Hydration for Aqueous Ions. *J. Solut. Chem. 1988 174* **1988**, *17* (4), 305–325. https://doi.org/10.1007/BF00650412.

(241) Burgess, J. Ion–Solvent Interactions. *Ions Solut.* **1999**, 45–61. https://doi.org/10.1533/9781782420569.45.

(242) García de Arquer, F. P.; Dinh, C. T.; Ozden, A.; Wicks, J.; McCallum, C.; Kirmani, A. R.; Nam, D. H.; Gabardo, C.; Seifitokaldani, A.; Wang, X.; Li, Y. C.; Li, F.; Edwards, J.; Richter, L. J.; Thorpe, S. J.; Sinton, D.; Sargent, E. H. CO2 Electrolysis to Multicarbon Products at Activities Greater than 1 A Cm−2. *Science (80-.).* **2020**, *367* (6478), 661–666. https://doi.org/10.1126/SCIENCE.AAY4217/SUPPL_FILE/AAY4217_GARCIADEARQUER_SM.PDF.

(243) Paul, P. P.; McShane, E. J.; Colclasure, A. M.; Balsara, N.; Brown, D. E.; Cao, C.; Chen, B. R.; Chinnam, P. R.; Cui, Y.; Dufek, E. J.; Finegan, D. P.; Gillard, S.; Huang, W.; Konz, Z. M.; Kostecki, R.; Liu, F.; Lubner, S.; Prasher, R.; Preefer, M. B.; Qian, J.; Rodrigues, M. T. F.; Schnabel, M.; Son, S. B.; Srinivasan, V.;

Steinrück, H. G.; Tanim, T. R.; Toney, M. F.; Tong, W.; Usseglio-Viretta, F.; Wan, J.; Yusuf, M.; McCloskey, B. D.; Nelson Weker, J. A Review of Existing and Emerging Methods for Lithium Detection and Characterization in Li-Ion and Li-Metal Batteries. *Adv. Energy Mater.* **2021**, *11* (17), 2100372. https://doi.org/10.1002/AENM.202100372.

(244) Swift, T.; Swanson, L.; Geoghegan, M.; Rimmer, S. The PH-Responsive Behaviour of Poly(Acrylic Acid) in Aqueous Solution Is Dependent on Molar Mass. *Soft Matter* **2016**, *12* (9), 2542–2549. https://doi.org/10.1039/C5SM02693H.

(245) Proto, A.; Bibbo, D.; Cerny, M.; Vala, D.; Kasik, V.; Peter, L.; Conforto, S.; Schmid, M.; Penhaker, M. Thermal Energy Harvesting on the Bodily Surfaces of Arms and Legs through a Wearable Thermo-Electric Generator. *Sensors (Switzerland)* **2018**, *18* (6), 1927. https://doi.org/10.3390/s18061927.

(246) Larsson, O.; Said, E.; Berggren, M.; Crispin, X. Insulator Polarization Mechanisms in Polyelectrolyte-Gated Organic Field-Effect Transistors. *Adv. Funct. Mater.* **2009**, *19* (20), 3334–3341. https://doi.org/10.1002/adfm.200900588.

(247) Potentials, S. E. Table of Standard Electrode Potentials. 2018, pp 1–2.